The Hong Kong Polytechnic University

Institute of Textiles and Clothing

Gas and Vapor Transport through Nano- and Micro- Fibrous Materials

Dahua Shou

A thesis submitted in partial fulfillment of the requirements for the degree of Doctor of Philosophy

July 2012

CERTIFICATE OF ORIGINALITY

I hereby declare that this thesis is my own work and that, to the best of my knowledge and belief, it reproduces no material previously published or written, nor material that has been accepted for the award of any other degree or diploma, except where due acknowledgement has been made in the text.

_____ (Signed)

Dahua Shou
_____ (Name of student)

Dedicated to my family

Abstract

Fibrous materials have a variety of applications, such as filtration, fuel cell, textile fabric, fiber reinforced composite, and tissue scaffold. Recently, of particular interest are fibrous preforms composed of nanofibers and microfibers, which are tailored to meet a range of advanced requirements. For many applications, permeability of gas flow and diffusivity of vapor diffusion are two important mass transport behaviors observed. However, the characterization of the transport phenomena in realistic fibrous structures is challenging and still not fully understood, especially in nano- and micro-scale regimes. Therefore, the current work is aimed at systematically bridging the microstructures to the transport properties of nano- and micro-fibrous materials, by analytically solving transport equations in equivalent fibrous structures based on deterministic and statistical methods.

Fibrous structures can be broadly classified into two types: single-scale and dual-scale. The absence of yarns makes the mean pore radius in single-scale mats of the same magnitude, and hence they can be characterized by a single permeability. However, after finer fibers or filaments are bundled into yarns, they are woven or stitched into different structures, which contain pore sizes in two distinctly different magnitudes and are therefore called dual-scale fibrous media. The single-scale fibrous medium is commonly referred to as a nonwoven web, which can be one-dimensional (1D: all fibers parallel with each other), two-dimensional (2D: all fibers parallel with the same plane), and three-dimensional (3D: all fibers distributed in different orientations in a cubic space) arrangements. Dual-scale fibrous media can be knitted or woven structures, which are always constructed by interlacing threads.

The first part of this study was aimed at studying gas flow through single-scale fibrous materials. For highly porous fibrous media, gas permeabilities from 1D ordered structure to randomly located 2D or 3D fiber assembles were determined by

Voronoi Tessellation Method and mixing laws. The slip flow on the fiber surface of nanofibers was particularly considered. For densely packed fibers, a modified scale estimate approach was utilized to predict the gas permeability.

In the second part, a permeability model throughout the range of porosities was obtained for single-scale fibrous layers, whose pore size distribution was found to statistically follow the fractal power law.

The third part investigated gas flow in dual-scale fibrous media, where complexities are introduced as the inter-yarn flow is coupled with the intra-yarn flow. A “slip” boundary at the interface between yarns and open channels was used to account for the coupled effect. A semi-analytical model was also provided for rapid predictions of permeabilities from unidirectionally aligned yarns to 3D woven fabrics.

The fourth part presented an analytical model of vapor diffusivities for 1D, 2D, and 3D randomly distributed fibers. The model was established by extending the 1D regular model to 1D random array through Voronoi Tessellation Method, and to 2D and 3D structures by mixing rules.

In the fifth part, a diffusivity model of nanofiber webs was derived as a function of porosity, fiber radius, and fractal dimensions, which statistically characterize the pore size distribution and tortuosity of fibrous media. To verify the proposed model, experimental measurements of water vapor diffusivities for electrospun nanofiber mats were conducted by inverted-cup test method.

All the models established in this study were well validated by the results collected from experiments in present study or related literature, numerical simulations, and past theoretical models. Moreover, the effects of structural parameters were extensively analyzed, and the following conclusions can be made:

1. Gas permeability of microfibers scales with the square of fiber radius, while vapor diffusivity of microfibers is independent of fiber/pore size.

2. In nanofiber mats, gas permeability is enhanced by slip effect, but vapor diffusivity is decreased due to Knudsen effect. Electrospun nanofibers are found to be good candidates of breathable materials experimentally and theoretically.

3. Both gas permeability and vapor diffusivity are not sensitive with in-plane fiber orientation, but increase with increasing through-plane fiber orientation.

4. In terms of fiber distribution, more random, more permeable, but less diffusive when porosity is high.

5. Comparing with squarely packed fibers, fibers with hexagonal configuration are more transversely permeable but less axially permeable in low porosity range.

6. Elliptical fibers with major axis parallel with flow direction are more transversely permeable than circular fibers, and they have similar permeability in the high porosity range.

7. The intra-yarn permeability increases the overall permeability of dual-scale fibrous materials when the ratio between them is more than 0.01.

Based on above models and findings, future work may be directed towards employing the models to specific uses, developing relevant software, improving models of coupled heat and moisture transfer, and designing optimized fibrous structures with controllable transport properties.

Publications Updated

International journals:

1. Shou, DH; Fan, JT; Ding F. Dual-scale modeling in fibrous porous media: hydraulic permeability predictions, submitted.

2. Shou, DH; Fan, JT; Ding F. An analytical model for gas diffusion though nanoscale fibrous media, submitted.

3. Shou, DH; Ye L; Tang YH; Fan, JT; Ding F. Transverse Permeability Determination of Dual-Scale Fibrous Materials, International Journal of Heat and Mass Transfer. 2013;58 (1-2):532-539.

4. Shou, DH; Fan, JT; Ding F. Effective Diffusivity of Gas Diffusion Layer in Proton Exchange Membrane Fuel Cells, Journal of Power Sources. 2013;225:179-186.

5. Shou, DH; Fan, JT; Ding F. Hydraulic permeability of fibrous porous media, International Journal of Heat and Mass Transfer. 2011;54 (17-18):4009-4018.

6. Shou, DH; Fan, JT; Ding F. A difference-fractal model for the permeability of fibrous porous media, Physics Letters A. 2010;374 (10):1201-1204.

7. Qin XH, Jia L, Lu WY, Shou DH, Fan JT. Stretching of the steady jet in electrospinning: theoretical analysis and experimental verification. Textile Research Journal. 2011;81(4):388-397.

International conferences:

1. Shou, DH; Fan JT; Ye L; Tang YH. Dual-scale permeability modeling in fibrous materials, The Fiber Society Spring 2012 Conference, St. Gallen, Switzerland.

2. Fan, JT; Shou, DH. Effective Permeability and Diffusivity of Fibrous Materials, The 2011 International Conference on Textile Engineering and Materials, Tianjin.

3. Shou, DH; Fan JT. Modeling moisture diffusion through nano and micro fibrous materials, The Fiber Society Spring 2011 Conference, Hong Kong.

Acknowledgements

I would like to convey my sincerest thanks to my chief supervisor, Prof. Jintu Fan, for his invaluable advice, excellent guidance, and insightful discussions throughout this project. I was always inspired by his enthusiasm in scientific pursuit and rigorous attitude towards research work. Also, I would appreciate him for encouraging me to carry out research studies liberally and offering me opportunities to study and make academic exchanges internationally.

I am very grateful to my co-supervisors, Professor Jihuan He in Soochow University and Dr. Feng Ding in The Hong Kong Polytechnic University, for their technical advice and useful discussions that contributed to this thesis.

Great thanks are sent to Prof. Lin Ye in Sydney University, who offered me the opportunity of studying in his group during my Attachment Program of PhD training. His wide knowledge broadened my mind, and his words “why are you doing that” continuously reminded me of the basic but important point in research.

My thanks also give to my colleagues who gave suggestions to my project or helped me in various aspects throughout my completion of this thesis. They include but not limited to Dr. Kausik Bal, Dr. Qing Chen, Dr. Fuan He, Dr. Maofei Mei, Dr. Manas Sarkar, Ms. Chao Sun, Ms. Maggie Tong, Dr. Xianfu Wan, Dr. Huijun Wu, Dr. John Wu, Mr. Boqi Xiao, and Mr. Lei Zhu in The Hong Kong Polytechnic University, Prof. Wang Huaiyuan in Northeast Petroleum University, Dr. Youhong Tang in Flinders University, Dr. Kunkun Fu in Tongji University, and Mr. Andy Wang in Sydney University.

Finally, I would gratefully acknowledge the PhD. Scholarship from The Hong Kong Polytechnic University.

Content

List of Figures

List of Tables

Nomenclature

a	Maximum radius of the yarn along x-direction, m
A	Major axis of an elliptical yarn, m
A_i	Constants to be determined
B	Minor axis of an elliptical yarn, m
c	Empirical constant
c_1	Empirical constant
c_e	Combination coefficient for high porosity limit
c_i	Correction factor
c_l	Combination coefficient for low porosity limit
C_v	Vapor density, gm^{-3}
d	Pore diameter, m
$\langle d \rangle$	Mean pore diameter, m
D	Space dimension

D_0	Fractal dimension
D_b	Bulk diffusivity, $m^2 s^{-1}$
D_{eff}	Effective diffusivity, $m^2 s^{-1}$
D_{equ}	Equivalent diffusivity, $m^2 s^{-1}$
D_f	Pore area fractal dimension
D_{Kn}	Knudsen diffusivity, $m^2 s^{-1}$
D_t	Tortuosity fractal dimension
D_{Tr}	Transition diffusivity, $m^2 s^{-1}$
h	Channel height, m
h_i	Thickness of i layer fibrous media, m
$h_{\min}$	Minimum channel height, m
h_p	Penetration depth of inter-yarn flow, m
H	Thickness of fibrous media, m
F	Drag acting on a unit length of fiber, $Pa \cdot m$

$f(S)$	Gamma distribution
i	Ordinal number
j	Empirical constant
$j(R_p)$	Diffusion rate of a single channel, $gm^{-2}s^{-1}$
J	Diffusive flux, $gm^{-2}s^{-1}$
k	Ratio of minimum and maximum pore radius
k_{fab}	Thermal conductivity of fabric, WK^{-1}
K	Permeability, m^2
K_c	Kozeny constant
K_e	Permeability at high porosity limit, m^2
$K_{eff,i}$	Effective fractional permeability, m^2
$K_{h,c}$	Permeability of hexagonal array of circular yarns, m^2
$K_{h,e}$	Permeability of hexagonal array of elliptical yarns, m^2
K_i	Inter-yarn permeability, m^2

K_l	Permeability at low porosity limit, m^2
K_p	Permeability of porous yarns, m^2
$\langle K_p \rangle$	Mean permeability of porous yarns, m^2
$K_{s,c}$	Permeability of square array of circular yarns, m^2
$K_{s,e}$	Permeability of square array of elliptical yarns, m^2
K_w	Weave permeability, m^2
K_y	Yarn permeability, m^2
Kn	Knudsen number
l	Radial distance, m
L	Length scale, m
L_c	Square side length, m
L_f	Length of the fiber, m
L_t	Total length of a channel, m
L_x	Side length of the representative cell in x-direction, m

L_y	Side length of the representative cell in y-direction, m
M	Fractal object
Ma	Mach number
max	Maximum
min	Minimum
n	Normal to the fiber surface
N	Population of pores or fibers
p	Pressure, Pa
q	Flow flux of a single channel, $m^4 s^{-1}$
q_d	Diffusion flux of a single channel, gs^{-1}
Q	Flow flux (2D), $m^3 s^{-1}$
	Flow flux (3D), $m^4 s^{-1}$
Q_d	Total fluxes of gas diffusion, gs^{-1}
Q_i	Inter-yarn flow flux (2D), $m^3 s^{-1}$

Q_p	Intra-yarn flow flux (2D), $m^3 s^{-1}$
r	Fiber/filament radius, m
R	Yarn radius, m
R_c	Cell radius, m
Re	Flow resistance, m^{-2}
R_f	Flow resistance, m^{-2}
R_p	Pore radius, m
R_y	Yarn radius, m
s	Effective channel length, m
S	Cell area, m^2
S_a	Adjacent yarn distance of 3D woven, m
S_p	Pore area, m^2
S_t	Total cross-sectional area, m^2
u	Fluid velocity, ms^{-1}

$\langle u \rangle$	Mean velocity, ms^{-1}
u_p	Intra-yarn velocity, ms^{-1}
u_{para}	Parallel velocity along the fiber axis, ms^{-1}
u_s	Slip velocity, ms^{-1}
u_y	Intra-yarn velocity, ms^{-1}
x	Coordinate system, m
y	Coordinate system, m

Greek symbols

α	Degree of randomness
α_s	Slip coefficient
β	Scale of a Gamma distribution
γ	Adjustable parameter
ϕ	Fiber fraction

μ	Fluid viscosity, Nsm^{-2}
μ_e	Effective viscosity, Nsm^{-2}
ε	Porosity
ε_i	Porosity fraction of regime i
ε_p	Percolation porosity
ε_w	Weave porosity
ε_y	Yarn porosity
ρ	Density, gm^{-3}
ρ_{media}	Porous medium density, gm^{-3}
ρ_{nylon}	Nylon density, gm^{-3}
λ	Mean free path of molecules, m
λ_e	Axis ratio of an ellipse
λ_v	Heat (de)sorption rate, Jg^{-1}
ψ	Stream function

θ	Azimuth
Γ	Gamma distribution function
Γ_f	Moisture (de)sorption rate, $gm^{-3}s^{-1}$
τ	Tortuosity
τ_{Kn}	Knudsen tortuosity
τ_M	Modified tortuosity
χ	Radio between the minimum and the total frontal areas

Chapter 1 Introduction

1.1. Background

In the past decades, fiber-based materials have attracted great attention from engineers and scientists in various areas, including filtration, fuel cells, functional clothing, thermal insulation, paper products, and medical science. Further development of various forms of fibrous products, particularly nano- and micro-fibrous materials and fiber reinforced composites, unfold a vigorous mass campaign for applications. Commonly, nanofiber has a diameter less than 1 micron (WIKI, 2012), and microfiber has a diameter of around 10 microns or less (Microfiber.com, 2012).

Among the applications, fibrous materials always serve as media, which allow air, vapor, particles, liquids, or heat to transfer through. Therefore, it is of great importance to understand the transport mechanisms in fibrous materials.

However, most of the structures of fibrous media are highly complex and difficult to describe. It is even more complicated to analyze the mass transfer behaviors within fibrous systems. Moreover, the range of the scales from nano to macro within one fibrous medium is huge, which further adds the complexity of transport behaviors. Modeling transport phenomena of fibrous media is therefore a great challenge and makes the present study interesting.

1.2. Fibrous structure

Fibrous medium is usually solid-void mixtures with the solid fibers in a slender circular/elliptical form, such as the one shown in Fig. 1-1. The unique properties of fibrous materials, different from some other categories of porous media, are their

breathability, compressibility, flexibility, and specific surface area. Particularly in textile science and engineering, fibrous materials can be mainly divided into two types: ordered fabrics and disordered nonwovens.

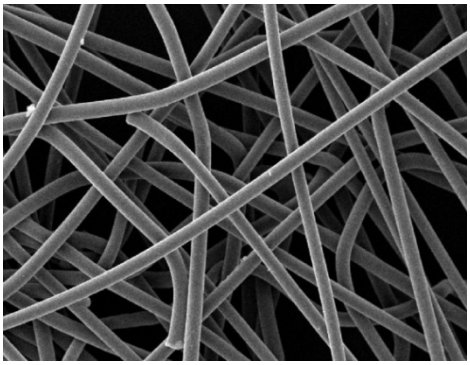

Figure 1-1: An example of microscopic image of a fibrous medium

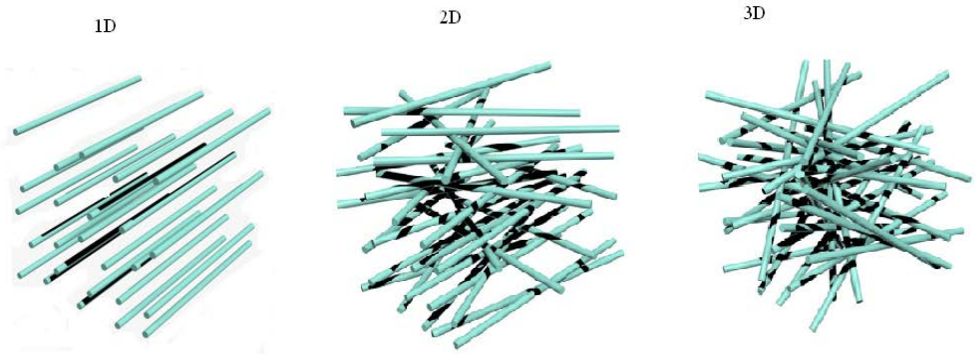

Figure 1-2: Illustration of 1D, 2D, and 3D fibrous media

Fibrous media in nonwoven form are generated by means of assembling fibers into a planar structure on the ground of research and applications. Although the nature of their structures are varied and complex, the nonwovens can be generally simplified as consisting of arrays of cylinders in three forms of formations, as shown in Fig. 1-2, viz. one-dimensional (1D) structure in which all fibers are parallel with one another; two-dimensional (2D) structure in which fibers lie in parallel planes with directional or random orientations; and three-dimensional (3D) structure in

which fibers are directionally or randomly oriented in space (Tomadakis and Robertson, 2005).

Ordered fabrics are made up of bundles of fibers after arrangements, such as weaving, knitting, crocheting, and knotting. Among them, woven structures (see Fig. 1-3) are the ones that are most widely applied in composites (Chen et al., 2006), which have additional features such as, unit cell, interlace spacing or gap, and interlace point (Mariatti et al., 2000). The popularity of woven composites is increasing due to the dual-scale structures that woven is made up of a bundle of filaments, known as yarns. The weaving of the yarns provides an additional interlocking which enhances strength better than what can be achieved by sole fiber matrix adhesion (Alavudeen et al., 2011).

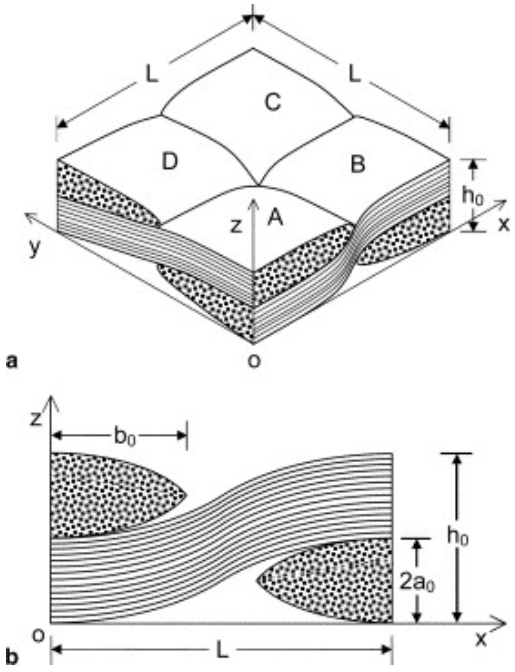

Figure 1-3: Unit cell of a plain weave fabric perform (Chen et al., 2006)

In contrast to the conventional fibrous materials with fiber radius larger than 10 microns, the radius of nanofiber is typically less than 0.5 micron or even smaller

than 50 nanometers (Gibson et al., 2001). The nanofiber assembles are expected to possess nano-scale texture and a very high surface to volume ratio, leading to different modes of transport properties by comparing to the macro-scale porous materials (Gibson et al., 2001). Particularly, a new type of fibers named electrospun nanofibers joins the family of fibrous materials and have gained increasing attention in the past decade (Subbiah et al., 2005). Electrospinning applies a high electrical charge to produce super-fine fibers from polymer solutions or melt polymers (Reneker et al., 2000, Li and Xia, 2004). Most electrospun nanofibers are prepared in a nonwoven form, but it can also be twisted or woven into an ordered structure (Bazbouz and Stylios, 2008). A schematic of an electrospun nanofiber mat and a conventional nonwoven is presented in Fig. 1-4.

(a)

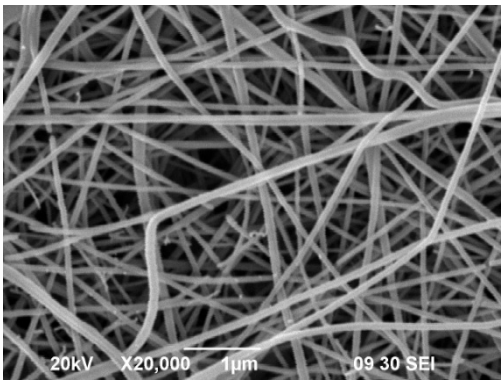

(b)

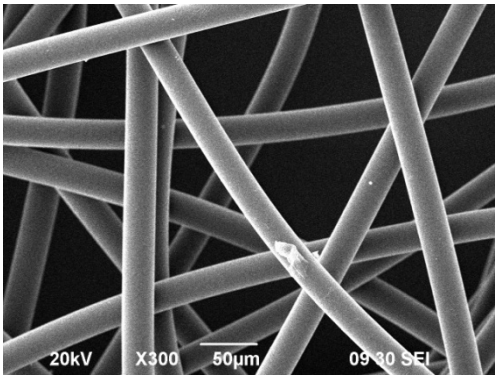

Figure 1-4: SEM images of (a) Nylon 6 electrospun nanofiber mat and (b) conventional nonwoven

1.3. Transport properties

Gas flow and vapor diffusion are the two main mass transport mechanisms involved in porous media (Bear and Bachmat, 1990), and also the targeted subjects in the present study.

It is generally assumed that the slow flow through fibrous porous media is dominated by viscosity at low Reynolds number, and the effects of gravity and inertia become negligible (Kim and Reneker, 1999). From a macroscopic view, the viscous permeability of fibrous media can be defined by Darcy's law (Darcy, 1856):

$$\langle u \rangle = -\frac{K}{\mu} \nabla p, \tag{1-1}$$

where K is Darcy hydraulic permeability, μ is the fluid viscosity, ∇p is the pressure gradient, and $\langle u \rangle$ is the average fluid velocity. Darcy's equation, as an expression of conservation of momentum, originated from determining permeability of porous media empirically in 1850s (Darcy, 1856). It has been served as a starting point for studying viscous flow in porous media.

The applicability of Eq. (1-1) is tarnished by the difficulty in accurately measuring the ratio of fluid flux against the directional pressure gradient through experimental measurements for different types of fibrous porous materials. In addition, it lacks of physical understanding of micro-structural influences on the permeability. To exactly describe the motion of fluid substances in a micro-scale regime, researchers employ Stokes equation, as follows (Gebart, 1992):

$$-\nabla p + \mu \nabla^2 u = 0. \tag{1-2}$$

Detailed fluid velocity distribution can be calculated based on solving Stokes equation with proper boundary conditions.

For dual-scale porous media, such as woven composites made up of permeable yarns, analytical technique is not capable of solving Stokes equation in both inter- and intra- yarn regimes simultaneously, and numerical simulation suffers from expensive computation (Nabovati et al., 2010). The Brinkman equation (Brinkman, 1947), dealing with the fluid flows in internal area of a porous medium by Darcy's law and in its outer boundary layer by Stokes equation, is therefore proposed for reducing computational complexity (Ahn et al., 1991):

$$-\nabla p + \mu \nabla^2 u - \frac{\mu}{K_p} u = 0, \tag{1-3}$$

where K_p is the Darcy permeability of the porous medium or the intra-yarn permeability in woven fabric.

Different from the pressure-driven gas flow, the movement of vapor molecules caused by concentration difference in a porous medium is known as diffusion (Smith and Hashemi, 2006). It takes place when the concentration of the molecules is higher in one region than the other. Vapor molecules will not stop migrating until there is an equalized concentration configuration throughout the carrier. The moving paths of molecules during diffusive motion process are random, but the most preferred migration of molecules will be in the direction of decreasing concentration. Diffusivities are calculated by postulating flux moving from regions of high to low concentration by using Fick's law (Smith and Hashemi, 2006):

$$J = -D_b \frac{\partial C}{\partial x}, \tag{1-4}$$

where J is the diffusion flux and measures the amount of migrated diffusive molecules, D_b is the bulk diffusion coefficient in open space without any confinement, C is the concentration of diffusive molecules, and x is the moving position.

Eq. (1-4) is analogous to Darcy's law in mathematical form, and it also lacks of microscopic study of structural effects. To overcome it, Fick's second law is applied (Nilsson and Stenstrom, 1995), viz.:

$$\nabla^2 C = 0, \tag{1-5}$$

which is expressed in the form of Laplace equation. The accurate concentration distribution can be calculated based on solving Eq. (1-5) with proper boundary conditions.

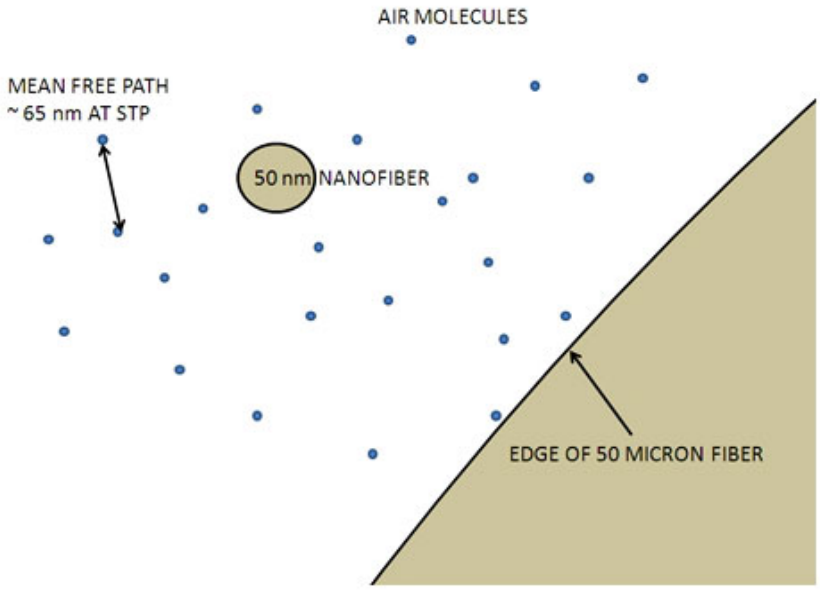

Figure 1-5: Air molecules near a nanofiber and a microfiber

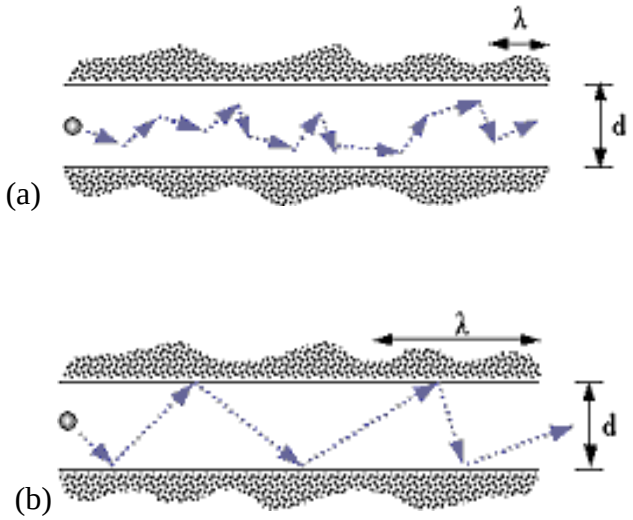

Figure 1-6: Schematic drawing of a molecule in a cylindrical pore in the case of (a) bulk diffusion and (b) Knudsen diffusion

To date, nanofibers and microfibers are being increasingly used in a range of novel applications. Unlike macroscopic problems in mass, momentum, or energy transport as described by traditional continuum equations, the movements and interactions of the nano-scale entities tend to be random walkers in microscopic world. For gas flow, the air molecule velocities are random near the surface of the fibers as seen in Fig. 1-5. The continuum theory assumes the average velocity of molecules fully in contact with the solid boundary of a microfiber is zero. This assumption is not strictly correct for nanofiber, as its radius is comparable to the mean free path (average distance covered by a moving particle between successive collisions) of fluid molecules and only a fraction of the air molecules actually contact the nanofiber (Smith, 2004). As such, the molecules without colliding with the nanofiber generate the slip flow (Smith, 2004).

For diffusion in porous media with large pores, movement of molecules is mainly blocked by their intermolecular collisions, and thus bulk diffusion occurs.

However, when the pore radius is comparable with the mean free path of diffusion molecule, molecular-wall collisions suffering from greater transport resistances will dominate (Brown, 1993), and Knudsen diffusion occurs as seen from Fig. 1-6.

1.4. Significance of transport properties in fibrous structures

Fluid flow and vapor diffusion in fibrous materials are significant and valuable as they are involved in a wide range of practical applications, including textile fabric, resin transfer molding (RTM), fuel cell, biological interfaces, and filtration, to say a few.

In textile and clothing engineering, fiber-based materials are dominantly used because fibrous structures have multifunctional characteristics, such as low weight and flexibility (Rantanen et al., 2000). More importantly, the fibrous structures can be tailored to meet a range of requirements, such as high moisture vapor diffusivity, controlled air permeability, and good thermal insulation. Therefore, fibrous materials have the great potential to be used as from protective clothing to daily wears with good comfort.

Resin transfer molding (RTM) is a promising manufacturing process of composite materials, which make the varieties of complex shapes in few simple steps and have control over mechanical properties by short cycle period (Ngo and Tamma, 2001). In RTM, the resin is drawn or injected into a shaped mold, which always contains the dual-scale woven preforms. Among the parameters, permeability is the critical processing factor which links the injection pressure with the mold filling time (Sadiq et al., 1995).

Proton exchange membrane fuel cell (PEMFC) is considered to be one of the leading candidates for the power sources of mobile, stationary, and portable devices

(Wee, 2007). The gas diffusion layer (GDL) of PEMFCs is a fibrous porous material with a layered structure, which not only provides the support of the fuel cell membrane, but also allows transport of reactants products, such as that oxygen diffusions through the GDL from the gas channel (GC) to the catalyst layer (CL), where it is combined with the protons and electrons from the anode to produce water (Litster and McLean, 2004). The produced water moves in a viscous form, which could condense and even block the porous GDL. Therefore, the permeability of liquid water and the diffusivity of water vapor, oxygen, and hydrogen are critical to the fuel cell performance.

Tissue engineering may allow for the reconstruction of breast, facial, skin, and other soft tissue defects in the human body (Gentleman et al., 2004). Fiber-based supporters are introduced to avoid the contraction of the scaffold by the constituent cells, which would severely reduce permeability and diffusivity of nutrient sources (Gentleman et al., 2004). Based on well predicted transport models, the incorporation of imposed fibers should enable the creation of larger constructs by allowing for greater nutrient transfer, and permit the creation of more complicated shapes of tissues.

Filters are also used to collect particles from the bulk fluid (Wang et al., 2006). The most common filter type is fibrous, which removes particles from a gas stream via solid fibers. The filter is generally characterized by their collection efficiency and pressure drop for air filtration. Therefore, a good understanding of the flow field and the resulting pressure drop is crucial in design and optimization of selective filtration systems.

1.5. Overall methodology

The literature review in Chapter 2 reveals the gap in the area of modeling gas

flow and vapor diffusion in fibrous materials. In order to solve the remaining problems, a systematic study will be conducted based on the overall methodology summarized in Fig. 1-7.

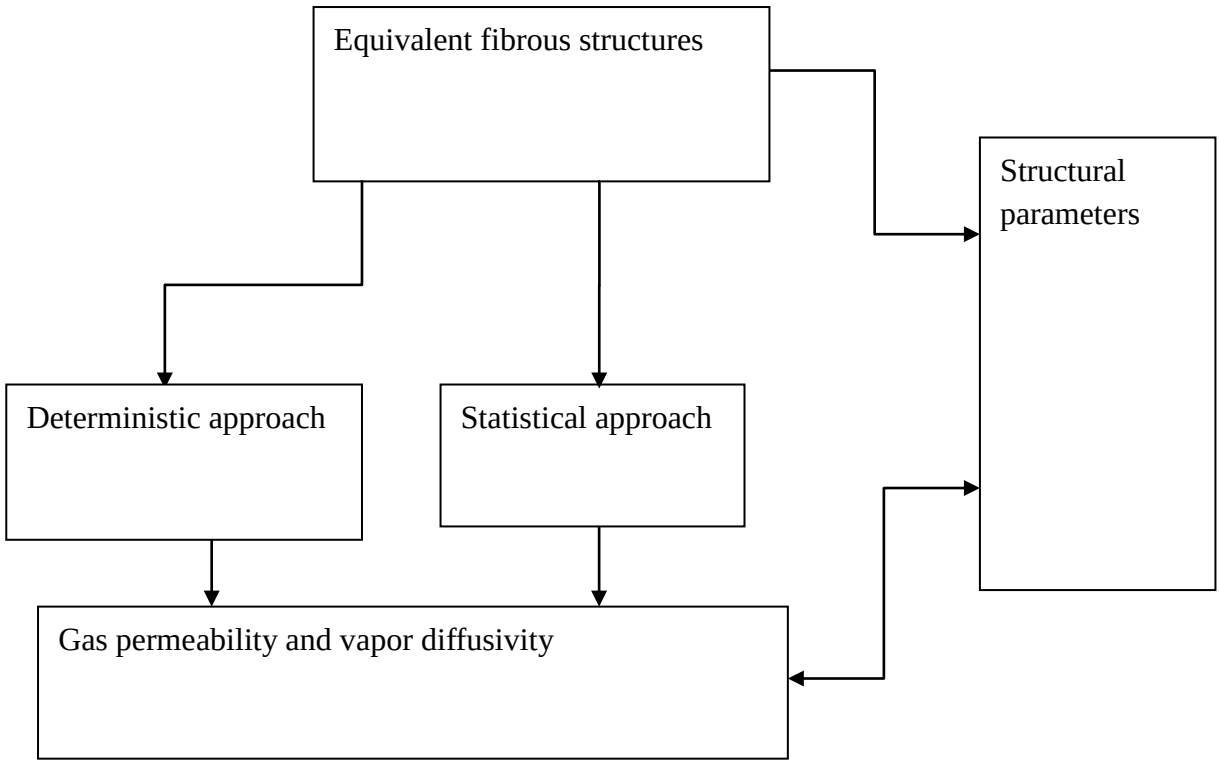

Figure 1-7: Outline of modeling methodology

Both of deterministic and statistical approaches are used to solve governing equations of gas and vapor transport in the equivalent fibrous matrix. Analytical solutions can be found within the properly equivalised fibrous matrix, which is used to represent the realistic fibrous structures. The deterministic method considers the affecting geometric details systematically, and the solution is therefore considered to be accurate, although it is sometimes difficult to derive. The statistical models, which describe the complex internal microstructures probabilistically or statistically, can provide rapid predictions of the transport trends, although they may be not as accurate as deterministic models. Therefore, the two methods are both presented in

this thesis, but the selection of the method depends on the specific end use of the fibrous structure. The predictions of all the models established in this study are compared with the data collected from the experiments in the present study or reported in the literature, previous numerical simulations, and existing theoretical models. Finally, the analysis of the structural parameters is conducted extensively.

1.6. Objectives of this study

The transport properties are very critical to the performance of fibrous materials, and this is the reason for the current intensive worldwide efforts to investigate transport phenomena in fibrous structures. To better characterize the relationship between the transport behavior and the fibrous medium, the present study aims to investigate the microscopic effect of fibrous structures towards the gas and vapor transfer mechanisms, and eventually provides macroscopic description of dependence of transport properties on structures. This thesis is focused on investigating transport properties in nano- and micro-fibrous materials, but all the models obtained in this study can also be used to deal with conventional or macro-scale fibrous preforms when the nano-scale effect is neglected.

Literature review in Chapter 2 shows that researchers have proposed a great number of analytical and numerical models in addition to experimental work. However, most of the analytical work studies the single-phase transport based on over-idealized structures of fiber beds, while the numerical studies are lack of theoretical analysis when simulating transport behaviors in realistic fibrous materials, or dealing with coupled and multi-phase transport within simplified homogenous structures. Therefore, this study is aimed at bridging the existing research to the ultimate models for various applications, where coupled and multi-phase transport takes place in the realistic complex fibrous media (see Fig. 1-8). To this end, this

thesis will extensively explore gas flow and vapor diffusion, respectively, in complex and realistic fibrous materials.

The studied morphological factors that are commonly used to describe fibrous media include: 1) porosity that is the ratio of the void volume to the total volume; 2) fiber radius; 3) fiber shape that is cross-section geometry of the fiber; 4) fiber orientation; 5) packing configuration that includes different packing arrangements; 6) nano-scale effect that describes unconventional phenomena arisen in nano- and micro-fibrous media; 7) randomness of fiber location that reveals the degree of disordered distribution of fibers; and 8) dual-scale effect that describes the influence of the intra-yarn flow on the system permeability.

To sum up, the main objectives of this project include:

1) To develop compact mechanistic models of gas permeability of single-scale fibrous materials from 1D to 3D structures, and investigate the affecting structural factors, such as porosity, fiber radius, fiber cross-sectional shape, fiber orientation, packing arrangement, slip flow, and randomness of fiber distribution.

2) To theoretically model gas permeability of dual-scale fibrous structures from aligned yarns to 3D woven fabric, and to investigate the influences of fiber shape, packing arrangement, and intra-yarn permeability.

3) To theoretically study vapor diffusion through fibrous media from 1D to 3D structures with consideration of Knudsen effect in nano-fibrous layer, and to conduct experimental measurements of vapor diffusion in electrospun nanofiber mats to verify the proposed model.

This project will improve the fundamental understandings of gas flow and vapor diffusion in fibrous media, especially in nano- and micro-scale regimes. In addition, the theoretical models with new findings of structural effects can serve as a foundation in the scientific and engineering fields, such as thermal protective clothing, sleeping bags, building construction, aircraft, filters, GDLs, and RTM composites. The developed models can also be applied to design nano- and micro-fibrous battings with required transport properties by hierarchy arrangement, structural optimizations, and integrations of different transport mechanisms.

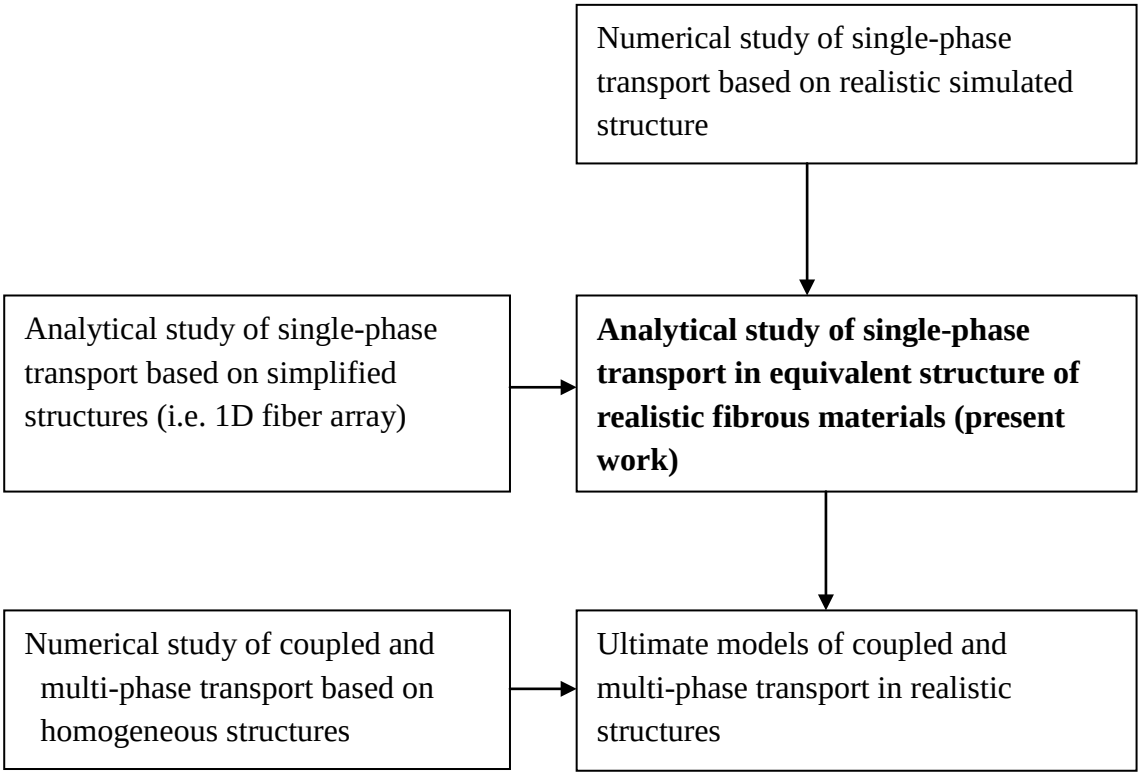

Figure 1-8: Relationship between previous studies, present work and ultimate model

1.7. Outline of this thesis

The remainder of the thesis is divided into seven chapters. Chapter 2 introduces a full literature review of transport properties of fibrous materials with research

methods and important conclusions. It ends with existing problems found in the literature. Chapter 3 and chapter 4 derive gas permeability models for single-scale fibrous materials based on deterministic and statistical approaches, respectively. Chapter 5 is focused on modeling dual-scale permeability. Chapter 6 obtains deterministic models of vapor diffusivity, and Chapter 7 presents a fractal model of vapor diffusivity. Chapter 8 summarizes the thesis and suggests the future work.

Chapter 2 Literature review

In human endeavor to utilize fibrous materials, it is fundamental to search for optimized performance and novel functionality. Therefore, the link between the microstructures and the resulting transport phenomena, which serves as the foundation for design and application of fiber materials, is of great scientific and engineered importance. Therefore, numerous studies of this area have been conducted based on analytical, numerical, and experimental methods.

This chapter reviews a class of representative publications with discussions and analysis. It is divided into five parts. The first part introduces different approaches employed to predict gas permeability of nonwoven fibrous materials. The second part refers to modeling gas flow in woven composites. The third part is focused on determining effective diffusivity of fiber assembles. The fourth part briefly discusses coupled heat and mass transfer in fiber-based materials. Existing problems are summarized in the fifth part.

2.1. Effective permeability of nonwoven fibrous media

Effective permeability, as a resulted property of slow viscous fluid flows, is one of key issues involved in applications of fibrous materials. Theoretical studies including pore-based model, cell-based model, scaling estimate model, and mixing rules, numerical simulations, and experimental measurements are critically reviewed. Effective permeability is a macroscopic scalar, but it lies in structural parameters such as porosity, fiber radius, fiber arrangements, and so forth. Hereby, the affecting microstructure factors are also analyzed.

2.1.1. Pore-based model

Fibrous materials are typical porous media, which are made up of solids and open voids. Many attempts have been made to relate the hydraulic permeability to the readily observable features of fibrous media, such as porosity and fiber radius. Among them, Kozeny-Carman (KC) equation is one of the most broadly used models, which assumes that porous media as consisting of a bundle of long tortuous pore channels (Tomadakis and Robertson, 2005). KC equation is expressed as:

$$K = \frac{\varepsilon \left\langle R_p \right\rangle^2}{4K_c}, \tag{2-1}$$

where ε is porosity, R_p is the pore radius, and K_c is the Kozeny constant. The mean pore radius $\left\langle R_p \right\rangle$ and porosity ε can be measured by a porosimeter.

A modified KC model was later proposed by using fiber radius instead of pore radius, because fiber radius is easier to measure and its size distribution is more uniform (Tomadakis and Robertson, 2005). The permeability model for randomly distributed fibers is given by (Tomadakis and Robertson, 2005):

$$K = \frac{\varepsilon}{4\ln^2 \varepsilon} \frac{\left(\varepsilon - \varepsilon_p\right)^{c+2}}{\left(1-\varepsilon_p\right)^c \left[\left(c+1\right)\varepsilon - \varepsilon_p\right]^2} r^2, \tag{2-2}$$

where, $\varepsilon_p = 0, c = 0,$ for 1D parallel;

$\varepsilon_p = 0.33, c = 0.707,$ for 1D normal;

$\varepsilon_p = 0.11, c = 0.521,$ for 2D parallel;

$\varepsilon_p = 0.11, c = 0.785,$ for 2D normal;

$\varepsilon_p = 0.037, c = 0.661,$ for 3D normal,

where, ε_p is the minimum porosity (or percolation threshold), and c is a constant varying with fiber structures, which are derived from recording moving distances of random-walk diffusive molecules by Monte Carlo simulations in numerical fibrous media (Tomadakis and Sotirchos, 1993a).

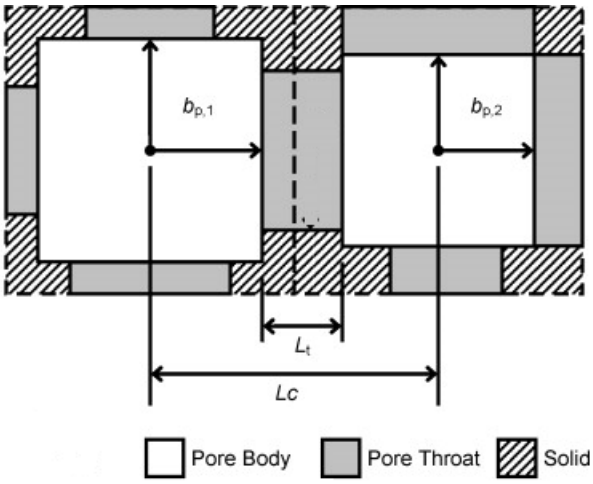

Figure 2-1: Representative diagram of two neighboring pore bodies and connecting throat (Gostick et al., 2007)

However, KC assumption does not hold at high porosity limit because the void pores promote interconnected flow rather than conduit flow. An alternative pore-based approach named as pore network modeling was then presented (Gostick et al., 2007). The basic idea of this method is mapping an indicative pore space continuum onto a lattice regularly or irregularly, as seen in Fig. 2-1. The pore space of fibrous media was idealized as consisting of a network collection of pore bodies communicating through pore throats, based on size distributions measured by porosimetry (Gostick et al., 2007). Nevertheless, the lack of detailed information of pore structures limits the further development of pore network modeling.

2.1.2. Cell-based model

Cell-based model assumes a representative unit cell, which is used to characterize the transport property of the whole fibrous system. The representative cell is regarded as existing repeatedly throughout the fibrous medium and has the same permeability with the whole system. With properly defined boundary conditions, accurate analytical solutions are available by solving Stokes equation, and the calculated permeability is always obtained without referring to tortuosity, specific surface area, and empirical shape factors. For a look at this area of literature, interested readers can be directed to a class of studies (Happel, 1959, Kuwabara, 1959, Keller, 1964, Sangani and Acrivos, 1982, Drummond and Tahir, 1984, Gebart, 1992, Tamayol and Bahrami, 2009). Among them, the lubrication approximation method, assuming the flow velocity is almost unidirectional, was always used to describe the channel flow between densely packed fibers with square and hexagonal manners. On the other hand, the effective medium approach, assuming all the regions outside the representative cell as an equivalent medium, was always employed to study the influences of neighboring fibers on the cell flow for loosely packed fibers. The representative models of cell-based methods are listed in Table 2-1.

The permeability model is generally expressed as a function of porosity, fiber radius, pore radius, and fiber geometric arrangement. As the fiber radius is generally uniform, the permeability model is preferred to be expressed by a dimensionless function of fiber radius (Johnson et al., 1986):

$$K / r^2 = f(\varepsilon). \tag{2-3}$$

Table 2-1: Summary of cell-based models of permeability

Models	Remarks
(Kuwabara, 1959) $K = \frac{-0.25\ln(1-\varepsilon) + 0.25 - \varepsilon - 0.25(1-\varepsilon)^2}{4(1-\varepsilon)} r^2$	• 1D flow transverse to dilute ordered array • Zero vorticity at the cell boundary
(Happel, 1959) $K = \frac{-0.25\ln(1-\varepsilon) + 0.5\frac{(1-\varepsilon)^2 - 1}{(1-\varepsilon)^2 + 1}}{4(1-\varepsilon)} r^2$	• 1D flow transverse to dilute ordered array • Zero shear stress at the cell boundary
(Happel, 1959) $K = \frac{-0.25\ln(1-\varepsilon) + 0.25 - \varepsilon - 0.25(1-\varepsilon)^2}{2(1-\varepsilon)} r^2$	• 1D flow parallel with dilute ordered array • Zero shear stress at the cell boundary
(Keller, 1964) $K = \frac{\sqrt{2}}{18(1-\varepsilon)}\left(1 - 2\frac{\sqrt{1-\varepsilon}}{\pi}\right)^{2.5} r^2$	• 1D flow transverse to dense square array • Force-based lubrication technique
(Sangani and Acrivos, 1982) $K = \frac{-0.25\ln(1-\varepsilon) + 0.262 - \varepsilon - 0.887(1-\varepsilon)^2}{4(1-\varepsilon)} r^2$	• 1D flow transverse to dilute square array • Least-squares technique
(Sangani and Acrivos, 1982) $K = \frac{-0.25\ln(1-\varepsilon) + 0.255 - \varepsilon - 0.25(1-\varepsilon)^2}{4(1-\varepsilon)} r^2$	• 1D flow transverse to dilute hexagonal array • Least-squares technique
(Drummond and Tahir, 1984)	• 1D flow parallel with square array

$K=\frac{-0.25\ln(1-\varepsilon)+0.251-\varepsilon-0.25(1-\varepsilon)^2}{2(1-\varepsilon)}r^2$	• Distributed singularities approach
(Drummond and Tahir, 1984) $K=\frac{-0.25\ln(1-\varepsilon)+0.323-\varepsilon-0.25(1-\varepsilon)^2}{2(1-\varepsilon)}r^2$	• 1D flow parallel with hexagonal array • Distributed singularities approach
(Gebart, 1992) $K=\frac{16}{9\sqrt{2}\pi}\left[\frac{1}{2}\left(\frac{\pi}{1-\varepsilon}\right)^{0.5}-1\right]^{2.5}r^2$	• 1D flow transverse to dense square array • Flux-based lubrication technique
(Gebart, 1992) $K=\frac{16}{9\sqrt{6}\pi}\left[\left(\frac{0.906}{1-\varepsilon}\right)^{0.5}-1\right]^{2.5}r^2$	• 1D flow transverse to dense hexagonal array • Flux-based lubrication technique
(Tamayol and Bahrami, 2009) Eq. (2-4)	• 1D flow transverse to square array • Modified lubrication technique • Studied cell aspect ratio
(Tamayol and Bahrami, 2009) Eq. (2-5)	• 1D flow parallel with square • Modified lubrication technique • Studied cell aspect ratio

The representative cell, which contains fibers arranged in a particular manner, is the smallest volume representing the basic characteristics of the dilute fibrous system, as shown in Fig. 2-2. This technique describes the structures of both square and hexagonal arrays of cylindrical fibers relying solely on the simple geometry and fiber

volume fraction. In 1959, Stokes equation for transverse permeability (i.e. permeability of fibers normal to flow) or parallel permeability (i.e. permeability of fibers parallel with flow) was solved with a zero shear stress boundary condition at the perimeter of circular cell (Kuwabara, 1959). Later, a similar approach was applied to study transverse permeability through 1D fibers, but with zero vorticity instead of zero shear stress (Happel, 1959). Kuwabara's model was reported to be able to deal with randomly located fibers, but only the ordered and homogeneous structure satisfied his assumption that the permeability of the unit cell was equal to the mean permeability of the fibrous system. In 1982, a new analytical solution by means of drag force, which can be transferred to effective permeability, was derived based on Least-squares technique for fibrous media with high limits of porosity (Sangani and Acrivos, 1982), where both square and hexagonal arrangements of fibers were considered. Later, an accurate solution for the two structures was presented by the distributed singularities approach (Drummond and Tahir, 1984).

(a) 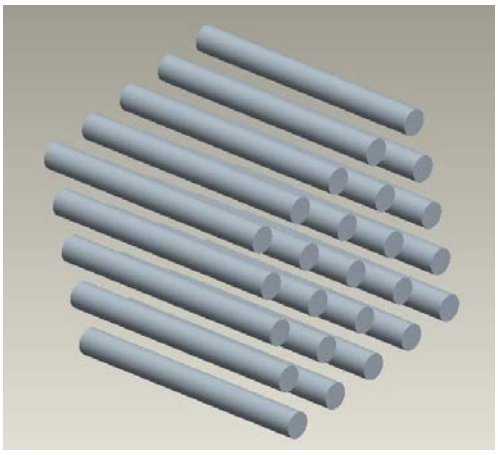 (b) 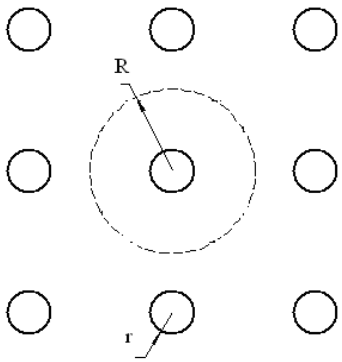

Figure 2-2: (a) Solid geometric and (b) plane geometric schematic of aligned cylindrical fibers in square pattern

In addition, it is interesting to find that the permeability of these arrays parallel

with flow is almost exactly twice of that when the fibers are transverse to the flow for those loosely packed fiber arrays (Johnson et al., 1986).

In order to predict the permeability of densely packing fibers, lubrication theory was applied by some researchers (Gebart, 1992, Keller, 1964). They found that most of the flow resistance or the pressure drop exists at the area near the narrowest slot between fibers. Keller considered the square array (Keller, 1964), while Gebart extended the square model to the hexagonal case (Gebart, 1992).

However, none of the above models predict well the permeability at moderate porosity (Tamayol and Bahrami, 2009), because the effective medium approximation and the lubrication approximation are valid only for the loosely and densely packed fiber arrays, respectively. Recently, a modified lubrication method was proposed to capture the flow trend in moderate porosity range by relating the border velocity of the channels between fibers with the average velocity of the system (Tamayol and Bahrami, 2009). They also found that the transverse permeability increases with the increasing aspect ratio of fiber distances between normal to and aligned with the flow direction in the cell, but the parallel permeability is not sensitive with the aspect ratio. The models of transverse permeability and parallel permeability are given as follows, respectively (Tamayol and Bahrami, 2009):

$$K=\left\{\frac{\pi}{24(1-\varepsilon)}+\left[\left(\sqrt{\frac{\pi}{4(1-\varepsilon)}}-1\right)^{3}\sqrt{\frac{(1-\varepsilon)}{9\pi}-\frac{\pi+1-\varepsilon}{8}}+2\right]\right\}\frac{\varepsilon}{2}r^{2}, \tag{2-4}$$

and

$$K=\left\{\frac{10}{\varepsilon_0^{1.5}}\left(2.27-1.27\varepsilon\right)+\frac{6+12\varepsilon_0}{\varepsilon_0^{0.5}(1-\varepsilon_0)^{2}}+\frac{18\varepsilon_0^{0.5}\tan^{-1}\left(\frac{1}{\varepsilon_0^{0.5}-1}\right)}{(\varepsilon_0-1)^{2.5}}\right\}^{-1}r^{2}, \tag{2-5}$$

where $\varepsilon_0 = \frac{\pi}{4(1-\varepsilon)}$.

2.1.3. Scaling estimate model

Based on the fact that most flow contributions exist near the narrowest gap between fibers (Gebart, 1992, Keller, 1964), Clague et al. (Clague et al., 2000) proposed a simple scaling estimate model of gas permeability based on Stokes equation. Clague et al. (Clague et al., 2000) selected the half distance $h_{\min}$ between cylindrical fibers as the characteristic length, over which the flow velocity changes rapidly. The scaling estimate model is given by (Clague et al., 2000):

$$K = ch_{\min}^2, \tag{2-6}$$

Later, Sobera and Klein (Sobera and Kleijn, 2006) argued that it is more proper to choose the actual velocity $u_0 = \langle u \rangle / \chi$ as the characteristic velocity, where χ is the radio between the minimum to the total frontal area between fibers, hence:

$$K = c\chi h_{\min}^2. \tag{2-7}$$

In addition, a correction factor was proposed to characterize the degree of disorder of fiber location (i.e., the variation of the distance between fibers (Sobera and Kleijn, 2006). It revealed that disordered fiber assembles are more permeable than those of regularly structured cases for both 1D and 2D arrays at the same porosity.

Recently, a tortuosity $\tau = \varepsilon^{-c_1}$ was added into the scaling estimate model of Eq. (2-7) to predict the permeability of fibrous materials from 1D to 3D structures (Tamayol and Bahrami, 2011). However, the scaling estimate model, which only

considers the critical geometric detail (i.e. $h_{\min}$), indeed intends to avoid referring to the statistical parameters such as tortuosity or pore size distribution. In addition, although the model is well verified by the experimental results collected from the literature, the agreement may be ascribed to the two empirical constants c and c_1, which can provide a more flexible fitting against the experimental values.

2.1.4. Mixing rules

Most cell-based and scaling estimate models are of high accuracy by comparing with the experimental and numerical results from the above literature, but neither of them can predict the permeability throughout the porosity range (Tamayol and Bahrami, 2009, Chai et al., 2011). To overcome this limitation, a mixed model was derived for transverse permeability of square array (Bruschke and Advani, 1993):

$$K = c_e K_e + c_l K_l, \tag{2-8}$$

where $c_e = 1 - \exp(0.8 - \frac{0.628}{1-\varepsilon})$ and $c_l = 1 - \exp(0.8 - \frac{0.628}{\varepsilon - 0.785})$ are combination coefficients, and K_e is the permeability model for loosely packed fiber, and K_l is the permeability model at low porosity (Bruschke and Advani, 1993).

The hydraulic permeability of 1D ordered fibers parallel with or normal to flow direction has been readily determined. However, it is difficult to predict the permeability of 2D and 3D structures that the hydraulic resistances of the fibers in different directions are interdependent and coupled, especially for those dense systems (Mattern and Deen, 2008). Accurate theoretical solutions are almost impossible considering the complex systems. An estimate as a function of fiber fraction ϕ was proposed for 3D arrays: $K(\phi) = \left[K_{norm}^{-1}(2/3\phi) + K_{para}^{-1}(1/3\phi) \right]^{-1}$,

which was obtained based on mixing flow resistances of fibers in normal and parallel flow direction, respectively (Johnson et al., 1986) .

2.1.5. Past experimental work

The first attempt at explaining the transport phenomenon of slow flow in porous media was conducted early in 1856 (Darcy, 1856). Based on the experimental observation, a mathematical form relating the flow flux linearly with the pressure difference was obtained, known as Darcy's law (Darcy, 1856). The fluid follows the Newton's law of viscosity and the porous medium is approximated homogeneous and isotropic. The effect of inertia and gravidity are not included as the Darcy's law focuses on viscous flows.

Based on Darcy's law, the permeability measurements require controlling either the pressure or fluid flux, and the most common experimental techniques include radial flow and channel flow measurements (Sharma and Siginer, 2010).

Diverse applications of fiber materials and testing fluids were used in different fibrous structures (Gostick et al., 2006b, Wiggins et al., 1939, Sullivan, 1942, DAVIES, 1952, Ingmanson et al., 1959, Lord, 1955, Wheat, 1963, Kirsch and Fuchs, 1967, Labrecque, 1968, Kostornov and Shevchuk, 1973, Sadiq et al., 1995, Rahli et al., 1997, Zhong et al., 2006). Fiber materials include glass rod, copper wire, glass wool, drill rod, copper wire, goat wool, hair, glass wool, kapok, rayon, Kapron fibers, and so forth. Testing fluids included water, air, alcohol, and so on. Fibrous geometric structures, from 1D parallel array to 3D assembles, from ordered structures to random matrix, from conventional fibers to nanofibers, from transverse flows to parallel, were all investigated. The permeability measurements are summarized in Table 2-2. Review work of experimental results is also available in literature (Jackson and James, 1986, Tomadakis and Robertson, 2005).

Darcy's law is a phenomenological model at the macroscopic level, which cannot go into the effects of microstructures. However, it is still the most commonly used technique as it can provide good permeability estimates, such as the empirical model of transverse permeability of 2D randomly layered fibrous media (DAVIES, 1952):

$$K / r^2 = \left\{16\left(1-\varepsilon\right)^{1.5}\left[1+56(1-\varepsilon)^3\right]\right\}^{-1}. \qquad (2\text{-}9)$$

Table 2-2: Summary of experimental measurement of nonwoven fibrous materials.

Authors	Remarks
(Wiggins et al., 1939)	• 3D flow through random structure • Glass rod, copper wire, and glass wool • Water
(Sullivan, 1942)	• 1D flow transverse/parallel with ordered/random array • Drill rod, copper wire, goat wool, and hair • Air
(DAVIES, 1952)	• 2D flow transverse to random layer • Glass wool, kapok, and rayon • Air
(Ingmanson et al., 1959)	• 2D flow transverse to random layer • Nylon fiber • Air
(Lord, 1955)	• 2D transverse flow through random

	layer • Silk, rayon
(Wheat, 1963)	• 2D transverse flow through random layer • Glass fiber • Air
(Kirsch and Fuchs, 1967)	• 1D flow transverse to ordered array • Kapron tube • Water
(Labrecque, 1968)	• 2D/3D flow through random structure • Nylon fiber • Water • Cross-section aspect ratio unimportant when less than 3
(Kostornov and Shevchuk, 1973)	• 2D flow transverse to random layer • Kapron fibers • Water and alcohol • Working fluid of water resulting in higher permeability than alcohol
(Sadiq et al., 1995)	• 1D flow transverse to square array • Nylon tube • Water
(Khomami and Moreno, 1997)	• 1D flow transverse to ordered array • Acrylic rod • Silicon oil
(Rahli et al., 1997)	• 3D flow through random structure • Bronze and copper rod

	• Water
(Zhong et al., 2006)	• 1D flow transverse to ordered array • Acrylic rod • Glycerol-water
(Gostick et al., 2006b)	• 2D flow transverse/parallel with random layer • GDL • Air

2.1.6. Numerical studies

Previous theoretical studies have to rely on approximately ordered structures of fibrous materials, while numeral approaches can deal with more complex and realistic cases with the dramatically growth of computational resources. The digital matrix to resemble the realistic fibrous structure is constructed first, where transport equations are calculated by the powerful numerical solvers. The numerical calculation can be indeed regarded as a numerical experiment.

Many attempts have been made to generate virtual structures that represent the studied fiber mat. A comprehensive model to describe the architecture of nonwoven network for use in tissue engineering and other applications was presented by Eichhorn and Sampson (Eichhorn and Sampson, 2005). Fibers were generally resembled as straight lines with given radius and length, and they were distributed by their core positions and orientations (Eichhorn and Sampson, 2005). Structural characteristics of fibrous network, such as the distribution of fibers, inter-fiber contacts, fiber contact distributions for integrity of the network systems, and the pore size distributions, were also provided (Eichhorn and Sampson, 2005). Later, Wang et al. (Wang et al., 2007a) applied the random generation-growth algorithm

and Monte Carlo method to construct random fibrous structures. After locating the fiber cores based on a core distribution probability and assigning an orientation for each fiber randomly, fibers keep growing until reaching given porosity of the system (Wang et al., 2007a). The morphology of simulating natural fibrous materials can be seen in Fig. 2-3. In 2005, Faessel et al. (Faessel et al., 2005) considered a 3D probabilistic random model, and the fibers are generated in a unit cell within a periodic elementary volume. Based on image analysis and X-ray tomography, the structural information about the fibrous system, such as fiber length, fiber diameter, curvature, orientation and position, can be easily extracted from the statistical distribution of the morphological properties of real fabrics (Faessel et al., 2005).

(a) 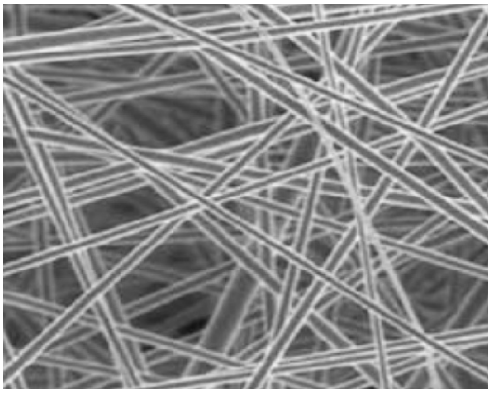 (b) 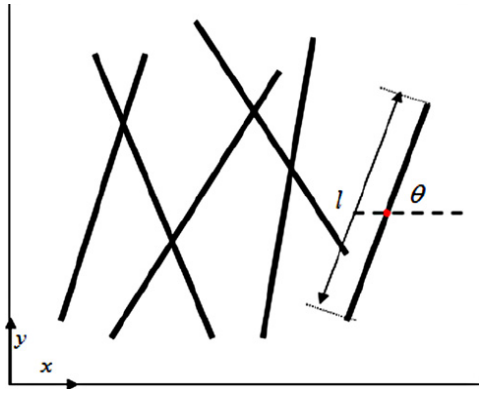

Figure 2-3: (a) Structure of a fibrous medium under SEM; (b) schematic illustration of grown fibers and parameters, with core position of fiber (red point), fiber length l, and fiber orientation θ (Wang et al., 2007a)

Table 2-3: Summary of numerical studies of permeabilities of nonwoven fibrous materials

Authors	Remarks
(Sangani and Acrivos, 1982)	• 1D flow transverse/parallel with square array • Multipole Expansion Method

(Higdon and Ford, 1996)	• 3D flow through ordered cell • Boundary Element Method
(Clague and Phillips, 1997)	• 3D flow through random structure • Slender Body Method
(Spaid and Phelan, 1997)	• 1D flow through hexagonal array • Lattice Boltzmann Method • Studied fiber cross-sectional shape
(Koponen et al., 1998)	• 2D flow through random layer • Lattice Boltzmann Method • Provided an exponent model
(Papathanasiou, 2001)	• 1D flow through ordered array • Finite Element Method • Provided an empirical model
(Sobera and Kleijn, 2006)	• 1D flow through one-layer random array • Finite Volume Method • Studied randomness of fiber distribution
(Tahir and Tafreshi, 2009)	• 2D/3D flow through random structure • Finite Volume Method • Studied fiber orientation
(Nabovati et al., 2009)	• 2D/3D flow through random structure • Lattice Boltzmann Method • Studied curvature and aspect ratio of fiber
(Hosseini and Tafreshi, 2010)	• 3D flow through random structure • Fluent • Studied slip flow
(Yazdchi et al., 2011)	• 1D flow transverse to 1D square array • Finite Element Method

	• Studied aspect ratio of fiber axis distance

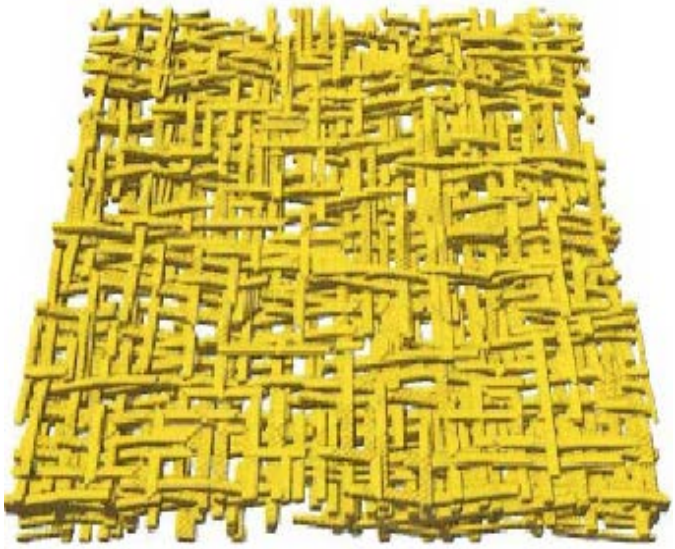

Figure 2-4: A numerical 2D fiber-web sample (Koponen et al., 1998)

The numerical studies on the flow through fibrous media are summarized in Table 2-3. Numerical simulation methods were also applied to more complex and realistic fibrous materials, covering a class of porosity ranges and fiber distribution from 1D to 3D structures. Viscous flow through ordered cylinders was numerically simulated based on different techniques (Sangani and Acrivos, 1982, Papathanasiou, 2001). In 1996, Higdon and Ford (Higdon and Ford, 1996) employed the Spectral Boundary Element Method to calculate the hydraulic permeability of 3D ordered fibrous media, including simple cubic, body centered cubic, and face-centered cubic fiber arrangements. Later, 3D randomly distributed monodisperse and polydisperse fibers were first investigated by using the Slender Body Theory (Clague and Phillips, 1997). Steady transverse flow through elliptical fiber array was investigated by the Lattice Boltzmann Method, demonstrating that the hydraulic permeability was not sensitive with a cross-sectional shape when the axis ratio was small (Spaid and Phelan, 1997). Later, Koponen et al. (Koponen et al., 1998) conducted Lattice

Boltzmann numerical simulations for layered structures (see Fig. 2-4), and they found that the overall permeability was dependent on porosity exponentially throughout a large range of porosities. To verify their scaling estimate model, Sobera and Kleijn (Sobera and Kleijn, 2006) applied Finite Volume Method to calculate the permeability of 1D and 2D ordered and random distributed cylindrical fibers, indicating that the overall permeability increases monotonously with the degree of randomness.

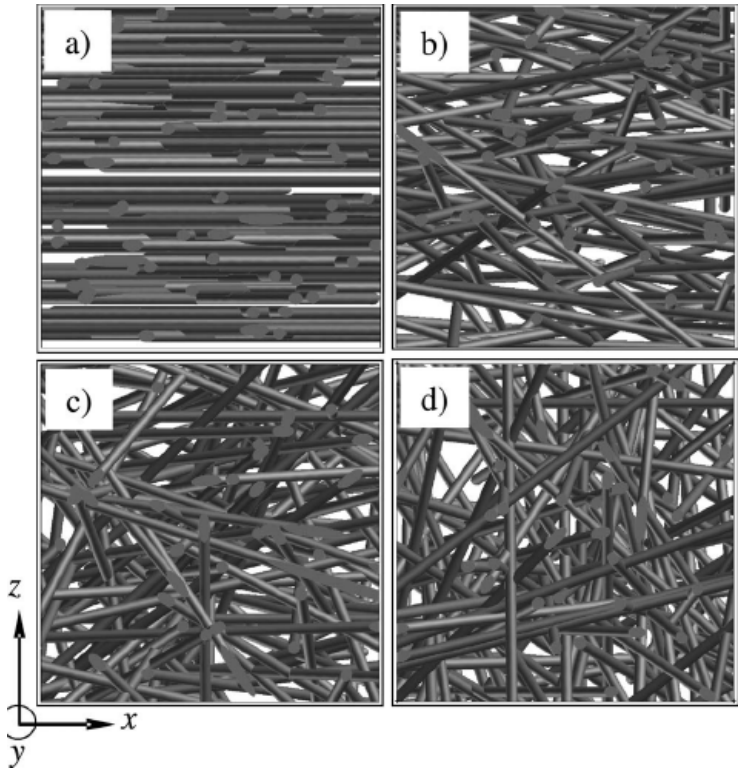

Figure 2-5: Examples of fibrous media with varying orientation distribution of fibers as (a) layered, (b) low through-thickness anisotropic, (c) moderate through-thickness anisotropic and (d) isotropic (Tahir and Tafreshi, 2009)

Recently, Stylianopoulos et al. (Stylianopoulos et al., 2008) modeled the permeability of fibrous media in terms of 3D artificial random networks using the Finite Element Method, and it was the first attempt to specifically examine the effect

of fiber orientation. It is showed that the highly aligned fibrous media are more permeable than moderately aligned ones when flow moves parallel to their preferred orientation, while the permeabilities of isotropic system and moderately or highly aligned ones are comparable with each other when they are perpendicular to the flow direction (Stylianopoulos et al., 2008). In 2009, Tahir and Tafreshi (Tahir and Tafreshi, 2009) studied the transverse permeability of fibrous systems and continued to evaluate the influence of fiber orientation (see fibers with different orientation in Fig. 2-5). They found that the permeability of fibrous media is in a positive relationship with the through-plane orientation of fibers, but is almost independent of the in-plane orientation.

In 2009, Nabovati et al (Nabovati et al., 2009) presented a semi-empirical model to predict the permeability of 3D random fibrous matrixes based on Lattice Boltzmann Method. In addition, they found that both of the fiber curvature and the aspect ratio of long fibers negligibly affected the permeability of fibrous media. Later, the permeability was found to decrease with the aspect ratio of fiber axis distance between along and normal to the flow direction, as shown from their Finite Element simulation (Yazdchi et al., 2011). In 2010, Hosseini and Tafreshi (Hosseini and Tafreshi, 2010) numerically studied the slip flow through 3D nano-fibrous media, and adopted the Maxwell first order approximation to describe the slip condition on the fibers. The simulation results reveal that the gas permeability in nano-fibrous media with slip effect is larger than the conventional models for coarse fibers.

2.2. Effective permeability of woven fibrous media

Based on the structural integrity and fiber architecture, woven fabrics can be generally classified into four patterns: discrete (staple fiber), continuous (filament yarn), planar interlaced (2D), and fully integrated (3D) structures (AMSC and

CMPS, 2002). It is reported that the structure of woven fabrics is always too complex to be precisely described mathematically (Nabovati et al., 2010). Good review of woven structural arrangement is available (Hearle et al., 1969). Among them, the plain bi-axial weave pattern is one of the most widely used patterns for textile woven fabrics and RTM performs (Nabovati et al., 2010).

One of the most unique features of woven fabrics is their fiber reinforcement interlaced and interloped in an ordered form, while nonwoven is in a more freely layered pattern. Another feature is that many woven performs are often made up of bundles of filaments, known as yarn. Those woven fabrics have two different length scales: radius of yarns and radius of filament. The yarn radius is about orders of magnitude larger than the filament radius. As a result, their transport properties become more difficult to formulate than single-scale fibrous materials, and numerical simulations are therefore widely adopted.

2.2.1. Monofilament

The geometric structure of different types of woven fabrics is difficult to formulate through mathematical descriptions. For computational purposes, the structure of woven fabric is generally approximated in a simple form of a periodic 2D or 3D representative cell (Nabovati et al., 2010). The plain bi-axial weave pattern, which is known as the most widely applied woven fabrics and will be studied in this project (Nabovati et al., 2010), is reconstructed in Fig 2-6. The fabric is composed of perpendicular yarns aligned along the x and y axes, which are interwoven to form a planar fabric sheet in the x-y plane.

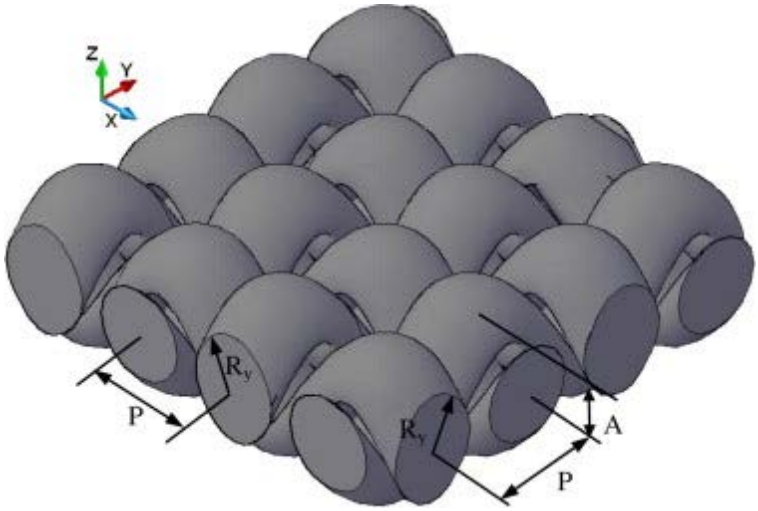

Figure 2-6: Schematic of the bi-axial plain woven fabric (Nabovati et al., 2010).

Pore-based models were always used to describe fluid flow through monofilament fabrics (Xu and Wang, 2005). However, the thickness of the fabric layer is roughly the same order of the yarn radius, which is not suitable for Hagen-Poiseuille law as used to describe the viscous flow through long tubes (Järvinen, 2007). In addition, the through-thickness pore between woven yarns is generally venture-shaped, which adds the difficulty in permeability determination.

The flow through monofilament woven fabrics was determined by the so-called orifice analogy (Armour and Cannon, 1968). In the orifice model, the open pores inside the woven fabrics were treated as a series of submerged orifices, and a discharge coefficient was used to characterize the pore size variation (Armour and Cannon, 1968). In 1996, a modified discharge coefficient in orifice model was presented, based on numerical simulations by Fluent (Lu et al., 1996). Lu et al. (Lu et al., 1996) studied four basic types of plain-weave fabrics: fours yarns alternate from top to bottom vice versa; one warp and one weft alternate; two warp or weft yarns alternate; no yarns alternate. Gooijer et al. (Gooijer et al., 2003) continued the

study of the four woven structures of Lu et al. (Lu et al., 1996). They explored the relationship between the flow resistance and the woven structure by simplifying the discharge coefficient, and the prediction of the orifice model was in closely agreement with the experimental results. Recently, yarns with elliptical cross-sectional shape were studied numerically and the discharge coefficient was modified accordingly (Wang et al., 2007b). The through-thickness permeability was found to increase inversely with the aspect ratio (i.e. semi-major axis vs. semi-minor axis) when the semi-major axis was normal to flow direction. The studies of permeabilites of monofilament woven fabrics are summarized in Table 2-4.

Table 2-4: Studies of permeabilites of monofilament woven fabrics

Authors	Remarks
(Armour and Cannon, 1968)	• 3D flow through monofilament woven • Orifice analogy
(Lu et al., 1996)	• 3D flow through monofilament woven • Orifice analogy and finite volume method • Studied four typical woven fabrics
(Gooijer et al., 2003)	• 3D flow through monofilament woven • Modified orifice analogy
(Xu and Wang, 2005)	• 3D flow through monofilament woven • Haggen-Poisuile law
(Wang et al., 2007b)	• 3D flow through monofilament woven • Fluent • Studied yarn cross-sectional shape

2.2.2. Multifilament

Characterizing fluid flow in multifilament woven fabrics is a challenging work

considering its dual-scale nature. Early studies on this problem were focused on 1D flow through fibrous media rather than realistic 3D case. In 1997, a numerical study of permeability for square arrays of multifilament yarns was conducted by Boundary Element Method (Papathanasiou, 1997). The yarns were circular and the intra-yarn flow was found to have positive effect on the overall permeability of the system. Elliptical yarns for hexagonal and square packing were investigated numerically by a computational fluid dynamics package (Phelan and Wise, 1996, Ranganathan et al., 1996) and Lattice Boltzmann Method (Spaid and Phelan, 1997). It was found that the overall permeability is not sensitive with cross-sectional shape of yarns when weave porosity is high, but increases with the axis ratio between the semi-major axis and the semi-minor axis of the elliptical yarn when fluid flows were parallel with the semi-major axis. Later, in order to express the numerical results in a predictable form, Papathanasiou (Papathanasiou, 2001) proposed a semi-analytical correlation of effective permeability for hexagonal packing configuration based on a great number of numerical values. The correlation is a function of inter-yarn and intra-yarn yarn permeabilities (Papathanasiou, 2001):

$$K_{eff} = K_{inter}\left[1+2.67\left(K_{inter}/K_{intra}\right)^{-0.89}\right], \tag{2-10}$$

where K_{eff} is the effective permeability of the multifilament fabric, K_{inter} is the weave permeability (i.e. the permeability of the fibrous system by assuming that the yarns are impermeably solid), K_{intra} is the permeability of the yarns. This relationship reveals the effects of inter-yarn permeability and intra-yarn permeability on the overall permeability of the fibrous system.

In 2006, Stokes flow was simulated simultaneously in both intra- and inter yarn areas by Wang et al. (Wang et al., 2006), and the overall permeability was calculated

by substituting back the ratio of pressure gradient and flow flux into Darcy's law. However, calculations of flows in the complex dual-scale structures are always time-consuming and computationally expensive (Nabovati et al., 2010). To reduce computational cost, some other researchers applied Stokes equation to compute the flow in the inter-yarn region of woven fabric, but applied Darcy's law to directly describe the micro-scale flow inside the yarns (Grujicic et al., 2004). Continuum of velocity field at the interface layer between inter-yarn and intra-yarn regions is satisfied, but it is difficult to address the shear stress continuum due to incompatible differential operators between second-order Stokes equation and first-order Darcy's law (Chen et al., 2010).

In another approach, Brinkman equation, of the same order as Stokes equation, was employed to describe the intra-yarn flow rather than Darcy's law. In 2000, Yu and Lee (Yu and Lee, 2000) developed an in-plane permeability model for woven fabric, in which 1D Brinkman equation and 1D Stokes equation were used to describe intra-yarn and inter-yarn flows, respectively, based on the rectangular unit cell. The predicted permeabilities were validated by experimental results and were found to be insensitive with microstructures of porous yarns. In the numerical models (Ranganathan et al., 1996, Phelan and Wise, 1996, Ngo and Tamma, 2001), Stokes equation was calculated in inter-yarn space and Brinkman equation was solved in intra-yarn region by powerful computational solvers. Song et al. (Song et al., 2004) used a control volume finite element method to predict the permeability tensor of woven fabrics, where the intra-yarn structure was assumed to be in the form of either square or hexagonal arrays of solid circular cylinders. The weave and yarn flow fields were computed separately, and the effect of the filament packing on the overall permeability was found to be small (Song et al., 2004). Experimental results were also obtained for the in-plane and out-of-plane permeability of plain woven fabrics and were found in good agreement with the simulated values (Song et

al., 2004). Tung et al. (Tung et al., 2002) employed the finite volume method for fluid flow simulation in the same basic weave geometries with Lu et al.'s (Lu et al., 1996), but replaced the solid yarns with the permeable yarns.

In 2006, a theoretical analysis was developed to characterize both inter-yarn permeability and intra-yarn permeability, and concluded that the two permeability values decide the time scales of resin impregnation between yarns and filaments (Zhou et al., 2006). In addition, the partially-saturated region was found to be a constant when the mold is sufficiently long (Zhou et al., 2006). Later, Song et al. (Song et al., 2009) studied the layer effect on transverse permeability of woven fabrics by a statistical analysis, and found that the mean permeability decreased with increasing number of fabric layers. The studies of permeabilites of multifilament woven fabrics are summarized in Fig. 2-5.

Table 2-5: Studies of permeabilites of multifilament woven fabrics

Authors	Remarks
(Ranganathan et al., 1996)	• 1D flow transverse to hexagonal array • Computational fluid dynamics package • Studied effects of intra-yarn permeability and fiber cross-sectional shape
(Phelan and Wise, 1996)	• 1D flow transverse to square array • Computational fluid dynamics package • Studied effects of intra-yarn permeability and fiber cross-sectional shape
(Papathanasiou, 1997)	• 1D flow transverse to square array • Boundary Integral Method • Studied intra-yarn porosity effect

(Spaid and Phelan, 1997)	• 1D flow transverse to square array • Lattice Boltzmann Method • Studied intra-yarn permeability effect and yarn shape
(Papathanasiou, 2001)	• 1D flow transverse to ordered array • Boundary Element Mmethod • Provides a semi-analytical correction
(Tung et al., 2002)	• 3D flow through plain fabric • Fluent • Studied four types of basic woven fabric
(Song et al., 2004)	• 3D flow through braided preforms • Finite Volume Method • Solved Brinkman equation in intra-yarn area
(Wang et al., 2006)	• 3D flow through woven filter • Fluent • Simulated flow in inter- and intra-yarns simultaneously
(Zhou et al., 2006)	• 1D flow transverse to ordered array • Studied effect of intra-yarn permeability on saturated flow length
(Song et al., 2009)	• 3D flow through layered preforms • Studied layer number effect
(Nabovati et al., 2010)	• 3D flow through multifilament woven • Lattice Boltzmann method • Provided a semi-analytical correction

2.2.3. Past experimental work

The process of measuring hydraulic permeability of woven fabrics is the same as that for nonwoven fabrics based on Darcy's law. For example, Sadiq et al. (Sadiq et al., 1995) studied transverse flow through an array of square-packed yarns with circular cross sections. These yarns were constructed by combining many solid cylindrical nylon fibers with finer radius.

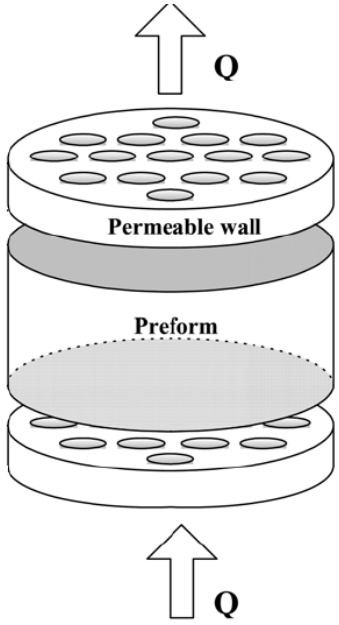

Figure 2-7: Permeable wall and preform employed for measurement of transverse permeability

Transverse permeability was always experimentally determined based on channel flow through a circular tube (Chae et al., 2007), as seen in Fig. 2-7. The main difference from previous experiment is that the circular tube contains thicker permeable compression plates, which provides an opportunity to measure the bulk and edge flow separately. The parallel circular channels in the compression loads also ensure a unidirectional fluid flows and make it possible to observe the edge effect directly (Chae et al., 2007).

Figure 2-8: Woven fabric tape

In 2007, a modified method was presented to measure transverse permeability of fibrous media by a translation of an in-plane measurement approach based on the radial technology (Wu et al., 2007). The main difference is the layout of the fiber reinforcement location comparing with other conventional experimental methods. The fiber layers were wound and placed on a mold (see Fig. 2-8), and the radical fluid flows entered into the fiber reinforcement composite along the through-plane direction. The new approach made it easy to visually observe the flow trace (Wu et al., 2007).

2.3. Effective diffusivity of fibrous materials

Effective diffusion of porous media is one of the most common and important transport phenomena encountered in natural processes and engineering applications. Understanding and prediction of effective diffusivity in fibrous materials are therefore very critical. In this part, the previous work on vapor diffusion in fibrous materials is reviewed from 1D simple to 2D and 3D complex structures.

2.3.1. Effective diffusivity of 1D fibers

A pore-scale model was applied to predict the effective diffusivity of unconsolidated 1D rectangular fibers (du Plessis et al., 2010). The tortuosity was expressed as the ratio of the diffusive path length to the streamwise displacement. However, the regular geometry of the diffusive streamlines in the pore-scale model differed from the actual concentration lines with curved shape by numerical simulations from Wang's (Wang, 2000).

Besides, Shen and Springer (Shen and Springer, 1981) calculated the diffusion equation through 1D impermeable cylinders with square packing configuration, and the model of effective diffusivity is expressed as follows:

$$\frac{D_{eff}}{D_b} = 1 - 2\sqrt{\frac{1-\varepsilon}{\pi}}, \tag{2-11}$$

which was widely applied to evaluate the influence of water vapor diffusion on the mechanical properties of composites (Li et al., 2002). Nevertheless, this model implied that the moisture vapor diffusion only move past the shadowed rectangular with the cross-section equal to the minimum gap between cylinders, which leads to under-estimating the effective diffusivity (Ogi and Takeda, 1997).

In 2002, Li et al. (Li et al., 2002) proposed an analytical model to describe gas diffusion of cylindrical system with both rectangular and hexagonal arrays arrangement. They assumed that gas diffusion traveled only in the voids between the solid fibers, and gas concentration at the every cross-section along the diffusion direction was uniform (Li et al., 2002). The fluid region was broken into zones in the cells repeating through the system, and diffusion equations were solved within them. The model was relied solely on porosity and structural geometry. Unfortunately,

their predicted effective gas diffusivity was smaller than previous experimental and numerical results for high porous media. Nilsson and Stenstrom (Nilsson and Stenstrom, 1995) also applied the unit cell method to represent the fibrous system, and obtained diffusivity model in terms of volume fraction of fibers by solving Laplace equation. It was further found that effective diffusivity is highly sensitive to the gap height between fibers at low porosity limit, but it varies less significantly with increasing porosity (Nilsson and Stenstrom, 1995).

2.3.2. Effective diffusivity of 2D and 3D fibers

For 2D and 3D fibrous materials, they are always assumed to consist of a bundle of tortuous channels, so the effective diffusivity can be related to the bulk diffusivity through porosity and tortuosity, given by a dimensionless form (Tomadakis and Sotirchos, 1993b):

$$\frac{D_{eff}}{D_b} = \frac{\varepsilon}{\tau}, \tag{2-12}$$

where D_b is the bulk diffusivity in the void, ε is the porosity, and τ is the tortuosity. Although the fiber volume fraction or porosity is easy to estimate or measure, the application of Eq. (2-12) is tarnished by the difficulty in accurately determining the value of tortuosity (Ahmadi et al., 2011).

It is almost impossible to solve transport equations though randomly distributed 1D fiber arrays and 2D or 3D performs. Thus, in order to model the diffusion through those realistic structures, a number of researchers turned to numerical techniques. Tomadakis and Sotirchos (Tomadakis and Sotirchos, 1993b) performed random-walk molecules simulations for 1D, 2D and 3D randomly positioned fibers. They measured the mean travelling distances of diffusive molecular inside the numerical

fibrous perform, and proposed the following semi-analytical model of effective diffusivity for randomly oriented fibrous systems (Tomadakis and Sotirchos, 1993b):

$$\frac{D_{eff}}{D_b} = \varepsilon \left(\frac{\varepsilon - \varepsilon_p}{1 - \varepsilon_p} \right)^c , \tag{2-13}$$

where, the parameters of the above equation c and ε_p were based on a least squares fit to the simulated results.

In another numerical study, the local effective gas diffusivity of a GDL medium was determined as a function of the local porosity and the local water saturation by a network model, where the solid structure was simulated as layers of continuously fiber screens and each layer was shifted by a randomly selected distances in plane (Nam and Kaviany, 2003). In 2008, Becker et al. (Becker et al., 2008) reconstructed an artificial fibrous structure numerically based on the structural information from a 3D tomography image of the GDL and proposed the model of effective gas diffusivity as a function of saturation coefficient of the GDL. Later in 2011, Becker et al. (Becker et al., 2011) extended their work to consider the effect of micro-porous layer coating (MPL). A class of numerical simulation schemes were also conducted in this field (Gostick et al., 2007, AlvarezRamirez et al., 1996, Hao and Cheng, 2009, Wang et al., 2010). In the PEMFC literature, the Bruggeman model was widely applied (Zamel et al., 2009), which is given by:

$$\frac{D_{eff}}{D_b} = \varepsilon^{1.5}. \tag{2-14}$$

However, Bruggeman diffusion model was derived for uniformly packed spherical particles rather than the differently oriented cylindrical fibers used in PEMFC.

What mentioned above are all about gas diffusion in ordinary regime, where the pore size of the fibrous medium is much larger than the mean free path λ of diffusive molecules and the repeated molecule-molecule collisions are dominate. When pore size is comparable with or smaller than λ, molecule-wall collisions increase and Knudsen diffusion occurs, which hinders molecule diffusion in small pore (Clifford and Hillel, 1986). In this regime, the equivalent diffusivity D_{equ} can be described by Bosanquet equation (Bosanquet, 1944):

$$D_{equ} = \left(\frac{1}{D_b} + \frac{1}{D_{Kn}} \right)^{-1}, \tag{2-15}$$

where $\mathrm{Kn} = \lambda / \langle d \rangle$ is Knudsen number, $\langle d \rangle$ is the average pore diameter, and D_{Kn} is Knudsen diffusivity. The value of D_b is given by kinetic theory as $D_b = \lambda u / 3$ when Kn<<1 in ordinary regime, and D_{Kn} is expressed as $D_{Kn} = \langle d \rangle u / 3$ when Kn>>1, where u is the mean molecular velocity (Zalc et al., 2004). From Eq. (2-15), the ordinary diffusivity is found to be a constant, while the Knudsen effect would prevents the passage of diffusive molecules when the pore size becomes in Knudsen regime. When $\mathrm{Kn} \sim 1$, the transition diffusivity D_{Tr} is equal to $\left(\frac{1}{D_b} + \frac{1}{D_{Kn}} \right)^{-1}$.

Eq. (2-15) shows that gas diffusion mechanisms are dependent on pore size. In many cases, the three types of diffusivities co-exist in a porous medium with a wide pore size distribution. The effective diffusivity is given by a composite form (Houst and Wittmann, 1994):

$$D_{eff}\varepsilon = \varepsilon_1 D_b + \varepsilon_2 D_{Tr} + \varepsilon_3 D_{Kn}, \quad (2\text{-}16)$$

where ε_1, ε_2, and ε_3 are the porosities in ordinary regime, transition regime, and Knudsen regime, separately. It is more accurate to consider the pore size distribution, but the porosities in different regimes are considerably difficult to measure.

In 2002, Mezedur et al. (Mezedur et al., 2002) proposed a 2D network model to investigate the effect of pore size, structure and randomness on the effective diffusivity of catalytic porous coatings. The model takes the variation of the lattice randomness to account for randomness effect of fiber distribution, and demonstrates that higher degree of randomness leads to lower effective mass diffusivity.

In 2008, Mu et al. (Mu et al., 2008) proposed a 3D pore network model to determine effective diffusion coefficient in fibrous porous system where Knudsen diffusion took place. Their model reveals that the pore size distribution accounts for the Knudsen effect decoupled in bulk diffusivity, and thus the effective diffusivity is strongly dependent on pore size (Mu et al., 2008).

2.3.3. Past experiment work

As the most reliable method, experimental measurement is often conducted to determine the effective vapor diffusivity of fibrous materials, by calculating the diffusive flux against the directional concentration gradient. Early in 1940, through-plane diffusion coefficient of a steel wool sample was measured using carbon disulfide and acetone vapor (Penman, 1940). In 1984, Bateman at al. (Bateman et al., 1984) employed NO gas to transfer through a 2D cellulosic filter and calculated its effective diffusivity. Recently, Gibson et al. (Gibson et al., 2001) applied a dynamic diffusion test cell method to measure vapor diffusivity of fibrous

media. Two parallel gas flows with different water vapor humidity were inputs of a test cell, where vapor diffused through the sample between the gas flows, and the effective diffusivity was obtained by measuring the relative humidity of gas flows leaving the cell. Huang and Qian (Huang and Qian, 2007) modified the dynamic cell method by directly using a water vapor source on one side of the sample instead of one entered gas flow used by Gibson et al. (Gibson et al., 2001). The evaporative moisture vapor resistance, which inversely demonstrates the ability of diffusion, was determined by measuring evaporative heat loss from the water evaporation (Chen et al., 2004, Fan and Chen, 2002). In 2011, LaManna and Kandlikar measured effective water vapor diffusion coefficient of GDLs considering the effect of microporous layer (MPL) coatings, GDL thickness, and polytetrafluorethylene (PTFE) loadings via the ex situ dynamic diffusion cell. However, the number of different kinds of potential fibrous samples throughout the range of porosity is very large, and the current experimental measurements are still complex and time-consuming.

2.4. Coupled heat and mass transfer in fibrous materials

In some applications of fibrous materials such as clothing and fuel cell, gas flow and vapor diffusion are coupled with heat transfer. For instance, the processes of heat and moisture transfer dynamically interact with each other in terms of moisture absorption/desorption and evaporation/condensation in clothing systems (Pan and Gibson, 2006). Heat transfer takes place through conduction in all of the phases, through radiation in the highly porous media, and through convection caused by moist air flow; moisture transfer occurs though diffusion, convection, absorption/desorption between the solid fiber and the surrounding air, and movement of condensed water (Pan and Gibson, 2006). The moisture absorption/desorption and phase change within the textile materials absorb or release heat, which further add

complexities of heat and moisture transfer.

A mathematical model was reported to describe coupled heat and moisture transfer in porous textiles (Henry, 1939), which is expressed in two equations:

$$\varepsilon \frac{\partial C_a}{\partial t} = \frac{D_a \varepsilon}{\tau} \frac{\partial C_a^2}{\partial x^2} - (1-\varepsilon)\Gamma_f, \tag{2-17}$$

$$C_v \frac{\partial T}{\partial t} = k_{fab} \frac{\partial T^2}{\partial x^2} + (1-\varepsilon)\lambda_v \Gamma_f, \tag{2-18}$$

where C_a is air density, C_v is vapor density, k_{fab} is thermal conductivity of fabric, Γ_f is moisture (de)sorption rate, and λ_v is heat of (de)sorption. The following assumptions were made: the local instantaneous temperature between fiber and moisture is in equilibrium; the concentration absorbed by fiber is promotional to local moisture vapor concentration; and the fiber volume is unaffected by moisture sorption (Henry, 1939). Henry's work established a basic framework to describe coupled heat and moisture transfer in textiles and other fibrous materials.

Later, the researchers considered more influencing factors. Motakef and Elmasri (Motakef and Elmasri, 1986) first modeled the transient heat and moisture transfer with condensation. Tao et al. (Tao et al., 1991) analyzed the frosting effect in an insulation slab with temperature below the triple point of water. Gibson and Charmchi (Gibson and Charmchi, 1997) developed a theoretical model by considering the effect of liquid water transport and accumulation, and flow convection. Fan et al. (Fan et al., 2000) considered the effect of water content on the effective thermal conductivity fibrous batting, and they also took radiative heat transfer into account. Li and Zhu (Li and Zhu, 2003) reported a new model to describe the coupled heat and moisture transfer with the additional condition of liquid diffusion, which was described as a diffusion process caused by the capillary

effect. Zhu et al. (Zhu et al., 2010) established a numerical model to simulate the coupled heat and liquid moisture transfer in hygroscopic fibrous media.

Most of the models are based on 1D partial differential equation and assume the fibrous system homogeneous and isotropic, although the recent researchers consider more and more affecting factors. Therefore, lack of microstructure information of fibrous media in 3D space exists in previous models, which may influence their accuracy and applicability.

2.5. Remaining problems

Experimental measurements are the final proofs, but time-consuming; numerical simulations, as computational experiments, cannot fully reveal the underlining mechanisms; analytical models are predictive, but sometimes may not be possible for complex structures. Therefore, different research methods should be integrated together in order to take the advantages of each of them. By and large, a predictive model is usually welcome, and this thesis will focus on theoretical modeling and validation of the models based on results from experiments and simulations.

Many theoretical studies have been conducted to study the transport properties of fibrous materials of 1D regularly structured array. However, the obtained models are based on over-idealized assumptions. With the increasingly development of computational techniques, it is feasible to model or reconstruct more complex and real fibrous media, and solve the transport equations by the powerful numerical solvers. Nevertheless, numerical simulations still cannot fully reveal the structural effects on transport mechanisms, especially in complicated nano- and micro-fibrous media. To sum up, four research gaps are identified from previous studies:

1. Incomprehensive models exist for transport properties of fibrous media. The

theoretical models of both permeability and diffusivity for realistic 2D and 3D fibrous structures are required, as the majority of past work is based on 1D assumption with over simplification.

2. The influences of different structural factors on transport properties of fibrous media have not been integrated systematically and therefore call for better understanding, as most of past studies tend to determine the resulting permeability or diffusivity rather than analyzing affecting parameters.

3. There is a lack of theoretical models to address the dual-scale effects in fibrous materials made up of permeable yarns. Numerical simulations are able to determine dual-scale permeability, but they are unable to illustrate clearly the analytical relationship between microstructures and gas permeability of fibrous media.

4. Few analytical studies are available for modeling transport behaviors in nano-scale fibrous media. Most studies are based on numerical simulations, which cannot provide a scale-dependent relationship between transport properties and microstructures of nanofibers.

Chapter 3 Deterministic models for flow through single-scale fibrous media

3.1. Introduction

Hydraulic permeability is one of the most important measures of characterizing transport phenomena in porous media. Although numerous studies have been conducted on this topic, accurate determination of hydraulic permeability taking into account of realistic and complicated structural influences of fibrous media remains challenging.

The early analytical solutions could be mostly found based on 1D array of ordered fibers (Happel, 1959, Kuwabara, 1959). In 1988, numerical results were obtained for the hydraulic permeability of 1D array of fibers towards normal and parallel flows (Sangani and Yao, 1988), but the accuracy of their results was limited by the computer power at that time. Higdon and Ford (Higdon and Ford, 1996) conducted a numerical simulation of calculating hydraulic permeability of 3D networks of fibers on regular cubic lattices by spectral boundary element formulation. Koponen et al. (Koponen et al., 1998) applied Lattice Boltzmann method to simulate flow in 2D randomly fibrous layers across a wide range of porosities and developed a semi-empirical model. Sobera and Kleijn (Sobera and Kleijn, 2006) determined hydraulic permeability of both orderly and disorderly 1D and 2D fibrous performs based on a modified scaling estimate rule, which was originally suggested by Clague (Clague et al., 2000). Recently, Tahir and Tafreshi

(Tahir and Tafreshi, 2009) solved Stokes equation in virtual fibrous media using finite volume method and found the transverse hydraulic permeability was almost not affected by in-plane fiber orientation, but increased with increasing through-plane fiber orientation.

From the above studies, it is clear that the theoretical studies are limited in the systems of ordered fiber arrays, and few analytical attempts try to link hydraulic permeability with the complex 2D and 3D geometry of fibrous media. The numerical studies can reconstruct the complex microstructures and determine the resulting permeability, but little theoretical analysis has been carried out so far to examine the influences of geometric structural factors. This is also becoming more of an important issue, thanks to the wide application of nanofiber and microfiber materials, for which the effect of slip flow should be addressed. Therefore, the current study is aimed at improving understanding of roles of different geometric formation factors including slip effect in gas flow through nano- and micro-fibrous materials.

In this chapter, viscous fluids though fibrous materials at high porosity and low porosity are studied respectively by deterministic method. All the models are compared with experimental and numerical results, and the influencing factors of microstructures are extensively analyzed. Finally, all the results are summarized in concluding remarks.

3.2. Fibrous structures with high porosity

In this part, permeability predictions of high porous fibrous media are conducted, from simple and ordered to complicated and random structures step by step. First, representative cell as a circular is used to describe the transport properties of 1D ordered fiber arrays, considering slip flow on the fiber surface. Second, Voronoi

Tessellation Method, which illustrates randomness of fiber location, is employed to determine the hydraulic permeability for randomly distributed fibers. Finally, a reasonable mixing rule is used to extend the 1D model to 2D and 3D structures. The calculation process can be illustrated from the construction of 3D or 2D fibrous materials from 1D fiber array, as shown in Fig. 3-1.

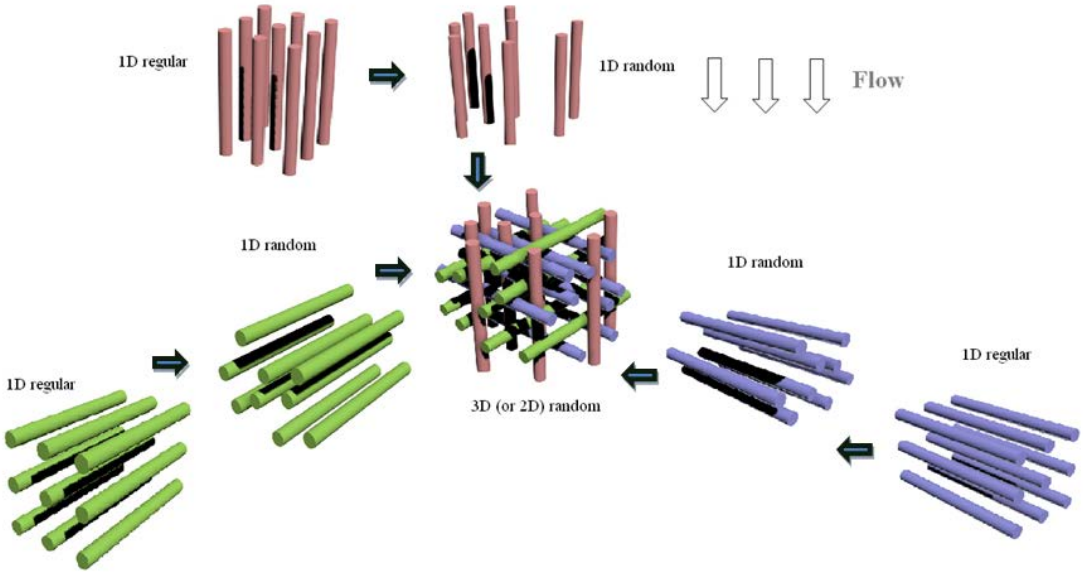

Figure 3-1: Illustration of 3D or 2D fibrous media as mixtures of 1D fiber arrays

3.2.1. 1D Ordered structures

A fibrous medium is assumed to be composed of periodical unit cells, which represent the geometric knowledge of the microstructure of the medium. The representative cell for 1D regular array of aligned fibers is shown in Fig. 3-2. With proper definitions of boundary conditions of the cell, an approximate solution is available by solving Stokes equation.

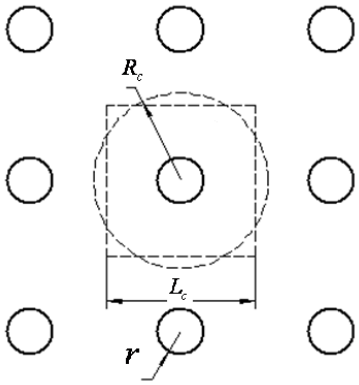

Figure 3-2: A unit cell in regular array of parallel fibers. The dotted circle is the unit cell with the same area as the square in dotted line.

Under the condition of low Reynolds number, the steady flow through the representative unit cell can be governed by Stokes equation:

$$-\nabla p + \mu \nabla^2 u = 0. \tag{3-1}$$

Derivation of Eq. (3-1) leads to Biharmonic equation in terms of stream function:

$$\nabla^4 \psi = 0, \tag{3-2}$$

where ψ is the stream function using cylindrical coordinates (l, θ) with velocity components (u_l, u_θ) as:

$$u_l = \frac{1}{l}\frac{\partial \psi}{\partial \theta}, u_\theta = -\frac{\partial \psi}{\partial l}. \tag{3-3}$$

On the fiber surface, the normal component of velocity vanishes, viz.:

$$\frac{1}{l}\frac{\partial \psi}{\partial \theta} = 0 \quad \text{for} \quad l = r. \tag{3-4}$$

Superfine fibers are fueling great interest in many fields and thus are particularly investigated in this work. The non-slip assumption is not strictly correct when fiber radius is comparable to the mean free path of fluid molecules (Huang et al., 2007). The slip flow, viz. the normal component of velocity is zero while the tangential velocity does not vanish, is therefore permitted to occur on the surface of the fibers (Huang et al., 2007). Note that rarefaction may also be a possibility of slip flow in micro porous system rather than in nano-scale regime, where mean free path of fluid molecules becomes much larger. It is found that Reynolds number Re, Mach number Ma and Knudsen number Kn satisfy the relationship: $\mathrm{Ma}/\left(\mathrm{Re}\cdot\mathrm{Kn}\right) \approx 0.05$ (Morini et al., 2004). In this work, viscous flow through nano- and micro-fibrous materials makes $\mathrm{Re} << 1$ and $\mathrm{Kn} < 1$, and thus it can be concluded that $\mathrm{Ma} << 0.05$, which is much lower than the threshold (i.e. 0.3) of gas compression and rarefaction (Anderson, 2001). Thus, the effect of compressibility and rarefaction of gas flow can be generally neglected in this study. For the flow around a fiber, the tangential velocity is proportional to the tangential stress when partial slip occurs, and the first-order slip boundary condition is applied (Brown, 1993):

$$u_s = \lambda \frac{\partial u}{\partial n}, \tag{3-5}$$

where u_s is the slip tangential velocity on the surface of fibers, and n corresponds to the normal direction of fiber surface. Since the Kn is defined as $\mathrm{Kn} = \lambda / r$, where λ is mean free path of air molecules and is also defined as the slip coefficient, the slip tangential velocity can be therefore expressed as:

$$u_s = \mathrm{Kn}\frac{\partial u}{\partial n} r. \tag{3-6}$$

According to Eq. (3-6), the slip tangential velocity around the fiber surface can be calculated as

$$\frac{\partial \psi}{\partial l} = r\mathrm{Kn} l \frac{\partial}{\partial l}\left(\frac{1}{l}\frac{\partial \psi}{\partial l}\right) \quad \text{for} \quad l = r. \tag{3-7}$$

For convenience and without losing generality, the unit cell can be assumed to be a square with an edge length L_c. The porosity ε for this arrangement of, both the unit cell and the whole fibrous media are determined by

$$\varepsilon = 1 - \frac{\pi r^2}{L_c^2}. \tag{3-8}$$

Consider an imaginary circular cell, which is coaxial with the given fiber and has the same area as that of the square cell as shown in Fig. 3-1. The circular cell is assumed to share the same permeability with the square and the whole system considering the fibrous media as homogeneity. The radius of the imaginary circular cell is $R_c = \frac{r}{\sqrt{1-\varepsilon}}$. For the continuous flow on the surface of the circular cell, its velocity is equal with the mean velocity of the effective medium outside the representative cell (Kuwabara, 1959):

$$\frac{1}{R_c}\frac{\partial \psi}{\partial \theta} = \langle u \rangle \cos\theta, \tag{3-9}$$

and its vorticity is found to be zero for flow because of the symmetry of flows between the adjacent representative cells, viz.,

$$\nabla^2 \psi = 0. \tag{3-10}$$

Particular solution of Eq. (3-5) is given by (Kuwabara, 1959):

$$\psi = (A_0 l + A_1 l^{-1} + A_2 l \ln(l/R) + A_3 l^3) \sin\theta, \tag{3-11}$$

where A_0, A_1, A_2, and A_3 are constants to be determined by fulfilling the boundary conditions of Eqs. (3-6 to 3-10). The solution of A_2 is readily obtained:

$$A_2 = \frac{(1-\varepsilon)(1+2\mathrm{Kn})\langle u \rangle}{-0.5\ln(1-\varepsilon) + 0.25 - \varepsilon - 0.25(1-\varepsilon)^2 + 2\mathrm{Kn}\left(-0.5\ln(1-\varepsilon) - 0.25 + 0.25(1-\varepsilon)^2\right)}. \tag{3-12}$$

The drag acting on a unit length of fiber can be expressed as (Brown, 1993):

$$F = \pi R_c^2 \nabla p, \tag{3-13}$$

or obtained by integrating stress components over the fiber surface with the help of Eq. (3-12) (Kuwabara, 1959), viz.,

$$F = 4\pi\mu A_2. \tag{3-14}$$

Substituting Eq. (3-13) to Eq. (3-14), one can calculate the dimensionless hydraulic permeability in the representative cell as:

$$K/r^2 = \frac{-0.5\ln(1-\varepsilon) + 0.25 - \varepsilon - 0.25(1-\varepsilon)^2 + 2\mathrm{Kn}\left(-0.5\ln(1-\varepsilon) - 0.25 + 0.25(1-\varepsilon)^2\right)}{4(1-\varepsilon)(1+2\mathrm{Kn})}. \tag{3-15}$$

Stokes equation of Eq. (3-1) is also used to compute the velocity u_{para} for flow parallel with the 1D fiber array. According to Eq. (3-6), the slip tangential velocity on the fiber surface aligned with flow direction can be expressed as

$$u_{para} = r\mathrm{Kn}\frac{\partial u_{para}}{\partial l} \quad \text{for} \quad l = r\,. \tag{3-16}$$

In addition, $\partial u_{para}/\partial n = 0$ is found on the bounder of the square due to the symmetry of flows between those square cells, where n is the normal to the square border. As the square cell is approximated by the circular cell with radius R_c, the following equation is obtained:

$$\frac{\partial u_{para}}{\partial l} = 0, \quad \text{for} \quad l = R_c. \tag{3-17}$$

The velocity satisfies stokes equation (3-1) and the boundary conditions Eq. (3-16) and Eq. (3-17) can be computed as

$$u_{para} = \frac{1}{4\mu}\nabla p\left[\left(l^2 - r^2\right) - 2R_c^2\ln(l/r) + 2\mathrm{Kn}r(r - R_c^2/r)\right]. \tag{3-18}$$

The mean velocity is the ratio of total flow rate against the total cell area, which is given by:

$$\langle u\rangle = \frac{1}{\pi R_c^2}\int_r^{R_c} 2\pi l u_{para}\,dl. \tag{3-19}$$

Substituting Eq. (3.19) into Darcy's law, the dimensionless permeability in the representative unit cell for flow parallel with fibers is readily obtained:

$$K/r^2 = \frac{-0.25\ln(1-\varepsilon) + 0.25 - \varepsilon - 0.25(1-\varepsilon)^2 + \varepsilon^2 \mathrm{Kn}}{2(1-\varepsilon)}. \quad (3\text{-}20)$$

3.2.2. 1D Random structures

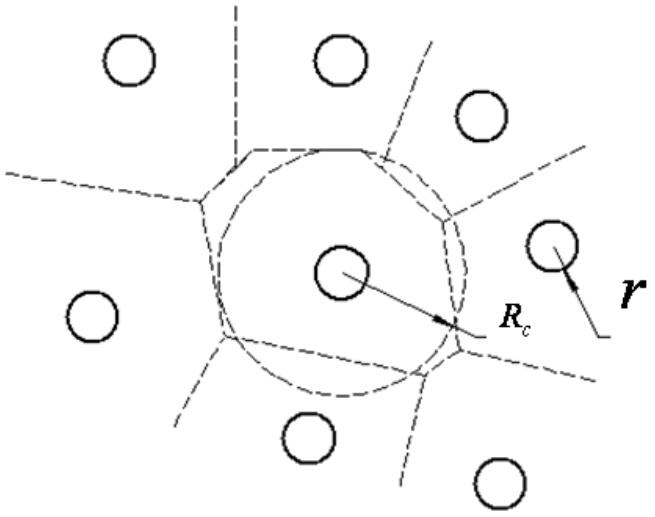

Figure 3-3: A unit cell in randomly distributed array of parallel fibers. The dotted circle is the unit cell with the same area as the voronoi polygon in dotted line.

This part considers the slightly more complicated and realistic case, in which 1D fiber arrays are randomly placed. Flows through the representative cells become more complex because of the disorder of cells. To characterize the effect of randomness, the Voronoi Tessellation Method (Ferenc and Neda, 2007) is applied in this study. A representative cell containing a fiber encircled by randomly located aligned fibers is shown in Fig. 3-3. Each fiber is assumed to be surrounded by a polygonal cell, whose boundaries are defined by the perpendicular bisectors of the lines joining each fiber axis with its nearest neighbor as defined by Voronoi Tessellation.

The mean area of the polygonal unit cell $\langle S \rangle$ is:

$$\langle S \rangle = \int S f(S) dS = \frac{\pi r^2}{1-\varepsilon}, \tag{3-21}$$

where S is area of a unit cell, and $f(S)$ is the probability density distribution function of the polygonal cell with area S. Comparing with the previous study that used the nearest inter-fiber distance to describe randomness degree (Sobera and Kleijn, 2006), this method is more reasonable by using the area distribution of polygonal cells to characterize randomness of fiber packing, because fiber randomness is generated by all neighboring fibers around the fiber rather than the nearest neighboring fibers. For polygonal cells containing fibers with random distribution, $f(S)$ are found to follow Gamma distribution (Chan et al., 1988). Moreover, the mean area square of the polygonal cells can be calculated as:

$$\langle S^2 \rangle = \int f(S) S^2 dS = \alpha \langle S \rangle^2. \tag{3-22}$$

where, $f(S) = \frac{S^{\beta-1}}{\Gamma(\beta)} \left(\frac{\beta}{\langle S \rangle} \right)^{\beta} \exp\left(-\frac{\beta}{\langle S \rangle} S \right)$ is a Gamma distribution function (Chan et al., 1988), $\Gamma(\beta)$ is a Gamma distribution, β is the scale parameter determined by α based on $\int \frac{S^{\beta-1}}{\Gamma(\beta)} \left(\frac{\beta}{\langle S \rangle} \right)^{\beta} \exp\left(-\frac{\beta}{\langle S \rangle} S \right) S^2 dS = \alpha \langle S \rangle^2$. For fully random distribution of the fibers, the coefficients are calculated as $\alpha = 1.28$ and $\beta = 3.61$ (Ferenc and Neda, 2007); for regular fiber distribution, it is apparent that $\alpha = 1$. Hence, the parameter α, which determines $f(S)$ based on Eq. (3-22), may provide a direct measure of the degree of randomness of fiber distribution.

And $f(S)$ will be written as $f(S,\alpha)$ in the following parts.

For a medium with $\varepsilon = 1$, the pressure gradient is surely constant throughout the medium. For fibrous system with extremely high porosity, it is also reasonable to assume the pressure gradient uniformly distributed in the porous medium. In addition, the pressure gradient in every representative cell is assumed to be equal to the macroscopic pressure gradient of the fibrous system based on the effective medium approximation. Therefore, an equivalent homogeneity (or 1D regular fiber array) is applied to calculate the hydraulic permeability as that of the original 1D randomly distributed fibers, which means that they share the same total Darcy permeability (or momentum of flow). Thus, the mean velocity of the random fibrous structure or the equivalent regular system is calculated based on conservation of momentum. The mean velocity of all polygonal cells $\langle u \rangle$ is volume-weighted, viz.,

$$\langle u \rangle = \frac{\int f(S,\alpha) u dS}{\langle S \rangle}, \tag{3-23}$$

where $\langle S \rangle$ is the mean area of polygonal cells.

Substitute Eqs. (3-15), (3-20), and (3-23) to Darcy's law, the dimensionless hydraulic permeability is obtained as $K/r^2 = \frac{\mu \int f(S,\alpha) u dS}{r^2 \nabla p \langle S \rangle}$ for flow through 1D fibers with a degree of randomness α.

Particularly, for flow normal to the fibers in 1D fully random (viz. $\alpha = 1.28$) fibrous system, the dimensionless permeability is given by

$$K/r^2 = \frac{\int f(S,1.28)\left[-0.5S^2\ln\left(\frac{\pi r^2}{S}\right)+\pi r^2 S-0.75S^2-0.25\left(\pi r^2\right)^2+2\mathrm{Kn}\left(-0.5S^2\ln\left(\frac{\pi r^2}{S}\right)-0.25S^2+0.25\left(\pi r^2\right)^2\right)\right]dS}{4\pi r^2(1+2\mathrm{Kn})\langle S\rangle}$$
$$= \frac{-0.64\ln(1-\varepsilon)+0.263-\varepsilon-0.25(1-\varepsilon)^2+2\mathrm{Kn}\left(-0.64\ln(1-\varepsilon)-0.097+0.25(1-\varepsilon)^2\right)}{4(1-\varepsilon)(1+2\mathrm{Kn})},$$

(3-24)

and for flow parallel with the fibers, the dimensionless hydraulic permeability is obtained as follows:

$$K/r^2 = \frac{\int f(S,1.28)\left[-0.5S^2\ln\left(\frac{\pi r^2}{S}\right)+\pi r^2 S-0.75S^2-0.25\left(\pi r^2\right)^2+\mathrm{Kn}\left(S^2-2\pi r^2 S+\left(\pi r^2\right)^2\right)\right]dS}{2\pi r^2\langle S\rangle}$$
$$= \frac{-0.64\ln(1-\varepsilon)+0.263-\varepsilon-0.25(1-\varepsilon)^2+\left(\varepsilon^2+0.28\right)\mathrm{Kn}}{2(1-\varepsilon)}.$$

(3-25)

where $f(S,1.28)=27.4\frac{S^{2.61}}{\langle S\rangle^{3.61}}\exp\left(-3.61\frac{S}{\langle S\rangle}\right)$ and $\pi r^2=\langle S\rangle(1-\varepsilon)$.

3.2.3. 2D and 3D structures

This part studies 2D and 3D fibrous media with varying fiber orientation. It is impossible to obtain the exact permeability of realistic 2D and 3D fibrous structures (Tamayol and Bahrami, 2009). However, it was suggested that the macroscopic permeability can be calculated by adding the contribution of flow resistances in three principal direction into a total drag in cubic space (Jackson and James, 1986). Thus, one needs to solve a closure problem to map the local permeabilities into combined permeability.

In this work, a fibrous medium is assumed to consist of network of representative cubic cells. In each cell, fibers may be located and oriented in different directions. The fiber orientation in the cubic cell can be statistically

characterized by the fractional length of the fibers oriented in x, y, or z direction, respectively (see Fig. 3-4), and the fiber fractional length is determined by the fiber fraction in the same direction. This assumption is used to model 2D and 3D permeabilities by combing the local flow contribution of 1D fibers in x, y, or z direction. The fibers are distributed regularly or randomly, and the microstructures are complex, but they can be considered as homogeneity at macro-scale. For the fibers oriented in the same principal direction and are regarded as a meso-scale system, they are also homogeneously located. Therefore, the whole system can be approximated as a collection of meso-scale systems, which are not overlapped by each other. The porosity of each meso-scale system is assumed identical with the overall porosity by considering the homogeneous feature of the whole system. It is difficult to find the exact solution of the system permeability as the meso-scale systems are interlaced. However, as the composite of the meso-scale systems, the overall fibrous system has upper and lower limits of permeability, viz. volume-averaged permeability model (or parallel network) and volume-averaged resistance model (or series network), respectively. Their relationship can be illustrated in Fig. 3-5.

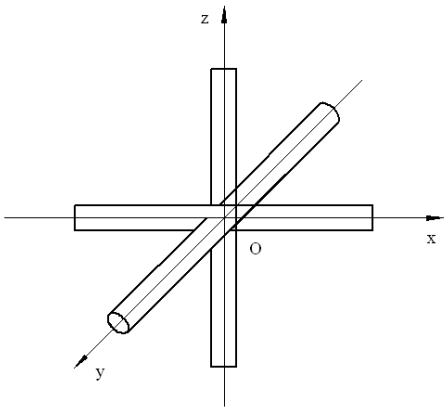

Figure 3-4: 3D view of fibrous media based on cubic lattice

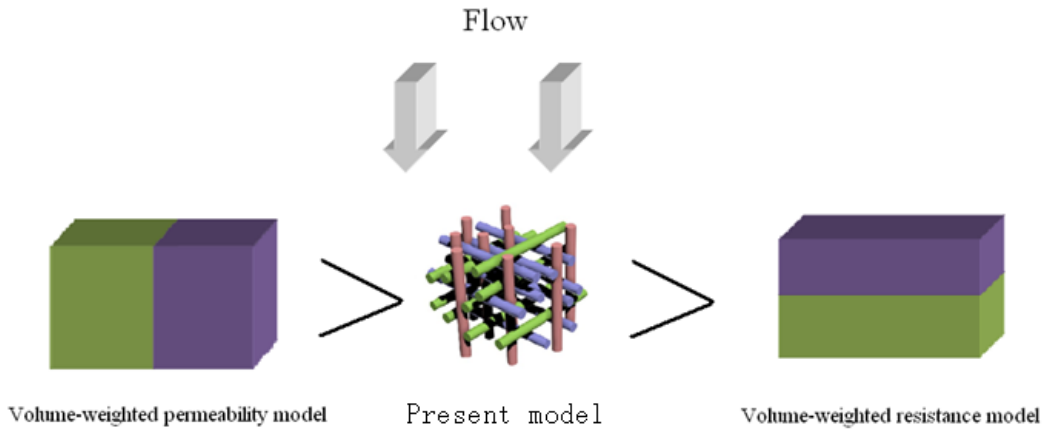

Figure 3-5: Relationship between the present model, volume-averaged permeability model, and volume-averaged resistance model

The volume-averaged permeability model is given by:

$$K_p(\phi) = \frac{\phi_{norm,x}}{\phi} K_{norm,x}(\phi) + \frac{\phi_{norm,y}}{\phi} K_{norm,y}(\phi) + \frac{\phi_{par}}{\phi} K_{par}(\phi), \tag{3-26}$$

and the volume-averaged resistance model is suggested as:

$$K_r(\phi) = \left[\frac{\phi_{norm,x}}{\phi} K_{norm,x}^{-1}(\phi) + \frac{\phi_{norm,y}}{\phi} K_{norm,y}^{-1}(\phi) + \frac{\phi_{par}}{\phi} D_{par}^{-1}(\phi) \right]^{-1}. \tag{3-27}$$

As the overall permeability of the fibrous system is between Eq. (3-26) and Eq. (3-27), an average estimate is adopted to estimate the system permeability. Its dimensionless form is given by

$$K/r^2 = \frac{1}{2r^2}\left[K_p(\phi) + K_r(\phi) \right]. \tag{3-28}$$

3.2.4. Results and discussion

The above-described models are compared with analytical expressions, numerical results and experimental data available in literature. For straightforward comparison, the reported results of drag coefficients, Kozeny constants or other relevant parameters are all converted into dimensionless permeability. In addition to model validation, this study also analyzes the affecting structural influences, particularly including degree of randomness, fiber orientation and Knudsen number (slip effect).

In this study, the randomness degree of fiber location is characterized by the value of α. For simulating moderately random fibrous medium, α is set as 1.07; and for highly random fibrous medium, $\alpha = 1.14$. The distribution of fiber orientation and space dimension can be effectively controlled by ϕ_x, ϕ_y, and ϕ_z. When $\phi_y = \phi_z = 0$, it demonstrates a 1D fibrous medium; when $\phi_z = 0$, $\phi_x \neq 0$, and $\phi_y \neq 0$, it becomes a 2D fibrous medium; when $\phi_z \neq 0$, $\phi_x \neq 0$, and $\phi_y \neq 0$, it refers to a 3D fibrous medium. In the 2D layered case, in-plane orientation varies from lowest to highest with ϕ_x decreasing from $1/2$ (2D isotropic) to 0 (1D fiber array normal to flow direction). For 3D fibrous media, through-plane orientation changes from lowest to highest level with ϕ_z from 0 (2D isotropic) to 1 (1D fiber array aligned with flow direction) while maintaining $\phi_x = \phi_y$. In addition, hydraulic permeabilities of fibrous media in continuum regime ($\mathrm{Kn} < 10^{-2}$) and in slip flow regime ($10^{-2} < \mathrm{Kn} < 1$) are discussed, respectively. Knudsen number is set as zero to study permeability of microfibers from Part A to Part C.

A. 1D array of fibers

The dimensionless permeability as a function of porosity for viscous flow

normal to 1D array of fibers is presented in Fig. 3-6 (a). The solid line is calculated using Eq. (3-15) for a regularly ($\alpha = 1$) distributed fibrous medium; the dotted line, the dash-dot line and dashed line are calculated using Eq. (3-24) for fully ($\alpha = 1.28$), highly ($\alpha = 1.14$) and moderately ($\alpha = 1.07$) random fibrous systems, separately. Fig. 3-6 (a) reveals that the hydraulic permeability for flow normal to the axis of 1D array of fibers increases with increasing degree of randomness. In addition, the present calculations are compared with the theoretical, experimental, and computational results, which include Sobera and Kleijn's (Sobera and Kleijn, 2006), who numerically obtained hydraulic permeability of randomly distributed system of a large amount of parallel cylinders using Finite Volume Method, Tomadakis and Robertson's (Tomadakis and Robertson, 2005), who obtained semi-analytical permeability estimates of 1D, 2D and 3D randomly fibers based on Monte Carlo simulations, Tamayol and Bahrami's (Tamayol and Bahrami, 2010b), who investigated transverse permeability of 1D ordered case analytically and experimentally, Kirsch and Fuchs's (Kirsch and Fuchs, 1967), who measured the hydraulic permeability of square arrays of Kapron fibers, and Acrivos and Sangani's (Sangani and Acrivos, 1982), who performed analytical studies of viscous permeability of square and hexagonal array of cylinders by multipole expansion method. It can be seen from Fig. 3-6 (a), the permeability prediction is in excellent agreement with the numerical values of Sobera and Kleijn (Sobera and Kleijn, 2006) for 1D fully random distributed fibrous media. For regular structure, the analytical and experimental data of regular structures by Tamayol and Bahrami (Tamayol and Bahrami, 2010b), the experimental measurements of Kirsch and Fuchs (Kirsch and Fuchs, 1967) as well as the computational and analytical results of Acrivos and Sangani (Sangani and Acrivos, 1982) agree closely with present model. In addition, permeability predictions of both square and hexagonal array of fibers (Sangani and Acrivos, 1982) are both identical with the proposed model, which reveals the fiber

arrangement of highly porous ordered structures is negligible.

The experimental and theoretical results of hydraulic permeability for the flow parallel with the unidirectional fibers are shown in Fig. 3-6 (b). Like in Fig. 3-6 (a), hydraulic permeability of unidirectional fibers increases with increasing degree of the randomly of fibers. The collected data are from Sullivan's (Sullivan, 1942), who reported data for the longitudinal viscous flow through randomly distributed wool, Sangani and Yao's (Sangani and Yao, 1988), who solved the Stokes equation numerically for longitudinal viscous flow through regular and random arrays of 1D cylinders, and Tamayol and Bahrami's (Tamayol et al., 2009), who calculated parallel flow through regular array of fibers numerically and theoretically, and also obtained another analytical model based on integral technique (Tamayol and Bahrami, 2009). The numerical results of Sangani and Yao (Sangani and Yao, 1988) are in good agreement with the present model, while the experimental results of Sullivan (Sullivan, 1942) are slightly greater than the perdition, which may be ascribed to the fact that the bundles of loose fibers became looser during experiment and eventually more big pores were generated. However, the prediction of Tomadakis and Robertson (Tomadakis and Robertson, 2005) is slightly larger than both previous experiments and the present model for longitudinal flow through 1D random structure.

Fig. 3-6 reveals that randomly distributed fibrous media are more permeable than those less random for flow both normal and parallel to the direction of fiber array. This can be understood by the fact that the permeability increase in big cells of random structure is much higher than the permeability decrease in small cells, because flow permeability scales with cell areas or pore radius square.

(a)

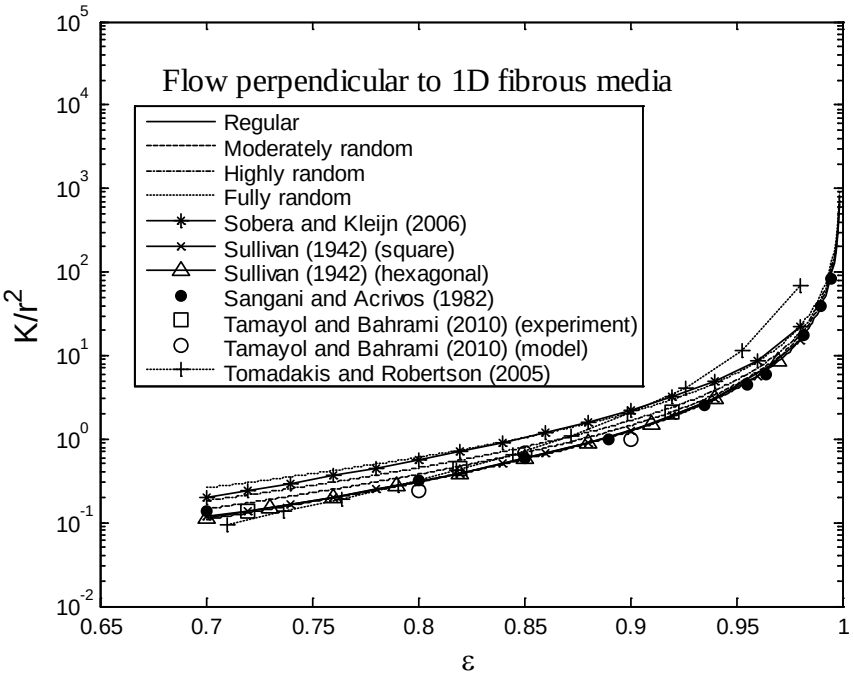

(b)

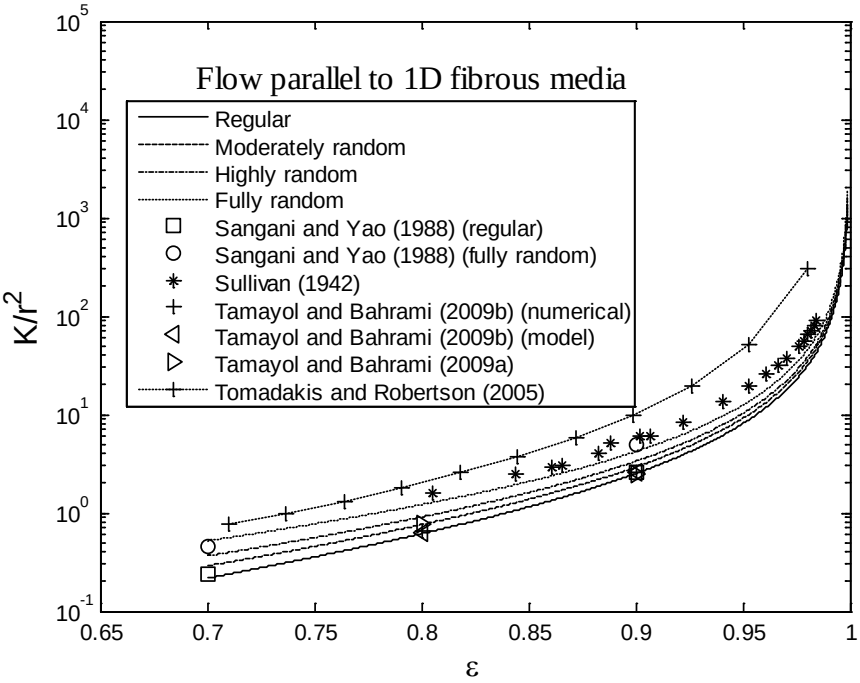

Figure 3-6: Dimensionless (a) normal and (b) parallel permeability against porosity for 1D fibers with varying degrees of randomness. The experimental, numerical and analytical results from literature are also added for comparison.

B. 2D layered fibrous media

The hydraulic permeability computed according to the present model for the flow normal to layered fibrous structures is compared with experimental measurements of past researchers in Fig. 3-7. Since conventional 2D fibrous webs are typically isotropic in the plane, $\phi_x = \phi_y = 1/2$ is adopted in the present model to represent the 2D layered fibrous structure. The following equation, which is calculated by Eq. (3-28), is the compact model of hydraulic permeability of 2D conventional layered fibrous web with fully random distribution of fibers:

$$K/r^2 = \frac{-0.64\ln(1-\varepsilon) + 0.263 - \varepsilon - 0.25(1-\varepsilon)^2 + 2\mathrm{Kn}\left(-0.64\ln(1-\varepsilon) - 0.097 + 0.25(1-\varepsilon)^2\right)}{4(1-\varepsilon)(1+2\mathrm{Kn})}, \quad (3\text{-}29)$$

which shares the same mathematical form with 1D random model of Eq. (3-24).

Past experimental data are obtained from Ingmanson's work (Ingmanson et al., 1959), who investigated the viscous flow through 2D glass, nylon and paper fibers, Wheat's work (Wheat, 1963), who measured the permeability of 2D layered fibrous mats, and Labrecque's work (Labrecque, 1968), who investigated the effect of fiber cross section on hydraulic permeability. Davies' empirical correlation (DAVIES, 1952), which was fitting his experimental results of transverse permeability through high porous fibrous filters, is also added for comparison. As can be seen from Fig. 3-7, experimental data including the empirical model fall closely to present model.

In 2D layered fibrous media, the fraction of fibers in z-direction ϕ_z is 0 as the fibrous medium is 2D layered structure, but the fractions of fibers in x-direction ϕ_x or y-direction ϕ_y is generally not 0. Fig. 3-8 presents that the calculated hydraulic permeability of 2D fully random fibrous media with different in-plane fiber

orientations. As the fraction of fibers in x-direction ϕ_x increases from 0 to $1/3$, and then to $1/2$, the fibers are distributed from unidirectionally or high in-plane fiber orientation to a moderately unidirectionally, and then to isotropically or low in-plane fiber orientation, separately. In Fig. 3-8, the present calculation based on Eq. (3-28) indicates that the hydraulic permeability is not sensitive to the changes of ϕ_x, i.e. in-plane fiber orientation. This phenomena was predicted by past researchers based on numerical simulations (Tahir and Tafreshi, 2009), but it was not verified by theoretical rigor until the present work.

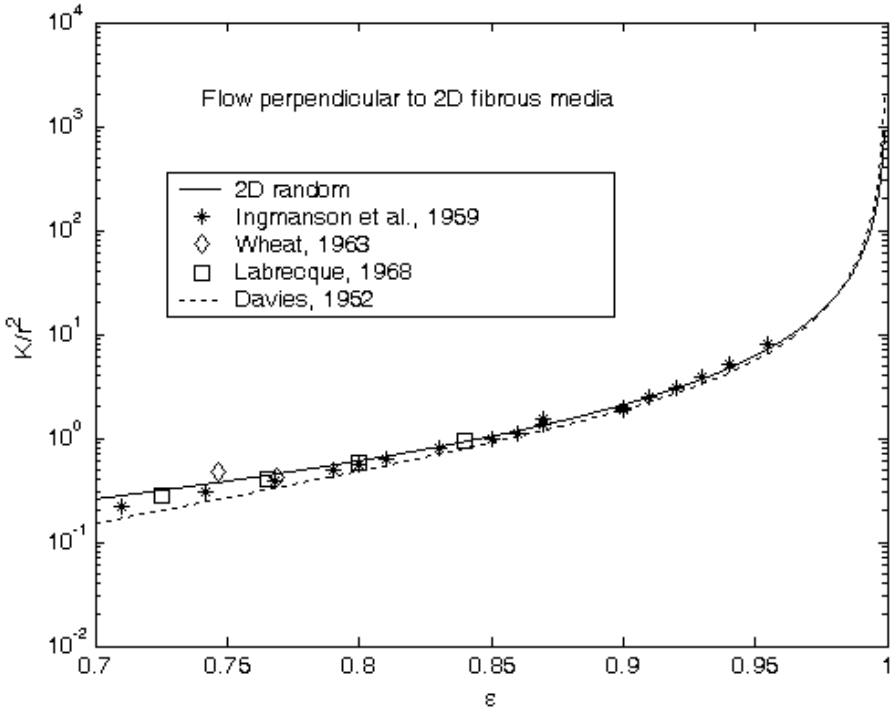

Figure 3-7: Dimensionless normal permeability as a function of porosity for 2D fibrous media. The experimental results and an empirical correlation from literature are also added for comparison.

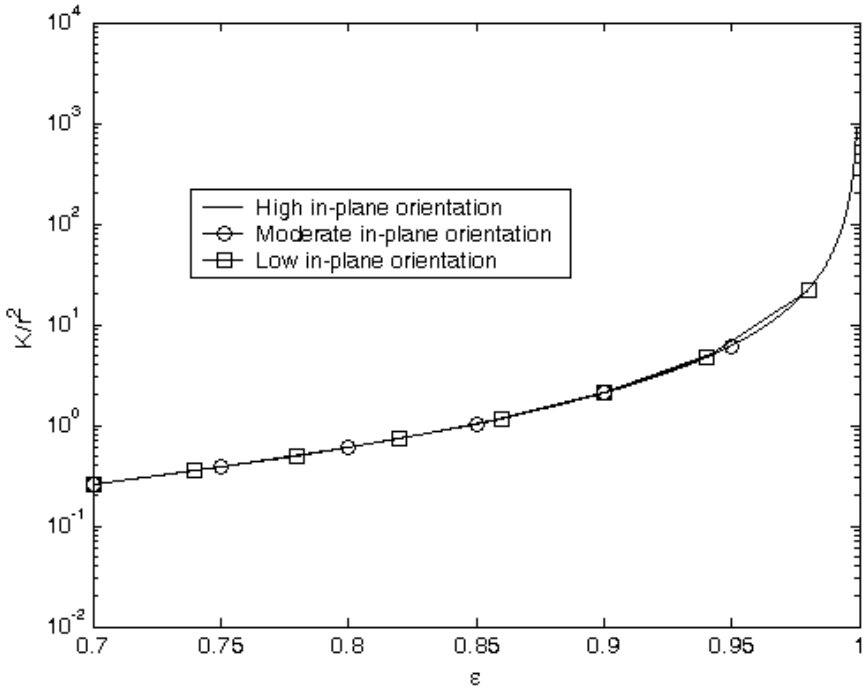

Figure 3-8: Comparison of dimensionless permeability of 2D fibrous media with different in-plane fiber orientations

C. 3D Fibrous media

Fig. 3-7 compares the calculated results using the present model for 3D isotropic fibrous media ($\phi_x = \phi_y = \phi_z = 1/3$) with the experimental and numerical data available in the literature. The following equation, which is calculated by substituting Eq. (3-26) and Eq. (3-27) to Eq. (3-28), is the compact model of hydraulic permeability of 3D randomly distributed fibrous media:

$$K/r^2 = \frac{1}{2r^2}\left[K_p(\phi) + K_r(\phi)\right], \tag{3-30}$$

where, the volume-averaged permeability model is given by:

$$K_p(\phi)=\frac{-0.64\ln(1-\varepsilon)+0.263-\varepsilon-0.25(1-\varepsilon)^2+(\varepsilon^2+0.28)\mathrm{Kn}}{6(1-\varepsilon)}$$
$$+\frac{-0.64\ln(1-\varepsilon)+0.263-\varepsilon-0.25(1-\varepsilon)^2+2\mathrm{Kn}\left(-0.64\ln(1-\varepsilon)-0.097+0.25(1-\varepsilon)^2\right)}{6(1-\varepsilon)(1+2\mathrm{Kn})},$$

(3-31)

and the volume-averaged resistance model is expressed as:

$$K_r(\phi)=\left[\frac{2(1-\varepsilon)}{3\left[-0.64\ln(1-\varepsilon)+0.263-\varepsilon-0.25(1-\varepsilon)^2+(\varepsilon^2+0.28)\mathrm{Kn}\right]}\right.$$
$$\left.+\frac{8(1-\varepsilon)(1+2\mathrm{Kn})}{3\left[-0.64\ln(1-\varepsilon)+0.263-\varepsilon-0.25(1-\varepsilon)^2+2\mathrm{Kn}\left(-0.64\ln(1-\varepsilon)-0.097+0.25(1-\varepsilon)^2\right)\right]}\right]^{-1}.$$

(3-32)

Along with the prediction in Fig. 3-9 are the experimental results collected from Carman's work (Carman, 1938), who conducted permeability measurements of randomly distributed beds of stainless steel wire crimps, Wiggins et al.'s work (Wiggins et al., 1939), who measured the hydraulic permeability of various 3D fibrous materials with several different kinds of test liquids, Brown's work (Brown Jr., 1950), who measured flow resistance to dry gas through 3D glass wool, Higdon and Ford's work (Higdon and Ford, 1996), who used a boundary element method to estimate the viscous hydraulic permeability of 3D networks of cylindrical fibers ordered in different cubic lattices, and more recently, Rahli et al.'s work (Rahli et al., 1997), who experimentally investigated the hydraulic permeability of randomly oriented chopped fibers of bronze and copper wires. Fig. 3-9 shows that most experimental data, which are obtained based on different fiber materials and testing fluids, agree closely with the proposed 3D fully random model. It is also interesting phenomenon that the proposed model is similar with the volume-averaged permeability model and volume-averaged resistance model in Fig. 3-9.

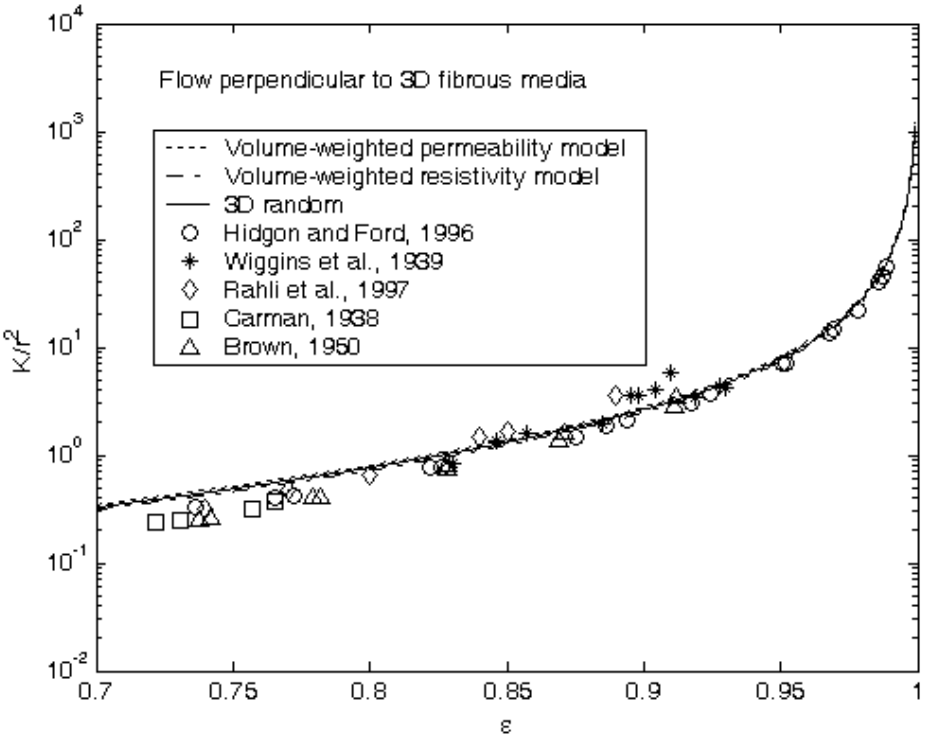

Figure 3-9: Dimensionless permeability as a function of porosity for a 3D fibrous media. 1D, 2D, and 3D models for regular structures, and the numerical and experimental results are also added for comparison.

To investigate the influence of the through-plane fiber orientation on the hydraulic permeability for flow normal to 3D fibrous media, a series of 3D structures with different through-plane fiber orientations are generated by changing the fraction of fibers in z-direction ϕ_z in steps, from 0 (2D layered random media with lowest through-plane orientation), to 1/3 (3D isotropic medium with moderate through-plane orientation), and then to 1 (1D fibers parallel to the flow with highest through-plane orientation), and maintaining the same fractions of fibers for x and y-directions ($\phi_x = \phi_y$). The calculated results plotted in Fig. 3-10 show that the hydraulic permeability for the flow normal to the 3D fibrous media increases

significantly with increase in the through-plane fiber orientation. Therefore, the 1D fibers or 2D layers normal to flow direction have the highest flow resistances, followed by 3D fiber assembles, and 1D fibers aligned with flow direction are most permeable.

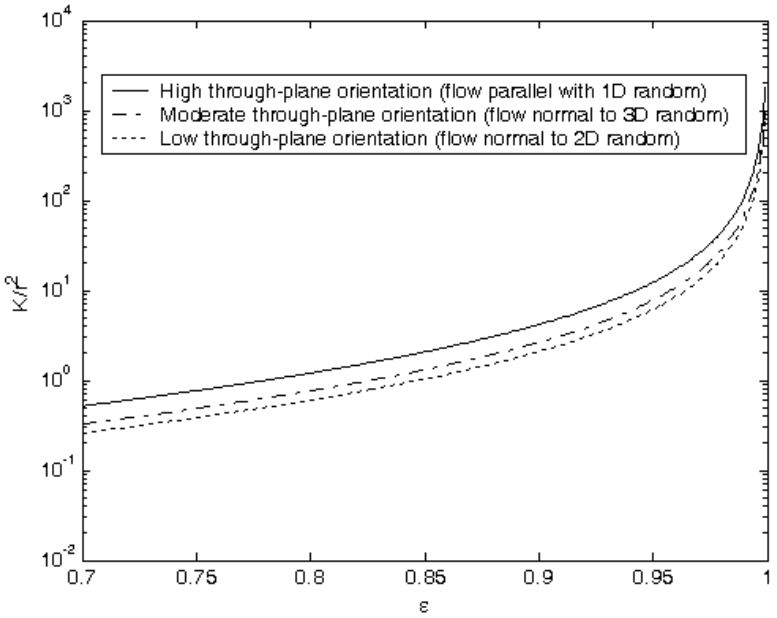

Figure 3-10: Comparison of dimensionless permeability of 3D fibrous media with different through-plane fiber orientations

D. Nanofiber arrays

This section specifically considers the viscous flow through 1D parallel nanofibers considering slip effect, although the present model can also be readily applied to 2D and 3D cases using Eq. (3-28). The dimensionless hydraulic permeability and Darcy hydraulic permeability of 1D fibrous media with different Kn are calculated using this model and are shown in Fig. 3-11 and Fig. 3-12, respectively.

(a)

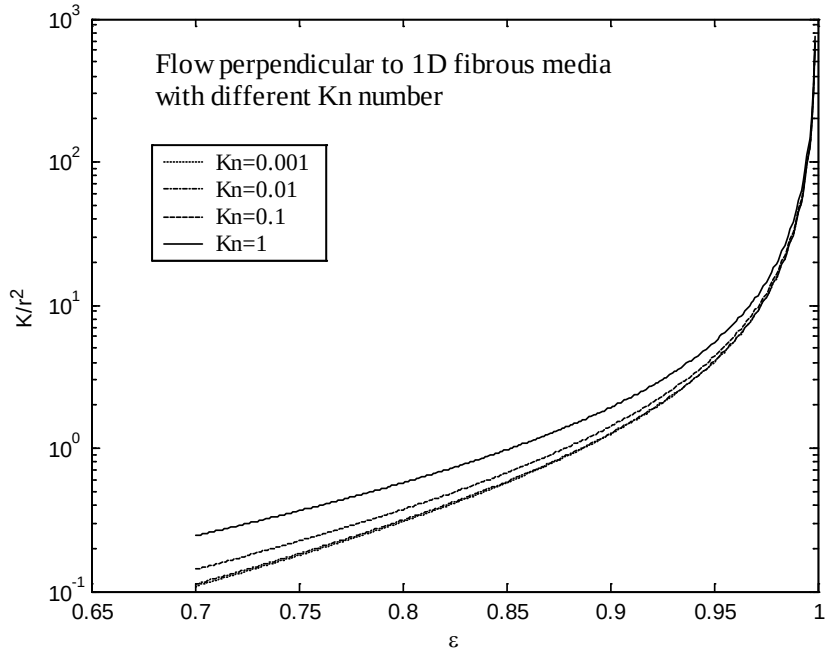

(b)

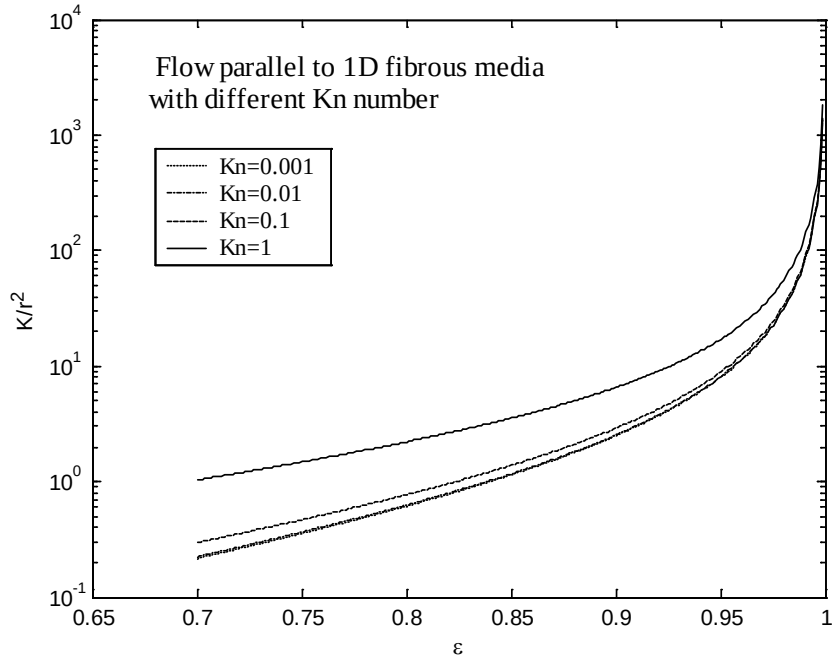

Figure 3-11: Comparison of dimensionless (a) normal and (b) parallel hydraulic permeability of 1D fibrous media with different Kn

(a)

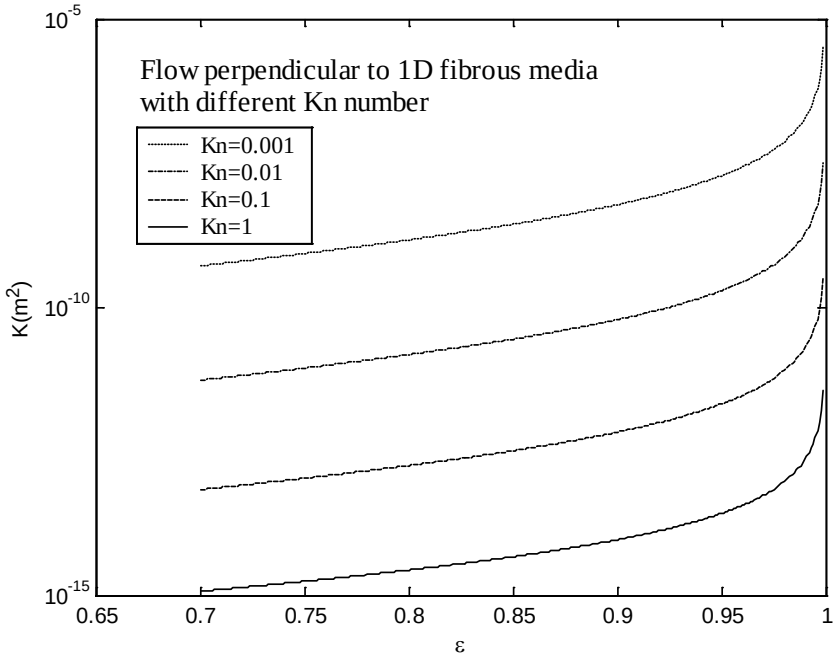

(b)

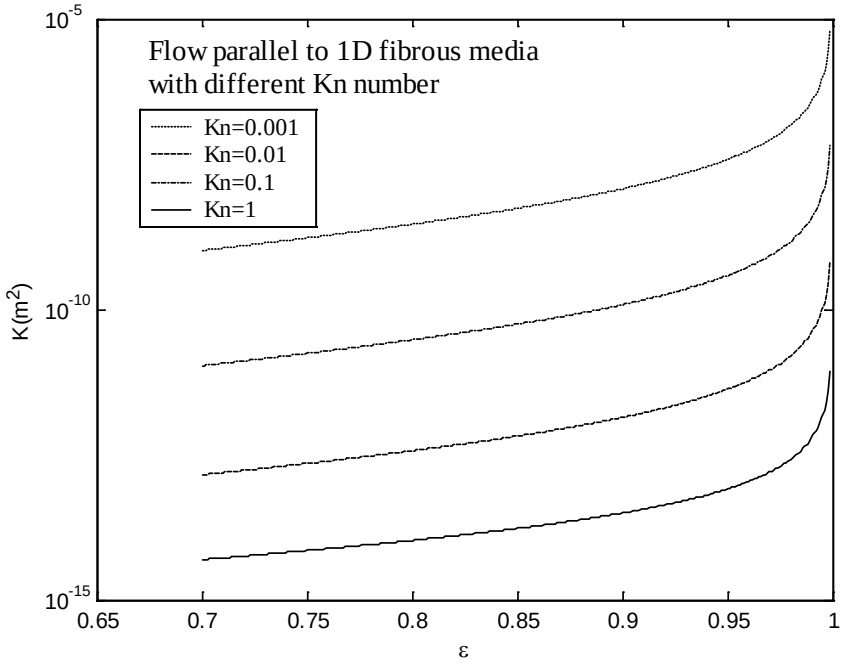

Figure 3-12: Comparison of (a) normal and (b) parallel Darcy hydraulic permeability of 1D fibrous media with different Kn

From Fig. 3-11 (a), it shows that the partial slip flow on the fiber surface ($10^{-2} < \mathrm{Kn} < 1$) increases normal dimensionless hydraulic permeability as compared to the no-slip case ($\mathrm{Kn} < 10^{-2}$ or $\mathrm{Kn}=0$). The effect of Kn on the longitudinal dimensionless hydraulic permeability is even more significant, as shown in Fig. 3-11 (b). This is understandable as all the partial slip flows on fiber surface are parallel with the macroscopic flow direction, and parallel flow suffers from more slip effect than transverse flow. However, both Fig. 3-12 (a) and 3-12 (b) reveal the Darcy hydraulic permeability of the fibrous media with higher Kn (i.e. more partial slip) is still much lower than that with smaller Kn. This can be ascribed to that the Darcy hydraulic permeability is proportional to the square of fiber radius, which greatly suppresses the slip effect on increasing permeability. Therefore, the effect of Darcy hydraulic permeability caused by fiber radius is much greater than the accompanied influence of slip flow. It can also been seen from Figure 3-11 that the slip effect on the hydraulic permeability is less pronounced at higher porosity of the fibrous media, which may be ascribed to their less specific interaction with flows.

3.3. Fibrous structures with low porosity

This section develops the model of hydraulic permeability for low porosity fibrous media from simple and ordered to complicated and random structures. First, modified scaling estimate method is proposed to predict the hydraulic permeability of 1D ordered structures. Afterwards, Kozeney-Carman approach is used to determine the hydraulic permeability of randomly distributed fibrous assembles for 2D and 3D.

3.3.1. 1D fiber arrays

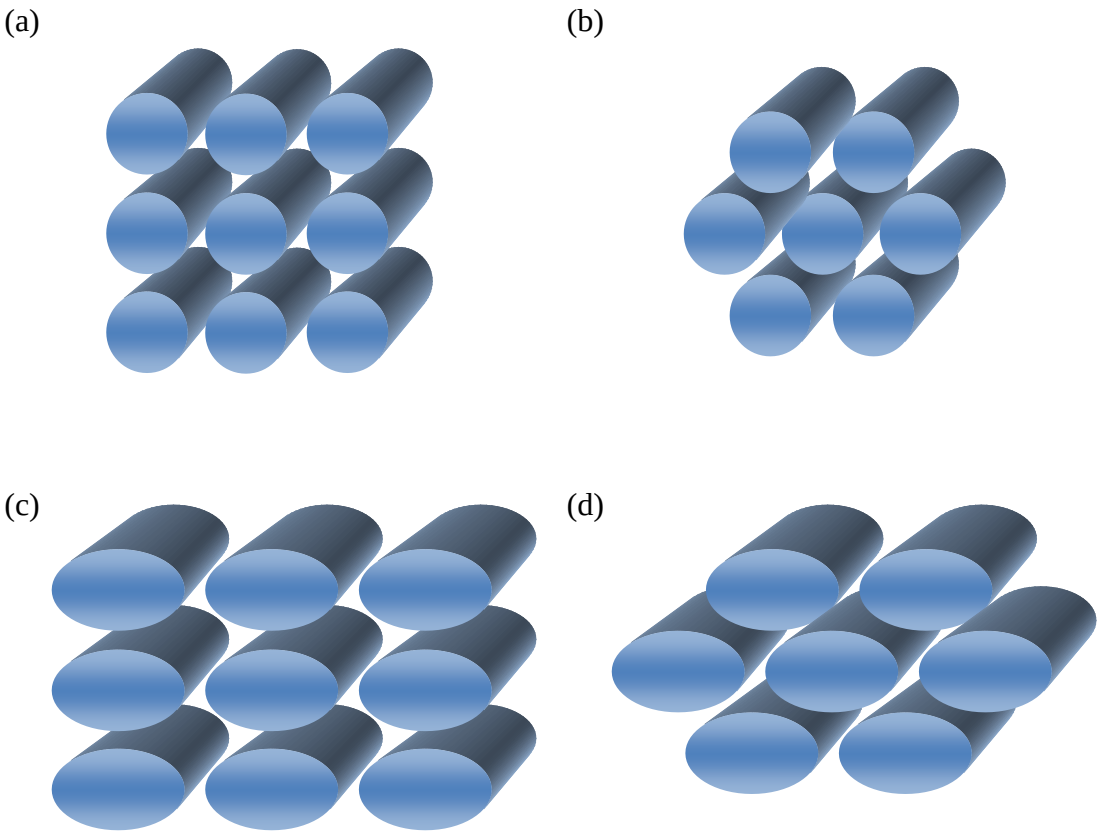

Figure 3-13: (a) Schematic of circular fibers in a square packing; (b) schematic of circular fibers in a hexagonal packing; (c) schematic of elliptical fibers in a square packing; (d) schematic of elliptical fibers in a hexagonal packing

Fibrous media are assumed to be composed of periodical representative cells. The cell contains arrays of solid fibers with different cross-sectional shapes and packing configurations. Shown in Fig. 3-13 include aligned yarns with different architectures, and the elliptical yarns reported here are generated by imposing the axis ratio $A/B=2$, where A is the major axis and B is the minor axis of an elliptical yarn.

A. Transverse flow through aligned fibers

Here, gas flow through an array of square packing circular fibers (see Fig. 3-14) is chosen as the example of performing solutions. The lubrication theory is employed

in this work. Lubrication theory describes fluid flow through a geometry in which one dimension is much smaller than the others, and here the velocity component in vertical direction (y-direction) is considered significantly smaller than that in horizontal direction (x-direction). Considering the flow in x-direction, Stokes equation can be simplified as (Chai et al., 2011):

$$\frac{dp}{dx} - \mu \frac{d^2 u}{dy^2} = 0. \tag{3-33}$$

The half distance $h_{\min}$ was selected between cylindrical fibers as the characteristic length (Clague et al., 2000), over which the flow velocity varies dramatically. They presented a scaling estimate as follows:

$$\nabla p \sim \mu \frac{\langle u \rangle}{h_{\min}^2}. \tag{3-34}$$

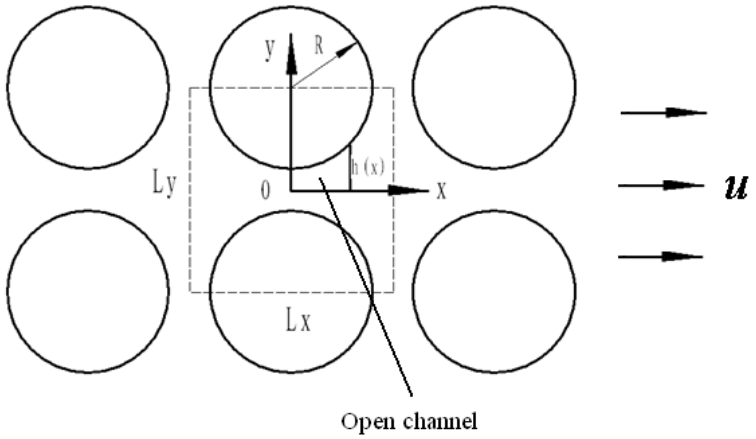

Figure 3-14: Circular yarns of square arrangement in the representative cell

Later, (Sobera and Kleijn, 2006) argued that it is more proper choosing the actual velocity $u_0 = \langle u \rangle / \chi$ as the characteristic velocity, where χ is the ratio between

the minimum area to the total frontal area as $2h_{\min}/L_y$. However, this prediction does not agree with experimental and numerical data in a wide range of porosities as shown in Section 3.3.3. It is believed that this is a consequence of neglecting effect of the curve shape of the fiber surface close to the area of the narrowest gap, which has been proven to have critical contribution of flow through fiber bundles (Gebart, 1992). Indeed, it is more reasonable to scale the pressure difference against the flow velocity within a length difference instead of the total cell width, because the "channel width square"-dependent velocities are not uniform or even in the same magnitude along the flow direction. A more generalized local scaling estimate is therefore suggested as follows:

$$\frac{dp}{dx} \sim \mu \frac{u(x)}{h^2(x)}, \tag{3-35}$$

where $h(x)$ is the half distance between fibers at the position of "x" along x-direction, and $u(x)$ is the corresponding mean velocity. Eq. (3-35) captures more structural details than the previous studies

Moreover, as the actual velocity $u(x)$ along flow direction in the open channel, which are formed by neighboring fibers (see Fig. 3-14), can be expressed as $\langle u \rangle L_y / [2h(x)]$ based on conservation of flow flux, re-writing Eq. (3-35) yields

$$dp = c\mu \frac{\langle u \rangle L_y}{h^3(x)} dx, \tag{3-36}$$

where L_y represents the side length of the representative cell in y-direction, and c is an empirical constant. Integrating Eq. (3-36) leads to the value of the pressure

difference between two positions $x = 0$ and $x = a$ in the channel:

$$\Delta p = c \frac{\langle u \rangle L_y}{\mu} \int_0^a \frac{1}{h^3(x)} dx. \tag{3-37}$$

For the fiber arrangement of Fig. 3-14, the half height of channel can be expressed as:

$$h(x) = h_{\min} + y(x), \tag{3-38}$$

where $y(x) = R - \sqrt{R^2 - x^2}$. As most pressure drop or flow resistances take place within a gap distance $|x| << R$ near $h_{\min}$, $y(x)$ is therefore given by (Gebart, 1992):

$$y(x) = R - \left[R - \frac{x^2}{2R} + 0(x^2) \right] \approx \frac{x^2}{2R}. \tag{3-39}$$

Substituting Eq. (3-38) into Eq. (3-37) results in:

$$\int_0^a \frac{1}{h^3(x)} dx = \int_0^a \frac{1}{\left[h_{\min} + y(x) \right]^3} dx, \tag{3-40}$$

where $y(x)$ is smaller than $h_{\min}$ in the region close to the narrowest gap between fibers, except those composed of extremely dense fiber arrays. If $y(x)$ is neglected, Eq. (3-40) would induce to $K \sim h_{\min}^2 \chi$, which has the same form with Clague et al.'s (Clague et al., 2000). Indeed, fiber surface shape or variation of $y(x)$ has considerable effect on pressure drop through the open channel according to Eq. (3-37)

and Eq. (3-40). Therefore, $y(x)$ will not be neglected in this study. Substituting Eq. (3-39) into Eq. (3-40) leads to:

$$\int_0^a \frac{1}{h^3(x)}dx = \frac{1}{h_{\min}^3}\sqrt{2Rh_{\min}}\int_0^{\sqrt{\frac{a}{2Rh_{\min}}}} \frac{1}{\left(1+t^2\right)^3}dt. \tag{3-41}$$

where $\int_0^{\sqrt{\frac{a}{2Rh_{\min}}}} \frac{1}{\left(1+t^2\right)^3}dt$ is a constant. Thus, rewriting Eq. (3-41) results in the following equation:

$$\Delta p = c\mu\frac{\langle u\rangle L_y\sqrt{R}}{h_{\min}^{2.5}}. \tag{3-42}$$

As most of the pressure difference is found to exist within the small area close to $h_{\min}$, Δp in Eq. (3-42) is reasonably equal with the total pressure difference throughout the representative cell. The hydraulic permeability of the representative cell is obtained as follows:

$$K = c\frac{h_{\min}^{2.5}L_y}{\sqrt{R}L_x}, \tag{3-43}$$

where L_x is the side length of the representative cell in x-direction. The dimensionless form of hydraulic permeability of solid circular fiber assembles is:

$$K/R^2 = c\left(\frac{h_{\min}}{R}\right)^{2.5}\frac{L_y}{L_x}. \tag{3-44}$$

Through a similar calculation process, the dimensionless permeability of solid elliptical fiber assembles is readily obtained, viz.,

$$K / AB = c\left(\frac{h_{\min}}{B}\right)^{2.5}\frac{L_y}{L_x}. \tag{3-45}$$

For different fiber arrangements, $h_{\min}$ is a function of porosity, fiber radius, and cell side lengths L_x and L_y:

$h_{\min} = \left(\sqrt{\frac{\pi}{1-\varepsilon}} - 2\right)R$ with $L_x = L_y$ for square packing circular yarns (Fig. 3-13a),

$h_{\min} = \left(\sqrt{\frac{\sqrt{3}\pi}{2(1-\varepsilon)}} - 2\right)R$ with $L_x = \frac{2\sqrt{3}}{3}L_y$ for hexagonal packing circular yarns (Fig. 3-13b),

$h_{\min} = \left(\sqrt{\frac{\pi}{1-\varepsilon}} - 2\right)B$ with $L_x = 2L_y$ for square packing elliptical yarns (Fig. 3-13c),

$h_{\min} = \left(\sqrt{\frac{2\pi}{\sqrt{3}(1-\varepsilon)}} - 2\sqrt{1-\frac{\pi}{8\sqrt{3}(1-x)}}\right)B$ with $L_x = \frac{4\sqrt{3}}{3}L_y$ for hexagonal packing elliptical yarns (Fig. 3-13d).

B. Parallel flow through aligned fibers

For flow parallel with fibers, they can be approximately regarded as flow through tubes with different packing (Tomadakis and Robertson, 2005). The viscous flow through such an irregular pore was widely characterized by a hydraulic radius, as the ratio of pore area and perimeter (Jia et al., 2008). However, even for an equilateral triangle, the difference between hydraulic radius-based model and the exact solution is significant (Bergelin et al., 1950). The error may be ascribed to that

a longer perimeter as a result of irregular shape of a pore, would lead to a much smaller hydrauilic radius but not the effective flow radius. In this study, the inscribed radius r_a is chosen as the characteristic length, as most flow fluxes exist in the inscribed polygon, which can be shown from the numerical simulation of velocity distribution in square packing array of fibers in Fig. 3-15. The inscribed fiber and the velocity distribution are difficult to characterize through the channels between fibers with elliptical cross-sectional shape, especially for those with high axis ratio. As thus, elliptical cases will not be considered in present study. For circular fiber, the dimensionless permeability for parallel flow is obtained as follows:

$$K / R^2 = c\left(\frac{r_a}{R}\right)^2 \varepsilon. \tag{3-46}$$

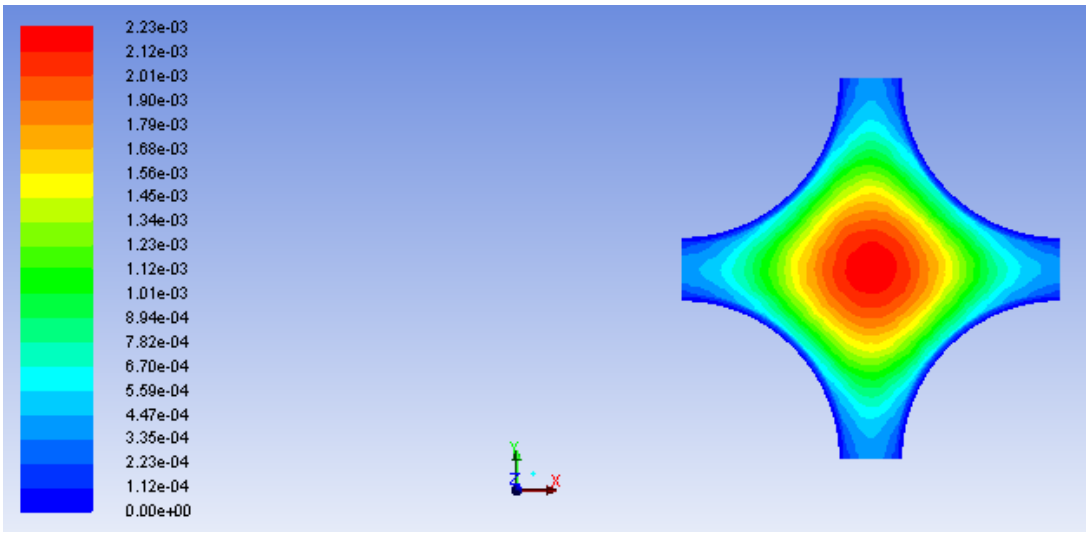

Figure 3-15: Velocity distribution of parallel flow though fibers of square arrangement

For different fiber arrangements, r_a varies depending on porosity, fiber radius, and packing configuration:

$r_a = \left(\sqrt{\frac{2\pi}{1-\varepsilon}} - 2 \right) R$ for square packing circular yarns (Fig. 3-13a),

$r_a = \left(\sqrt{\frac{2\sqrt{3}\pi}{3(1-\varepsilon)}} - 2 \right) R$ for hexagonal packing circular yarns (Fig. 3-13b).

3.3.2. 2D and 3D fiber mats

It is difficult to characterize the structural information of 2D and 3D fibrous media at low porosity. However, their geometric parameters can be assumed to follow the Kozeny-Carman form that the fibrous systems are assumed as bundles of tortuous channels formed by the closely packed fibers. Here, Kozeny-Carman approximation is applied to permeability prediction, which yields:

$$K = \frac{\langle R_p \rangle^2}{4K_C} \tag{3-47}$$

The mean pore size R_p is expressed as $R_p = \frac{\varepsilon}{1-\varepsilon} r$ (Tomadakis and Sotirchos, 1991). Considering the relationship between mean pore radius and fiber radius, Eq. (3-47) is re-written in the following form:

$$K / r^2 = \frac{\varepsilon^3}{4K_C (1-\varepsilon)^2}, \tag{3-48}$$

or

$$K / r^2 = c \frac{\varepsilon^3}{(1-\varepsilon)^2}, \tag{3-49}$$

where c is a geometric factor, depending on microstructures of the fibrous system.

3.3.3. Results and discussion

The present analytical model requires inputting geometric factors, which include fiber radius, porosity, fiber shape, packing configuration, etc. To evaluate the model, the model is applied to fit the values of numerical, experimental and analytical data available in the literature. For better comparison, all the collected data are converted to dimensionless permeability. As such, for circular fibers, the hydraulic permeability K is divided by square of fiber radius R^2; for ellipse fibers, the hydraulic permeability K is divided by the product of semi-major and semi-minor axis AB.

A. Transverse flow through circular fibers

Aligned fibers are the simplest representations of fibrous porous media. For transverse flow though aligned solid fibers with square packing and circular cross-section, a comparison between the present model and previous studies is presented in Fig. 3-16 (a). Experimental data are collected from Bergelin et al.' (Bergelin et al., 1950), who measured viscous permeability of heat exchange tubes, Sadiq et al.'s (Sadiq et al., 1995), who used nylon fibers. Numerical results are Sangani and Acrivos's (Sangani and Acrivos, 1982), who applied numerical technique to predict the hydraulic permeability of periodic square arrays of fibers normal to flow direction. By fitting with experimental and numerical data, a constant $c = 0.4$ is used in the model of dimensionless permeability based on Eq. (3-44):

$$K / R^2 = 0.4\left(\sqrt{\frac{0.785}{1-\varepsilon}} - 1\right)^{2.5}, \tag{3-50}$$

which provides an excellent prediction over a wide range of porosities. Sobera and Kleijn's estimate (Sobera and Kleijn, 2006) is also plotted for comparison. As can be seen in Fig. 3-16 (a) with logarithmic scale of permeability, Sobera and Kleijn's

model has much greater deviation from the experimental data than the proposed model, which may be attributed to the fact that they did not consider the curved interface between the flow and the fiber near the region of the narrowest gap.

The other ordered arrangement of fibers is hexagonal packing. Following Sangani and Acrivos's numerical work (Sangani and Acrivos, 1982), Higdon and Ford (Higdon and Ford, 1996) applied spectral boundary element method to calculate the hydraulic permeability through parallel hexagonal circular cylinders. The calculated hydraulic permeability can be excellently fitted by the present model with $c = 0.2$, as seen from Fig. 3-16 (b). Based on Eq. (3-44), the model for circular fibers in hexagonal packing is given by:

$$K / R^2 = 0.2\left(\sqrt{\frac{0.907}{1-\varepsilon}} - 1\right)^{2.5}. \tag{3-51}$$

(a)

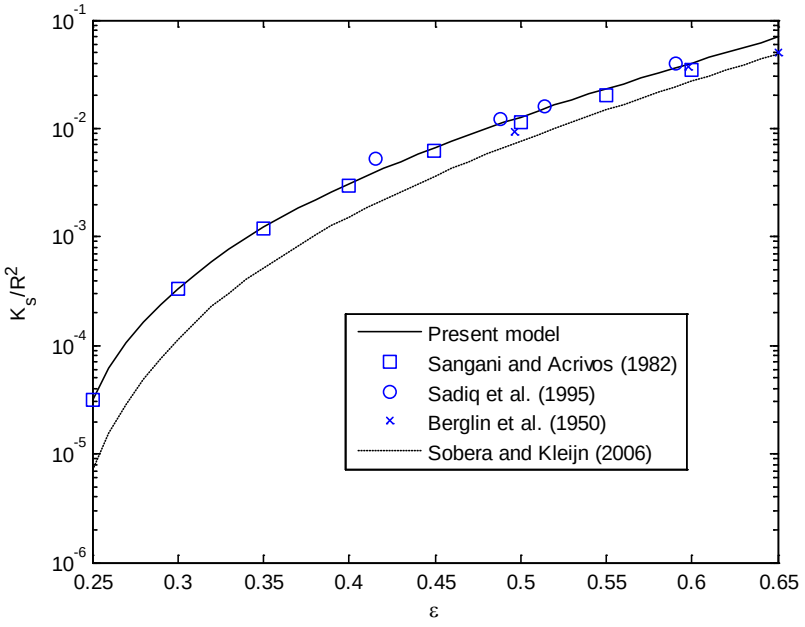

(b)

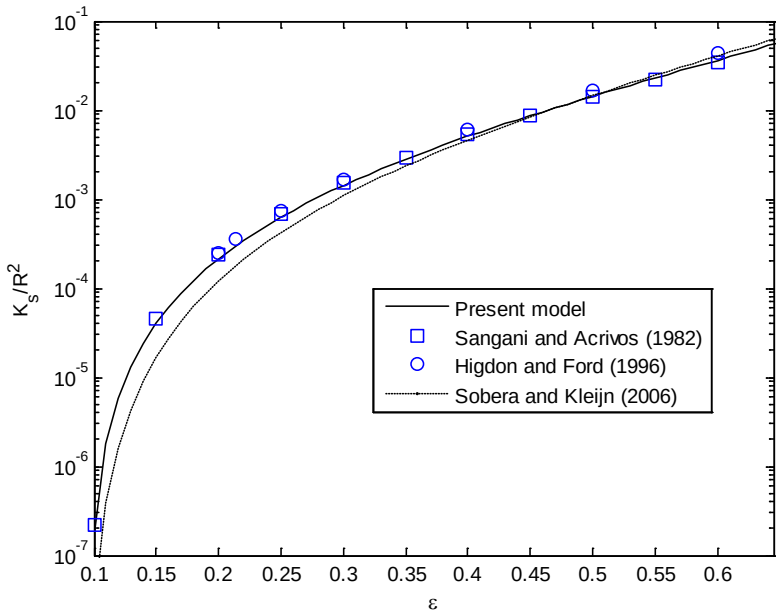

Figure 3-16: (a) Comparison of the present model of transverse permeability with experimental and numerical results for circular solid fibers with square packing configuration; (b) comparison of the present model of transverse permeability with numerical data for circular solid fibers with hexagonal arrangement. Sobera and Kleijn's estimate (Sobera and Kleijn, 2006) is also added for comparison.

Large discrepancies are observed between the numerical data and Sobera and Kleijn's model (Sobera and Kleijn, 2006) when porosity is small, as seen in Fig. 3-16 (b). Comparing strictly with the square packing structure, the hexagonal matrix is more permeable when the fibers are packed densely.

B. Transverse flow through elliptical fibers

Next, the theoretical model for 1D elliptical fiber arrays is validated by past results obtained through computational fluid dynamic (CFD) simulation. A

computational fluid dynamics package called FIDAP was used to simulate fluid flows through 1D elliptical fiber arrays with square packing and a cross-sectional ratio of 2 and it was shown that the small regime close to the smallest gap captures most pressure gradient in a representative cell (Phelan and Wise, 1996). In Chapter 5, a compact theoretical model expressed as Eq. (5-23) is proposed and validated for squarely packed elliptical fibers, by solving Stokes equation strictly between the elliptical fibers in a representative cell. From Fig. 3-17 (a), the best fitted model of Eq. (3-45) is given by:

$$K / AB = 0.21\left(\sqrt{\frac{0.785}{1-\varepsilon}} - 1\right)^{2.5}, \tag{3-52}$$

which agrees perfectly well with the collected values and Eq. (5-23).

(a)

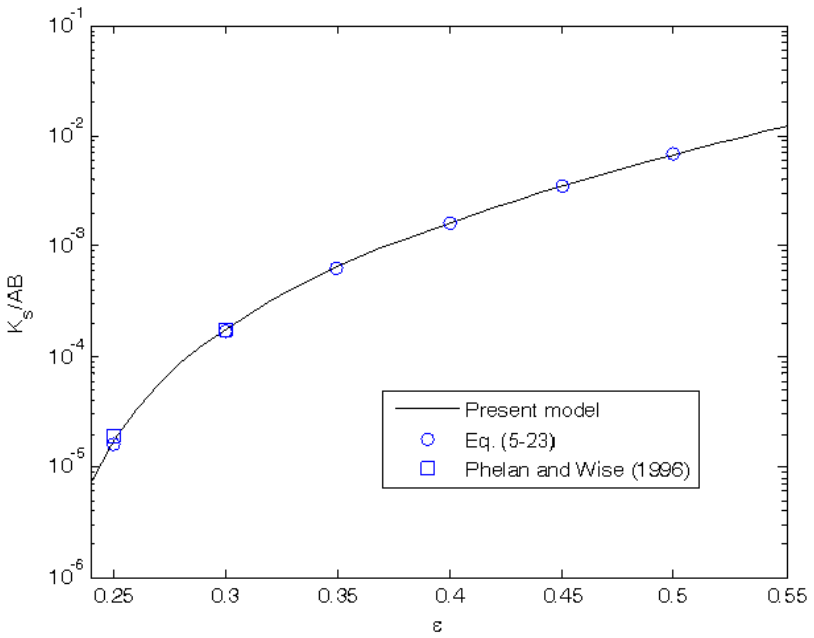

(b)

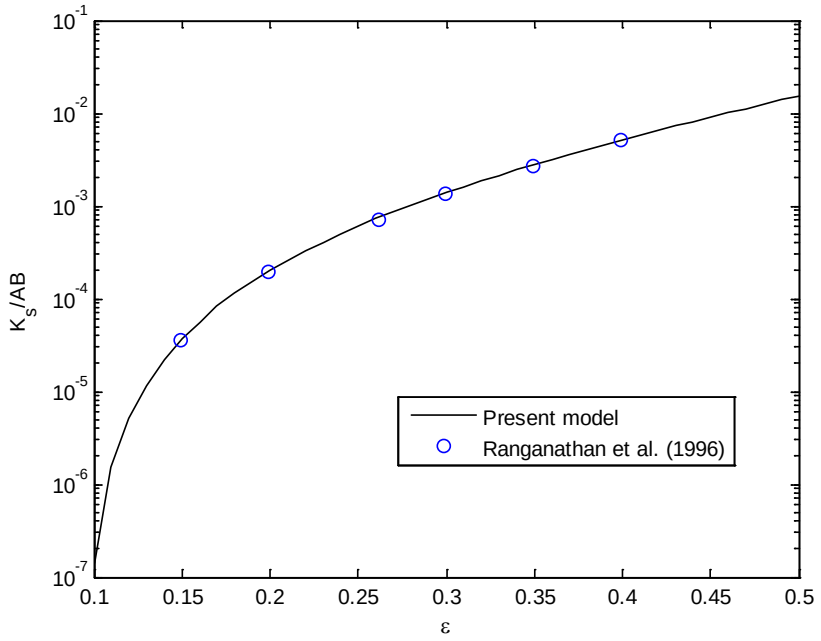

Figure 3-17: (a) Comparison of the present model of transverse permeability with numerical values for elliptical solid fibers with square arrangement; (b) comparison of the present model of transverse permeability with numerical simulations for elliptical solid fibers with hexagonal arrangement

In addition, the model of Eq. (3-45) for arrays of hexagonal packed elliptical yarns with axis ratio 2 is obtained:

$$K / AB = 0.13\left(\sqrt{\frac{0.680}{1-\varepsilon}} - \sqrt{1-\frac{0.227}{1-\varepsilon}}\right)^{2.5}, \qquad (3\text{-}53)$$

where the predicted values of which compare with the computed results by Ranganathan et al. (Ranganathan et al., 1996). Satisfactory agreement is found between prediction and simulation in Fig. 3-17 (b), indicating reliability of this prediction.

For the effect of fiber cross-sectional shape, the hydraulic permeability of parallel fibers with elliptical cross-section (major axis parallel with flow direction) is more permeable than the circular at the highly dense limit under the same porosity, which can be found by comparing Fig. 3-16 and Fig. 3-17.

C. Parallel flow through circular fibers

For parallel flow through ordered fibers, a comparison between the modified scaling estimate and previous results from literature is presented in Fig. 3-18. Experimental results are collected from Sullivan's (Sullivan, 1942), who conducted measurements to study the fiber-touched structures for both square and hexagonal packed pattern, and from Skartsis et al.'s (Skartsis et al., 1992), who measured resin flow rate through square-packed carbon fibers. Numerical data are summarized from Shih's (Shih, 1967), who simulated flow through fiber-touched structure with hexagonal packing, from Higdon and Ford's (Higdon and Ford, 1996), who computed the hydraulic permeability of periodic square arrays of fibers aligned with flow direction, and recently, from Tamayol and Bahrami's (Tamayol and Bahrami, 2010a), who calculated axis permeability of ordered fibers by Fluent. By fitting the plots of experimental and numerical results, a constant $c = 0.04$ is adopted to provide the model of dimensionless permeability for square packing based on Eq. (3-46):

$$K / R^2 = 0.04\left(\sqrt{\frac{2\pi}{1-\varepsilon}} - 2\right)\varepsilon, \tag{3-54}$$

and $c = 0.18$ for hexagonal packing:

$$K / R^2 = 0.18\left(\sqrt{\frac{2\sqrt{3}\pi}{3(1-\varepsilon)}} - 2\right)^2 \varepsilon. \tag{3-55}$$

(a)

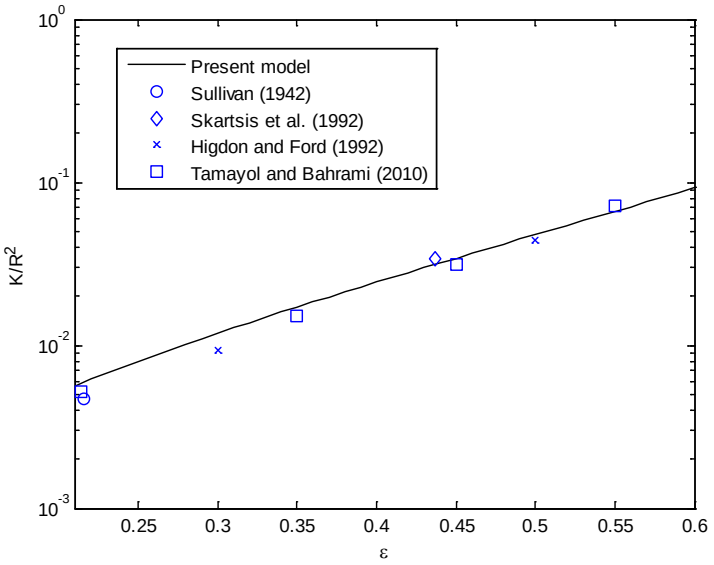

(b)

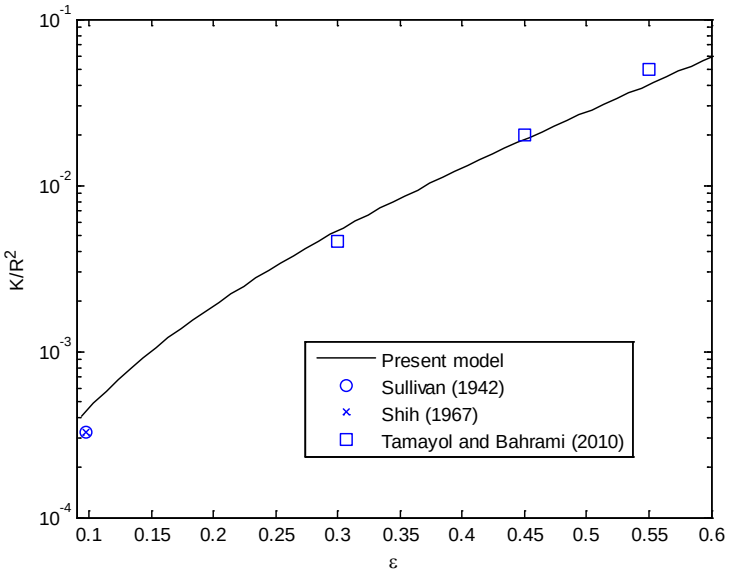

Figure 3-18: (a) Comparison of the present model of parallel permeability of square packing with experimental and numerical values; (b) comparison of the present model of parallel permeability of hexagonal packing with experimental and

numerical values collected from literature

The proposed model provides an excellent prediction against a wide range of porosities. Comparing with square packing structure, hexagonal array is less permeable, which has an opposite trend with that of transverse permeability.

D. Transverse flow through 2D and 3D fibrous media

For transverse flow though 2D and 3D fibrous materials, a comparison between the model in this study and the collected experimental results are presented in Fig. 3-19. In fact, few fibrous materials with densely packed fibers exist in actual applications, as the fibrous medium tends to be high porous media when fibers located randomly in 2D and 3D space. Kostornov and Shevchuk (Kostornov and Shevchuk, 1977) measured transverse flow through 2D randomly oriented fibers using testing fluids of alcohol and water. By fitting their experimental results using the present model, a constant $c = 0.4$ is found for the dimensionless permeability based on Eq. (3-49):

$$K / R^2 = 0.4 \frac{\varepsilon^2}{(1-\varepsilon)^3}, \tag{3-56}$$

Rahli et al. (Rahli et al., 1997) carried out permeability measurements on randomly layers made by chopped fibers of bronze and copper wire. The constant value, $c = 0.2$, is adopted to fit the numerical data the best as seen from Fig. 3-19 (a). The corresponding model is expressed as:

$$K / R^2 = 0.2 \frac{\varepsilon^2}{(1-\varepsilon)^3}. \tag{3-57}$$

(a)

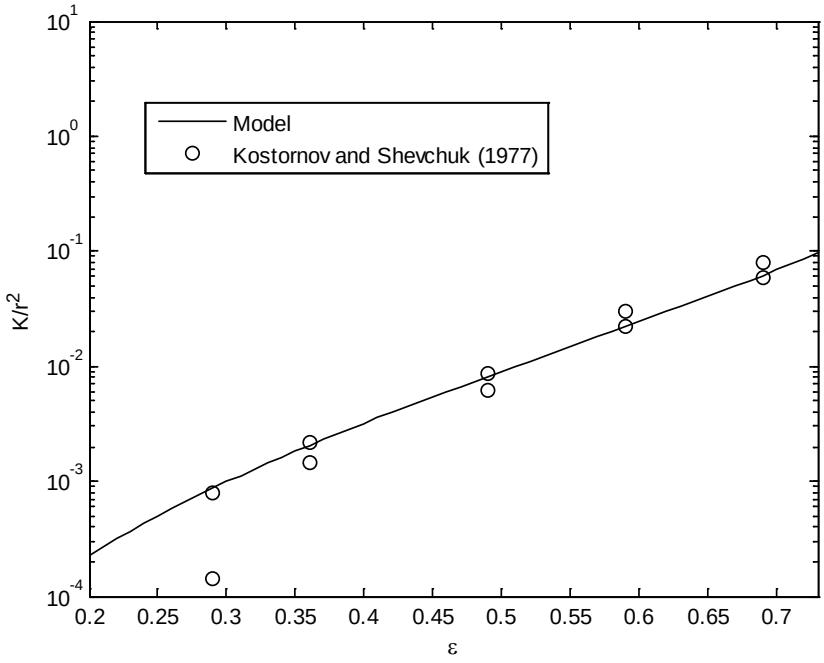

(b)

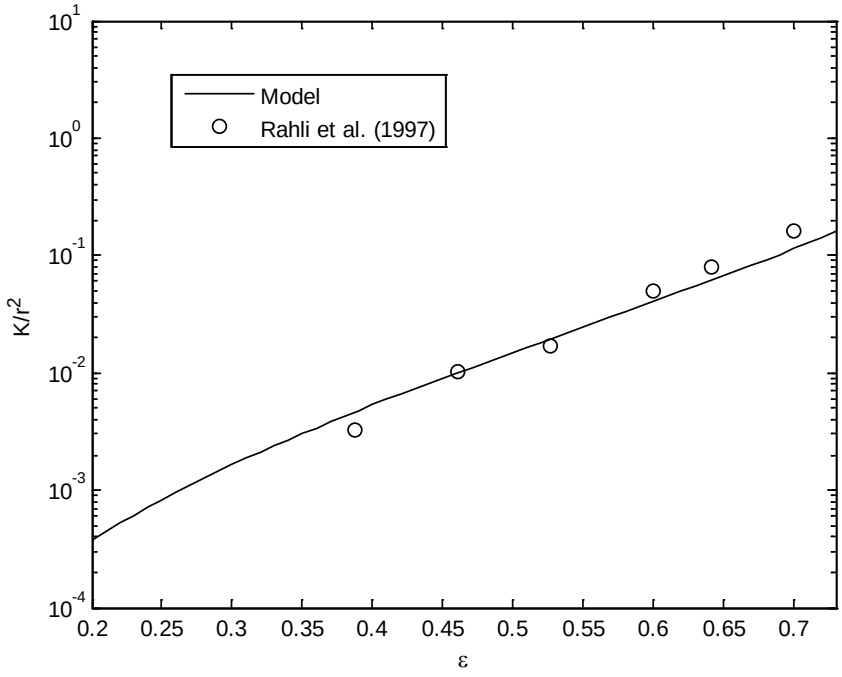

Figure 3-19: Comparison of the present model of transverse permeability of (a) 2D and (b) 3D fibrous materials with experimental results

3.4. Concluding remarks

Discrepancies were found between existing analytical values and experimental results, as the past researchers applied 1D ordered model to predict permeability of the actual fiber beds, which indeed could be 2D and 3D. To overcome it, theoretical studies were conducted here to determine hydraulic permeability of realistic fiber beds based on properly equivalent structures. Note the challenge is to find the balance between simplifying realistic fibrous structures and solving governing equations analytically.

Representative cell method, Voronoi Tessellation method, and mixing law were applied in steps to develop an analytical model of hydraulic permeability from simplified to realistic fibrous structures in high porosity range ($\varepsilon > 0.7$). The fibrous structures were characterized by equivalent fiber matrixes, where the fibers were in three principal directions with different degrees of randomness and different fiber fractions. The model was validated with the available theoretical, experimental and numerical results from literature. With the new model, the effect of Knudsen number or slip flow on the hydraulic permeability was also investigated. It can be concluded that hydraulic permeability increases with increasing degree of randomness of fiber distribution, and the hydraulic permeability of fibrous media is almost independent of in-plane orientation, but increases with increasing through-plane orientation. The slip flow increases the longitudinal permeability more significantly than the transverse permeability of 1D fiber arrays.

Viscous gas flow through aligned fibers was also studied in means of modified scaling estimate method at relative low porosity area ($\varepsilon < 0.6$). This versatile and predicable model, considering the minimum distance between fibers as the most critical effect on transverse permeability, is in excellent agreement with

experimental, numerical and analytical results collected from literature. It is also found that permeability of aligned fibers with elliptical cross-sectional are similar with circular fibers at a constant porosity, but more permeable at the low porosity limit. For hexagonal packing configuration of fibers, their permeability is found to be slightly greater than the squarely located fibers. For parallel flow through fibers, the inscribed radius was selected as the characteristic length, as most of the flow fluxes exist within the inscribed regular polygon. The model shows that the hexagonal structure has more flow resistances than the square case at a constant porosity in low porosity range, which is opposite to the trend of transverse flow. Kozeny-Carman approximation was applied to predict the hydraulic permeability of 2D and 3D densely packed fibers, and the models are all successfully verified by experimental and numerical results.

However, a complete permeability model of fibrous materials covering porosities from high to low limit remains to be developed. Scaling estimate models for fibers with elliptical cross-section are not obtained, because it is difficult to accurately determine the inscribed radius between elliptical fibers, and the inscribed polygon may not be able to capture the most contribution of flows along fiber axis considering the extremely irregular geometry between fibers.

Chapter 4 Statistic models for flow through single-scale fibrous media

4.1. Introduction

It is difficult to propose a deterministic model of hydraulic permeability in fibrous materials throughout porosities. Fortunately, it is found that microstructures of disordered porous media can be statistically described by fractal geometry (Mandelbrot, 1982), which can be used to determine permeability of fibrous media in a wide porosity range.

The disordered structures are analogous to a class of natural objects such as rivers, coastlines, and lakes, which are complex and difficult to describe using Euclidean geometry with integer dimensions 0-3. These objects are observed to demonstrate self-similar patterns, or fractal (Mandelbrot, 1982). They are generally not exactly self-similar, but statistical self-similar, which implies these objects exhibiting self-similarity in some average sense. A fractal object is always related to the length scale by a power law (Mandelbrot, 1982):

$$M(l) \propto l^{D_0}, \tag{4-1}$$

where D_0 is the fractal dimension, $M(l)$ can be a quality, or length, or volume, or area of the object, and l is the length scale.

In this chapter, the pore size distribution, which is the integration of various structural parameters including fiber orientation, disorder of fiber distribution, and medium dimensions, is used to predict permeability of randomly distributed fiber

layers based on fractal theory.

4.2. Model generation

It is shown that the size distribution of pores in realistic porous media or fibrous materials follows the fractal power law (Yu and Liu, 2004):

$$N(L \geq R) = (R_{\max} / R)^{D_f}, \tag{4-2}$$

where, D_f is the pore area fractal dimension, $0 < D_f < 2$ in two dimensions, and R and $R_{\max}$ is the pore radius and maximum pore radius, respectively. N is the cumulative population of pores whose radiuses are greater than or equal to R. In order to make Eq. (4-2) practically manageable, the smallest pore radius observed is assumed as $R_{\min}$. Moreover, pores with radius smaller than $R_{\min}$ are ignored, which is reasonable as smaller channels are much less permeable than larger pores from Hagen-Poiseuille equation. Thus, the total number of pores N_t, from $R_{\min}$ to $R_{\max}$, can be expressed as:

$$N_t(L \geq R_{\min}) = (R_{\max} / R_{\min})^{D_f}. \tag{4-3}$$

Based on the equation above, the fractal dimension D_f in two-dimensional spaces is given by (Yu, 2008):

$$D_f = 2 + \frac{\ln \varepsilon}{\ln\left(R_{\max} / R_{\min}\right)}. \tag{4-4}$$

Since the pore radius varies discretely considering the basic characteristic of

fractal geometry, it is appropriate to apply the difference approach to describe the relationship of pore numbers and pore radius. From Eq. (4-2), the difference on two adjacent pore numbers with respect to R yields:

$$dN = -D_f R_{\max}^{D_f} R^{-D_f-1} dR, \tag{4-5}$$

Substituting Eq. (4-3) into Eq. (4-5) leads to:

$$-\frac{dN}{N_t} = D_f R_{\min}^{D_f} R^{-D_f-1} dR = f(R)dR, \tag{4-6}$$

where, $f(R) = D_f R_{\min}^{D_f} R^{-D_f-1}$ is the probability density function of the pore radius, and it satisfies the following relationship:

$$\int_{R_{\min}}^{R_{\max}} f(R)dR = 1. \tag{4-7}$$

Apparently, when the number of the pores is sufficiently large, it is reasonable that the variation of pore size is regarded as continuum variable.

Real fibrous porous media are assumed to consist of a bundle of tortuous tubes, where the flow rate through a single tortuous tube, $q(R)$, is given by Hagen-Poiseuille equation as follows (Denn, 1980):

$$q(R) = \frac{\pi R^4}{8\mu\tau}\nabla p, \tag{4-8}$$

where, τ is tortuosity of the channel. The total flow rate Q_t through a cross-section can be obtained by integrations of arrays of individual flow rate based on Eq. (4-8):

$$
\begin{aligned}
Q(R) &= \int_{R_{\min}}^{R_{\max}} q(R)dR \\
&= \frac{\pi}{8\mu\tau}\frac{D_f}{4-D_f}R_{\max}^4\left(1-\left(\frac{R_{\max}}{R_{scale}}\right)^{4-D_f}\right)\nabla p \\
&\approx \frac{\pi}{8\mu\tau}\frac{D_f}{4-D_f}R_{\max}^4\nabla p.
\end{aligned}
\tag{4-9}
$$

where $2 > D_f > 0$ in the two-dimensional space, the exponent $4 - D_f > 2$. It is apparent $\left(\frac{R_{\min}}{R_{\max}}\right)^{4-D_f} \to 0$ for generally $R_{\min} \le 0.1R_{\max}$ in fibrous porous media, which can be observed in Fig. 1-4. The present study assumes $R_{\min} = 0.1R_{\max}$.

The porosity of every cross section is approximated as the total volume porosity, and the total cross area A_t is related to the total pore area A_p by (Yu, 2008):

$$
A = \frac{A_p}{\varepsilon}, \tag{4-10}
$$

where the total pore area A_p can be obtained by summing up:

$$
A_p = \int_{R_{\min}}^{R_{\max}} \pi R^2 dN = \frac{D_f}{2-D_f}R_{\max}^2\left(1-\varepsilon\right), \tag{4-11}
$$

Therefore, the total cross sectional area A_t of a unit cell normal to the flow direction is

$$
A_t = \frac{\pi D_f}{2-D_f}\frac{1-\varepsilon}{\varepsilon}R_{\max}^2. \tag{4-12}
$$

Thus, the mean velocity can be readily obtained:

$$\begin{aligned}\langle u\rangle &= \frac{Q}{A_t} \\ &= \frac{1}{8\mu\tau}\frac{2-D_f}{4-D_f}\frac{\varepsilon}{1-\varepsilon}\nabla p R_{\max}^2.\end{aligned} \tag{4-13}$$

In Eq. (4-13), all the parameters have clear physical meanings and no empirical constants exist. This model can be used to calculate average velocity of general porous media, and the flow rate is found to be strongly dependent on the maximum pore radius of the fibrous materials.

However, the pore size of fibrous media is always difficult to measure, but not for fiber radius. The mean pore radius $\langle R_p\rangle'$ is given by:

$$\langle R_p\rangle' = \int_{R_{\min}}^{R_{\max}} Rf(R)dR = \frac{D_f}{D_f-1}R_{\min}, \tag{4-14}$$

and be approximated by a function of porosity and fiber radius r (Sampson, 2003):

$$\langle R_p\rangle' = -\frac{\pi^{0.5}}{2}\left(1+\frac{\pi}{2\ln\varepsilon}\right)r. \tag{4-15}$$

The mean hydraulic pore radius $\langle R_p\rangle'$ as the ratio of pore area and pore perimeter, is usually larger than the mean flow pore radius $\langle R_p\rangle$ calculated from Hagen-Poiseuille law, and the relationship between them is given by (Lifshutz, 2005):

$$\langle R_p\rangle = \frac{\langle R_p\rangle'}{2.336}. \tag{4-16}$$

Substituting Eq. (4-16) into Eq. (4-15) leads to:

$$\left\langle R_p \right\rangle = \frac{-\frac{\pi^{0.5}}{2}\left(1+\frac{\pi}{2\ln\varepsilon}\right)r}{2.336}. \tag{4-17}$$

The tortuosity of 2D random fibrous porous media can be calculated by the following widely used equation from (Tomadakis and Robertson, 2005):

$$\tau = (\frac{1-0.11}{\varepsilon-0.11})^{0.785}. \tag{4-18}$$

Finally, the mean velocity is obtained by substituting Eq. (4-17) and Eq. (4-18) into Eq. (4-13):

$$\left\langle u \right\rangle = \frac{4-2D_f}{4-D_f}\left(\frac{D_f-1}{D_f}\right)^2 \frac{\varepsilon(\varepsilon-0.11)^{0.785}}{1-\varepsilon}\left(1+\frac{1.57}{\ln\varepsilon}\right)^2 \frac{r^2}{\mu}\nabla p. \tag{4-19}$$

Therefore, the dimensionless permeability of fibrous media is given by:

$$K/r^2 = \frac{4-2D_f}{4-D_f}\left(\frac{D_f-1}{D_f}\right)^2 \frac{\varepsilon(\varepsilon-0.11)^{0.785}}{1-\varepsilon}\left(1+\frac{1.57}{\ln\varepsilon}\right)^2. \tag{4-20}$$

Eq. (4-20) indicates that the permeability model of fibrous porous layer is a function of area fractal dimension and porosity, and every parameter has clear physical meaning.

4.3. Results and discussion

An abundance of experimental results and mathematical models are available for fluid flow normal to 2D fibrous porous media. In Fig. 4-1, the predicted permeability of Eq. (4-20) is compared with the experimental data from several literature sources (Johnson et al., 1996, Kostornov and Shevchuk, 1977, Ingmanson et al., 1959, Wheat, 1963, Gostick et al., 2006a). The experiments were conducted by using air or water within a variety of fibrous materials such as nylon fibers, glass

fibers and filter pads. As evident in Fig. 4-1, the permeability prediction agrees with the experimental data throughout the porosity ranges. The comparison between the present model and an empirical model (Johnston, 1998) also shows a comparable agreement in Fig. 4-1, although the empirical model over-predicts gas permeability in low porosity range. Therefore, the proposed analytical model, which is covered by the experimental data over the entire range of porosity, can provide a rapid prediction of transport trend of gas flow.

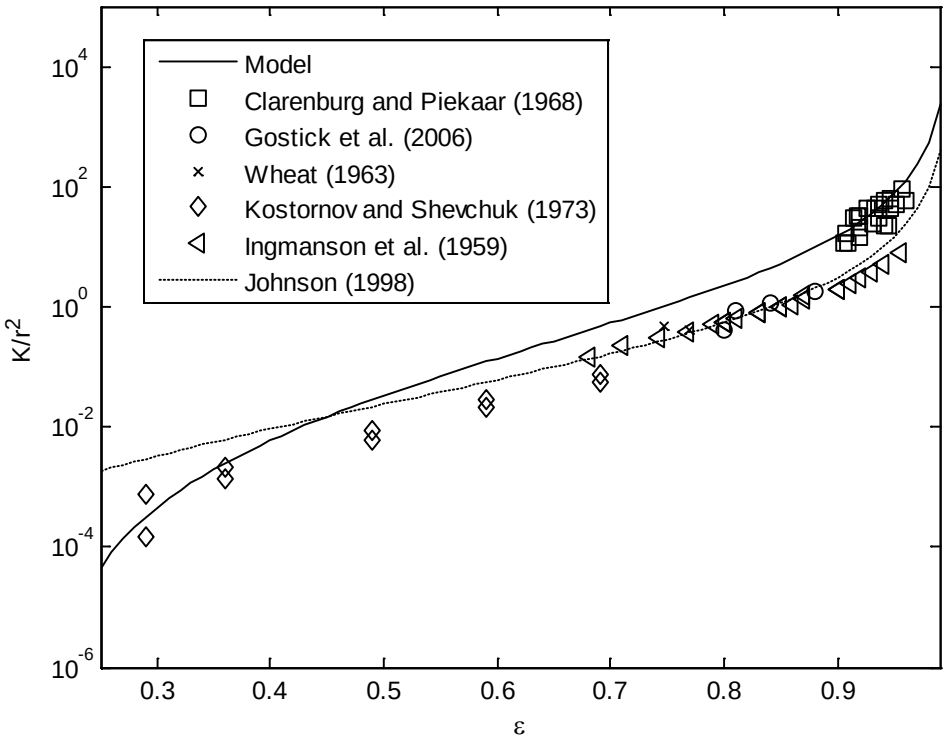

Figure 4-1: Comparison between the fractal model and experimental results

4.4. Concluding remarks

A fractal approach was applied to model the permeability of 2D layered fibrous media. The model of dimensionless permeability is expressed as a function of porosity and fractal dimension, and the prediction of permeability agrees well with

the experimental results. It is also found that the overall permeability is great sensitive with the maximum pore size of the fibrous system. This statistical model of permeability predictions is available over the whole range of porosities, while the deterministic models reported in Chapter 3 are only applicable to fibrous materials at high porosity or low porosity regimens. Note that the fractal model is not as accurate as the deterministic models as it is based on statistical information of fibrous structures and estimate of the ratio between minimum and maximum pore sizes, but it can rapidly provide a qualitative prediction of transport trends.

However, the fractal distribution of pore size is more like a phenomenology. Further physical understanding of the generation of fractal geometry in both natural and scientific areas is required.

Chapter 5 Deterministic models for flow through dual-scale fibrous media

5.1. Introduction

Fiber arrays and nonwovens can be considered as single-scale fibrous materials, which were studied in Chapter 3 and Chapter 4. In woven or knitted fabric materials, the void pores in the yarns and between the yarns are always in two different scales, which make the transport behaviors more complex.

Apart from experimental measurements, previous models of dual-scale permeability of fibrous materials were based on numerical simulations of fluid flows in both intra- and inter yarns domains simultaneously (Wang et al., 2006). The overall permeability was then calculated by back substituting the ratio of pressure gradient and flow flux into Darcy's law.

To reduce computational cost, Brinkman equation was used to describe fluid flows in intra-yarn area. For instance, Phelan and Wise (Phelan and Wise, 1996) and Ngo and Tamma (Ngo and Tamma, 2001) performed numerical simulations based on Brinkman equation and Stokes equation inside and outside the porous yarns, respectively.

Although great progress has been made in numerically determining dual-scale permeability of fibrous materials, it is still difficult but necessary to find the analytical link between the dual-scale microstructures and the resulting permeability.

To this end, this chapter is aimed at theoretically modeling gas flow through dual-scale fibrous materials. The inter-yarn permeability is determined by Stokes equation with a “slip” flow boundary in the interface between yarns and open channels, while the intra-yarn permeability is calculated by Darcy’s law instead of solving Brinkman equation numerically. Based on this modification, the overall transverse permeability of fibrous media is determined by a network treatment of interconnected sub-areas in terms of inter-yarn and intra-yarn permeabilities. The proposed dual-scale model is expressed as a function of porosity, fiber radius, fiber shape, and packing pattern. In addition, a simple but effective semi-analytical model is provided for quick prediction. The categories of important geometric factors considered in the dual-scale model are illustrated in Fig. 5-1.

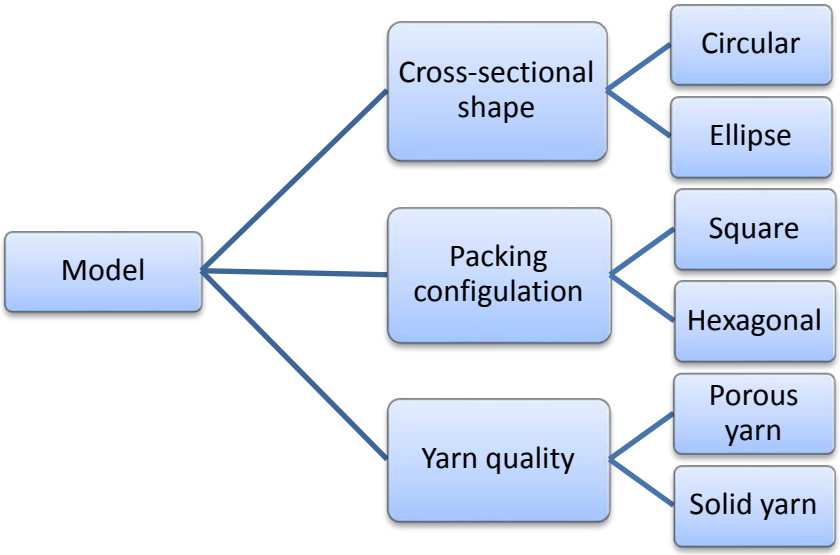

Figure 5-1: Category of geometric factors

The assumptions in this study are necessarily made, viz.:

1. The aligned yarns are made up of straight filaments. The cross-section of all filaments is circular.

2. All the filaments are impermeable, and the flow takes place only in the voids between filaments and yarns.

3. The fiber radius is much larger than the mean free path of the fluid molecules, and thus continuum hypothesis of Newton's law holds.

5.2. Aligned yarns

In dual-scale fibrous media, it is necessary to define the two relevant porosities: the yarn porosity ε_y, as the ratio of the void volume to the total volume of a yarn; and the weave porosity ε_w, as the ratio of the void volume to the total volume of the weave assuming all the yarns are solid.

5.2.1. Model generation

The permeabilities of inter-yarn and intra-yarn are determined respectively before conducting the network treatment. Higher fiber volume fractions are of most interest in composite applications (Phelan and Wise, 1996). Thus, the lubrication approach, dealing well with flow in densely packed particles or cylinders, is employed to calculate the inter-yarn permeability. The velocity component in vertical direction (y-direction) is found to be much smaller than that in horizontal direction (x-direction) (Li et al., 2002). Under such circumstance, Stokes equation can be simplified as:

$$\frac{dp}{dx} - \mu \frac{d^2u}{dy^2} = 0. \qquad (5\text{-}1)$$

The Brinkman relationship (Brinkman, 1947), which has been successfully and widely applied to calculate intra-yarn permeability in dual-scale porous materials

(Ngo and Tamma, 2001, Ranganathan et al., 1996, Phelan and Wise, 1996), is re-written as follows:

$$-\frac{dp}{dx}+\mu_e\frac{d^2u_p}{dy^2}-\frac{\mu}{K_p}u_p=0. \tag{5-2}$$

where K_p is the intra-yarn permeability, u_p is the volume averaged velocity of intra-yarn region, and μ_e is the effective viscosity in the porous yarn. K_p can be determined by Eq. (3-50) and Eq. (3-51) for squarely and hexagonally packed fibers, respectively. Brinkman equation has the same order of differential operator with Stokes equation, so the continuity of shear stress across the fluid/porous interface is ensured.

Beavers and Joseph (Beavers and Joseph, 1967) carried out experiments of measuring permeability in a hollow channel bounded by a porous medium at the interface and found the velocity at the interface different from the average filter velocity within the porous material. The interface velocity is named as “slip” velocity in this thesis. Beavers and Joseph (Beavers and Joseph, 1967) found the “slip” velocity proportional to the shear rate of the open channel flow at the interface by a scale analysis:

$$\frac{du}{dy}=\frac{\alpha_s}{\sqrt{K_p}}\left(u_s-\left\langle u_p\right\rangle\right), \tag{5-3}$$

where, α_s is considered as slip coefficient, u_s is the slip velocity at the interface, $\left\langle u_p\right\rangle$ is the average filter velocity in the porous medium.

Parallel flows through an open channel and a bounding porous medium can be

seen in Fig. 5-2. The flow deep in the porous medium is dominantly pressure-driven, while the flow near the interface is mainly driven by the shear of the open-channel flow. The porous medium is assumed homogeneous, so the pressure gradient along the flow direction is uniformly distributed. The pressure gradient in the porous medium can be expressed as: $\frac{dp}{dx} = \nabla p = -\frac{\mu}{K_p}\langle u_p \rangle$, which is substituted into Eq. (5-2). Therefore, the simplified Brinkman equation is given by:

$$\frac{\mu}{K_p}\langle u_p \rangle + \mu_e \frac{d^2 u_p}{dy^2} - \frac{\mu}{K_p} u_p = 0. \tag{5-4}$$

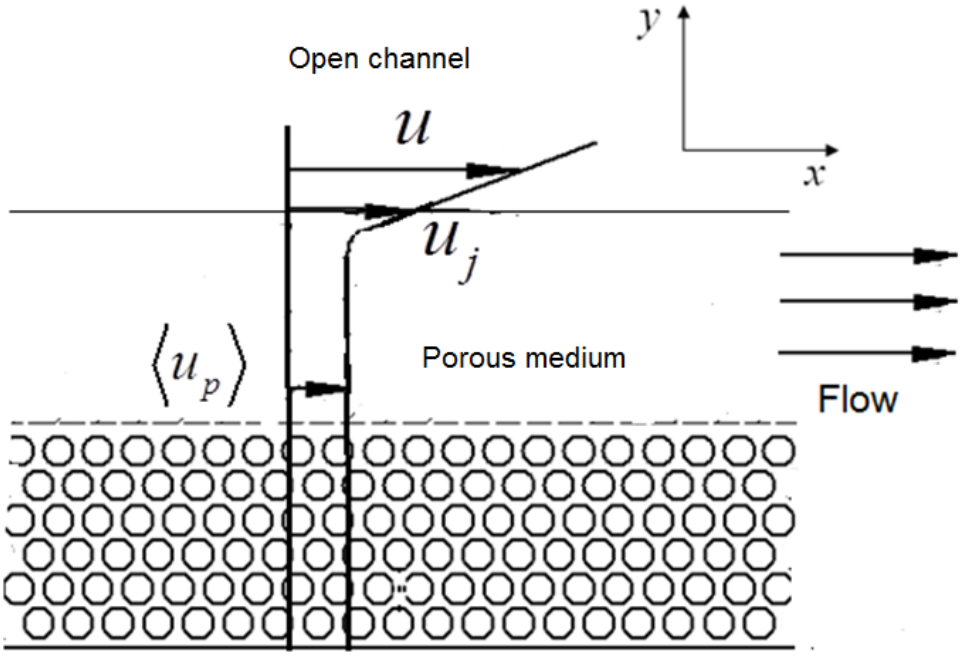

Figure 5-2: Schematic of velocity profile in a porous medium and in the adjacent open channel

Based on that $u(0)$ is equal to u_j and $u(y)$ increases to zero with decreasing y ($y \le 0$) deep in the porous medium, the solution of Eq. (8) is obtained:

$$u_p(y) = \left(u_s - \langle u_p \rangle\right) e^{y/\sqrt{K_p}} + \langle u_p \rangle. \quad (5\text{-}5)$$

The penetration depth of flow in the porous medium is of order $\sqrt{K_p}$ (Saffman, 1971). In the intra-yarn space, it is found that $\sqrt{K_p} < r$ when $\varepsilon_y < 0.9$ in Fig. 3-6, and common yarns contain 1000 to 12000 filaments (Phelan and Wise, 1996). Therefore, the penetration depth is much smaller than the yarn radius and the intra-yarn flow can be approximately characterized by the Darcy permeability K_p.

There are several types of stress boundary conditions between the porous medium and the fluid layer (Alazmi and Vafai, 2001). The latest model of Ochoatapia and Whitaker's (Ochoatapia and Whitaker, 1995) introduced a shear stress jump condition based on the non-local form of the volume-averaged Stokes equation:

$$\frac{\mu}{\varepsilon}\frac{du}{dy}\bigg|_{y=0} - \mu\frac{du_p}{dy}\bigg|_{y=0} = \gamma\frac{\mu}{K_p}u_p(0), \quad (5\text{-}6)$$

where the effective viscosity of the porous medium is taken as μ/ε, and β is an adjustable parameter related to microstructures of the porous medium. The parameter γ on the order of one is always experimentally determined and varies with the flow velocity, which is always an unknown of the problem (Goyeau et al., 2003). It is shown that γ has negligible effect on the results of flow velocity in fluid/porous layers (Alazmi and Vafai, 2001), so the exact determination of β is not important for the present purpose of developing a simplified model of permeability. Therefore, it is assumed $\gamma = 0$ in this study and the interfacial condition of continuum shear stress is satisfied:

$$\mu_e\frac{du}{dy}\bigg|_{y=0} - \mu\frac{du_p}{dy}\bigg|_{y=0} = 0. \quad (5\text{-}7)$$

Substituting Eq. (5-3) and Eq. (5-5) into Eq. (5-7) results in $\alpha = \sqrt{\mu_e / \mu}$. It is difficult to accurately determine μ_e / μ for any given porous system (Neale and Nader, 1974), but assuming μ_e equal to μ provides satisfactory correlations of experimental and numerical results in a great many cases (Yu and Lee, 2000, Ranganathan et al., 1996, Phelan and Wise, 1996, Ngo and Tamma, 2001). Therefore, $\alpha = 1$ is considered here and the "slip" velocity is given by:

$$u_s = \sqrt{K_p}\frac{du}{dy} + \langle u_p \rangle. \tag{5-8}$$

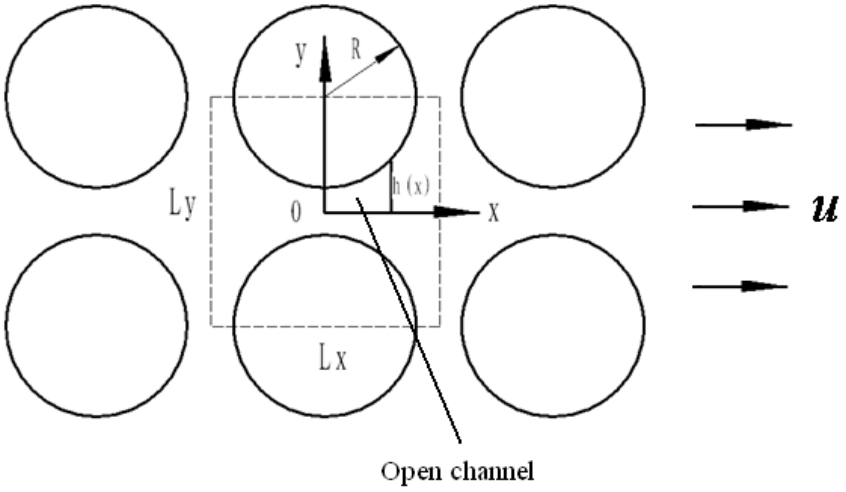

Figure 5-3: Schematic of flows in the open channel between fibers in the representative cell

Solving Eq. (5-2) and considering the boundary conditions of $u\left[h(0)\right] = u_s$ and $\left.\frac{du}{dy}\right|_{y=0} = 0$ provides the parabolic velocity profile in the channel in Fig. 5-3:

$$u(x)=-\left[\frac{h^2(x)}{2}\left(1-\frac{y^2}{h^2(x)}\right)+h(x)\sqrt{K_p}+K_p\right]\frac{1}{\mu}\frac{dp}{dx}, \tag{5-9}$$

where $h(x)$ is the half height of the channel between yarns. The relevant inter-yarn permeability can be easily derived from Darcy's law:

$$K_i=\frac{h^2(x)}{2}\left(1-\frac{y^2}{h^2(x)}\right)+h(x)\sqrt{K_p}+K_p. \tag{5-10}$$

The macro-scale flow flux Q through the network is the sum of the sub-fluxes of inter-yarns (Q_i) and intra- yarns (Q_p), which reads,

$$Q=Q_i+Q_p=\frac{KL_y\Delta p}{\mu L_x}, \tag{5-11}$$

where $Q_i=2\int_0^h K_i dy$, $Q_p=\left(L_y-2h\right)K_p$, and L_x and L_y represent the side lengths of the representative cell in x-direction and y-direction, respectively. Thus, the pressure drop of the cell can be calculated as:

$$\Delta p=2Q(x)\mu\int_0^{L_x/2}\frac{1}{\frac{2}{3}h^3(x)+2h^2(x)\sqrt{K_p}+L_yK_p}dx. \tag{5-12}$$

where L_x and L_y represent the side lengths of the representative cell in x-direction and y-direction, respectively. With the total flow rate $Q(x)=\langle u\rangle L_y$ and Darcy's law $\langle u\rangle=\frac{K}{\mu}\frac{\Delta p}{L_x}$, the general model of the overall permeability K can be obtained based on Eq. (5-12):

$$K = \frac{L_x}{2L_y\left(\int_0^a \frac{1}{\frac{2}{3}h^3(x)+2h^2(x)\sqrt{K_p}+L_yK_p}dx + \int_a^{L_x/2} \frac{1}{\frac{2}{3}h^3(x)+2h^2(x)\sqrt{K_p}+2hK_p}dx\right)}, \qquad (5\text{-}13)$$

where a is the largest cross-sectional length of the yarn along x-direction. Note that the yarns are considered as consisting of bundles of regularly parallel filaments, so Eq. (5-13) can also be applied to calculate the intra-yarn permeability with $K_p = 0$ with filaments instead of solid yarns.

A. Circular yarns in square configuration

The overall permeability of dual-scale fibrous materials with different packing arrangements and cross-sectional shapes can be calculated based on Eq. (5-13).

(a)

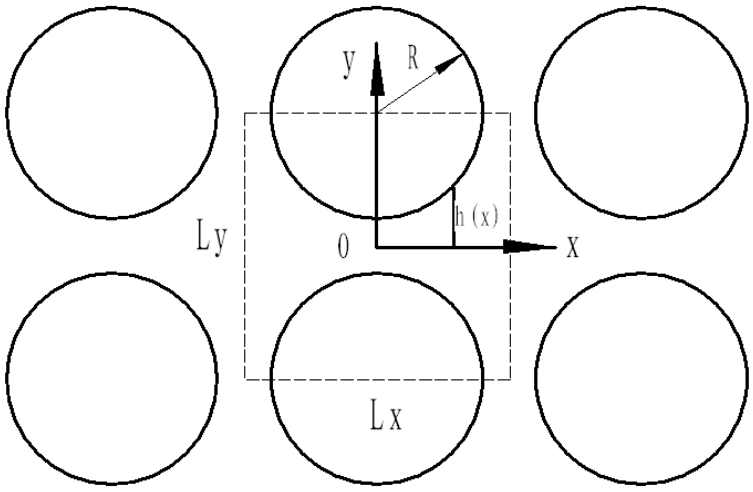

(b)

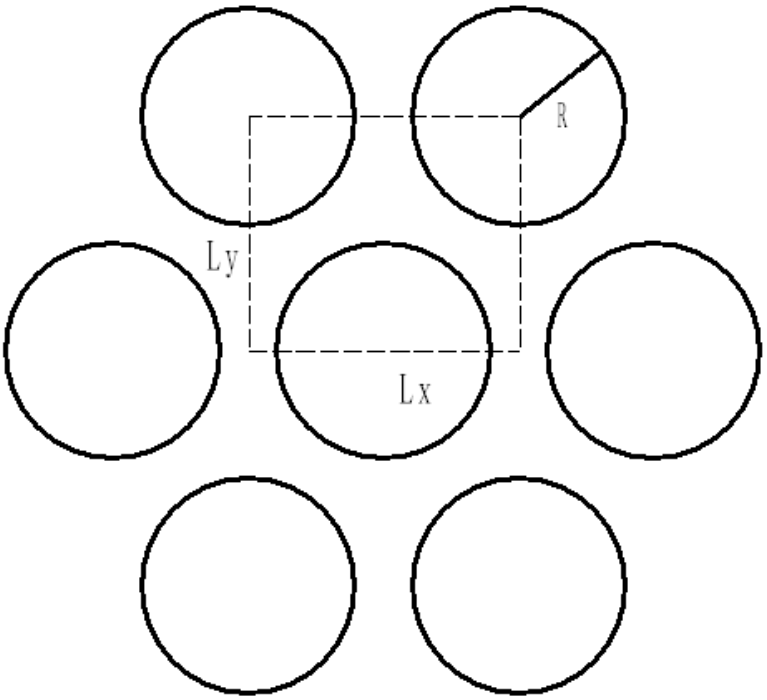

(c)

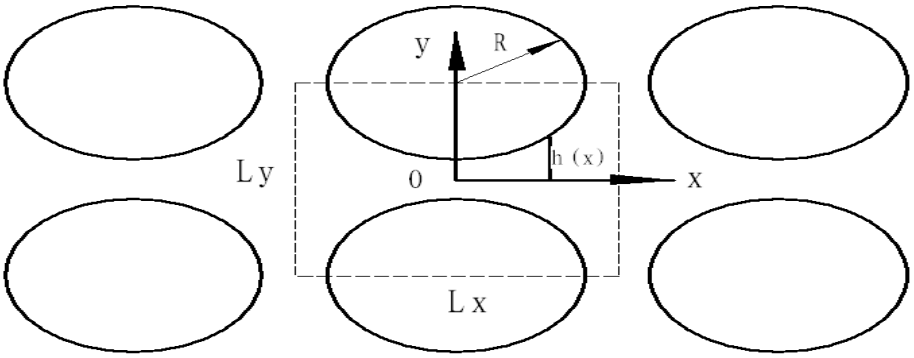

(d)

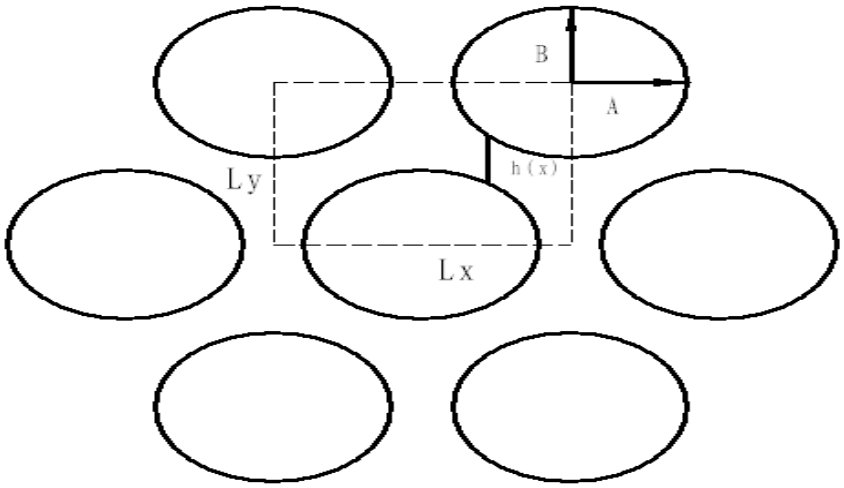

Figure 5-4: (a) Circular yarns of square arrangement, (b) circular yarns of hexagonal arrangement, (c) elliptical yarns of square arrangement, and (d) elliptical yarns of hexagonal arrangement in the representative cell

The model is expressed in terms of porosity and fiber radius, both of which are relatively easy to measure. Herein, the weave porosity ε_w (assuming all yarns are solid) is written as:

$$\varepsilon_w = 1 - \frac{\pi R^2}{L_x L_y}, \tag{5-14}$$

where R is the yarn radius. For square packing pattern of yarns in Fig. 5-4 (a), the side lengths of the representative in both x-direction and y-direction are equal, viz:

$$L_x = L_y = R\sqrt{\frac{\pi}{1-\varepsilon}}. \tag{5-15}$$

The half height of channel is $h(x) = L_y / 2 - \sqrt{R^2 - x^2}$ when $|x| \le R$; and $h(x) > L_y / 2$ when $L_x / 2 \ge |x| > R$.

The form of the permeability model for square array of circular yarns $K_{s,c}$ can be simplified by neglecting the integration term between a and $L_x / 2$, i.e. setting $a = R$ in Eq. (5-15), because there is no solid surface in that area to apply any resistance against flow. The simplification is proved accurate in the next section. The models of other structures also follow this simplification. The model of circular yarns in square configuration is therefore given by:

$$K_{s,c} = \frac{1}{2\int_0^R \frac{1}{\frac{2}{3}\left(\frac{1}{2}R\sqrt{\frac{\pi}{1-\varepsilon}} - \sqrt{R^2 - x^2}\right)^3 + 2\left(\frac{1}{2}R\sqrt{\frac{\pi}{1-\varepsilon}} - \sqrt{R^2 - x^2}\right)^2 \sqrt{K_p} + R\sqrt{\frac{\pi}{1-\varepsilon}}K_p} dx}. \quad (5\text{-}16)$$

B. Circular yarns in hexagonal configuration

Next, it comes to the question of hexagonal packing, which is presented in Fig. 5-4 (b). Both of yarns of square and hexagonal packed configuration have filaments with square packing (see Fig. 5-5 (a)) or hexagonal packing (see Fig. 5-5 (b)). The pressure drop over each slot in the hexagonal array is apparently the same as in the square case, so the pressure drop over the representative cell is twice of square case in Eq. (5-14).

The half height of the channel between yarns is $h(x) = \frac{\sqrt{3}}{3}L_y - \sqrt{R^2 - x^2}$ when $|x| \le R$. The side lengths of the cell for hexagonal arrangement of yarns are as follows:

$$L_x = \sqrt{\frac{2\sqrt{3}}{3}\frac{\pi}{1-\varepsilon}}, \tag{5-17}$$

and

$$L_y = R\sqrt{\frac{\sqrt{3}}{2}\frac{\pi}{1-\varepsilon}}. \tag{5-18}$$

Substituting Eqs. (5-16, 5-17 and 5-18) into Eq. (5-15) leads to the overall permeability of hexagonal structure $K_{h,c}$, which is given by:

$$K_{h,c} = \frac{1}{2\sqrt{3}\int_0^R \frac{1}{\frac{2}{3}\left(R\sqrt{\frac{\sqrt{3}}{2}\frac{\pi}{1-\varepsilon}} - \sqrt{R^2-x^2}\right)^3 + 2\left(R\sqrt{\frac{\sqrt{3}}{2}\frac{\pi}{1-\varepsilon}} - \sqrt{R^2-x^2}\right)^2 \sqrt{K_p} + R\sqrt{\frac{\sqrt{3}}{2}\frac{\pi}{1-\varepsilon}}K_p}dx}. \tag{5-19}$$

(a)

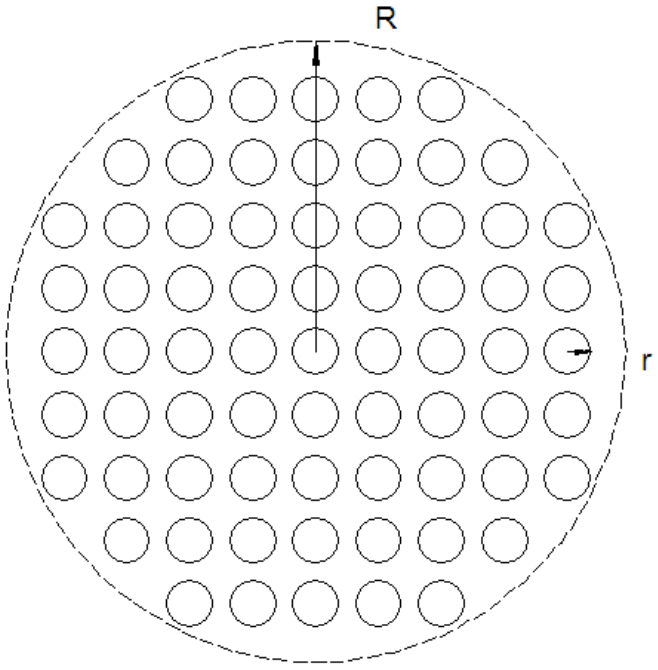

(b)

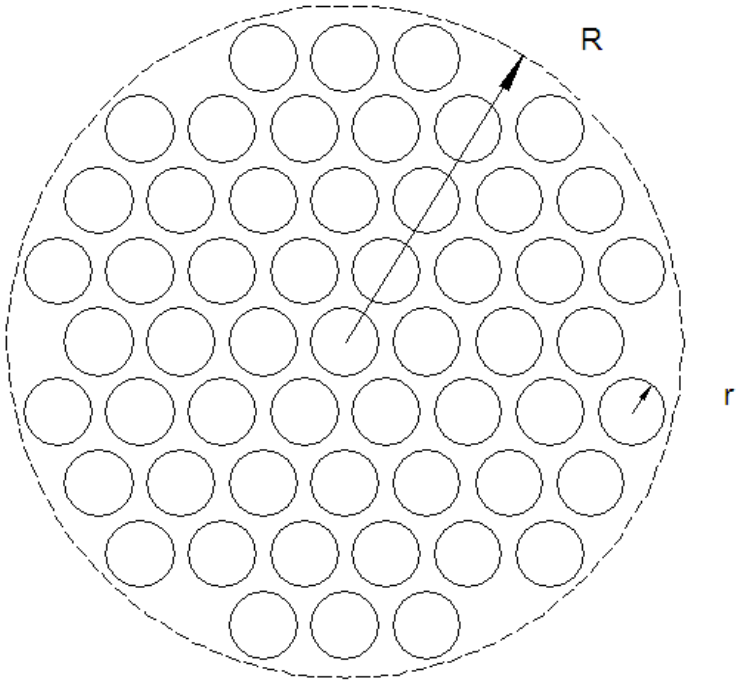

(c)

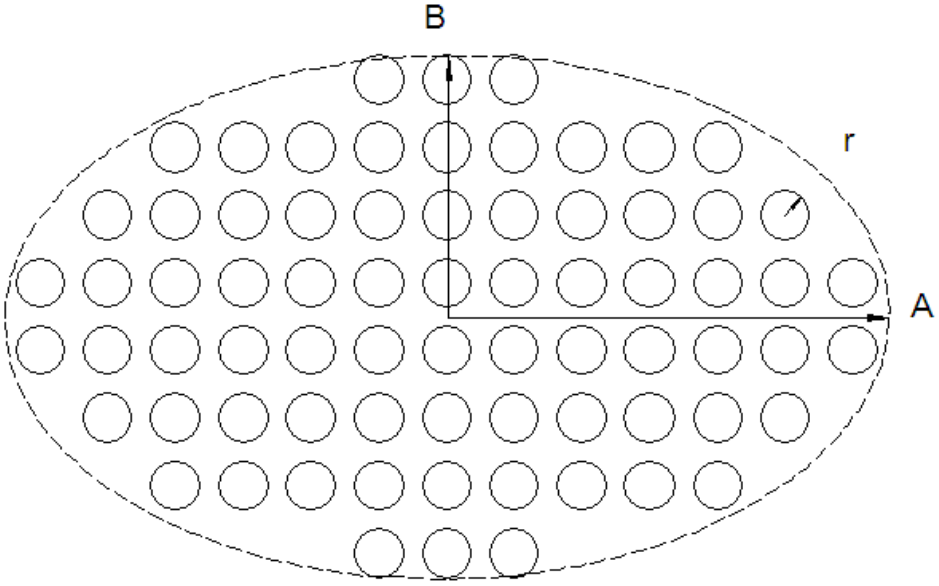

(d)

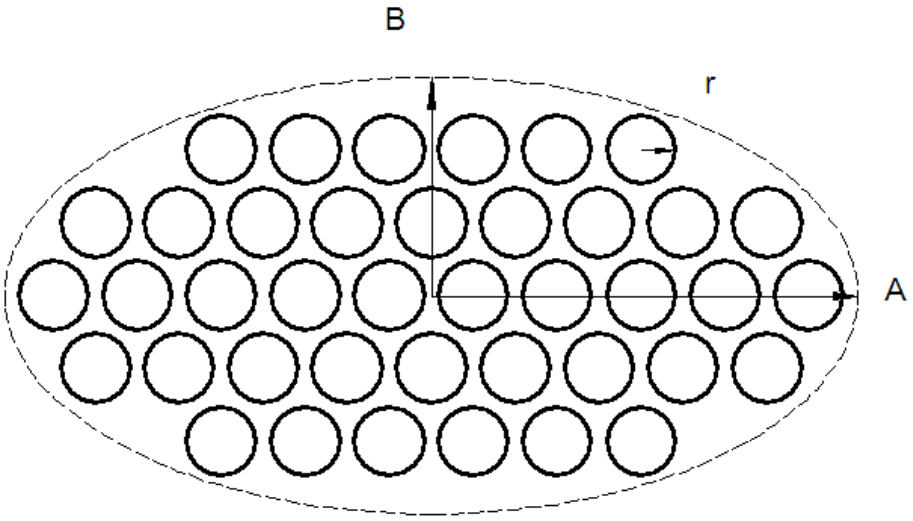

Figure 5-5: Schematic of (a) a circular yarn made up of squarely packed filaments, (b) a circular yarn made up of hexagonally packed filaments, (c) an elliptical yarn made up of squarely packed filaments, and (d) an elliptical yarn made up of hexagonally packed filaments

C. Elliptical yarns in square configuration

For more general cases such like compressed fibrous layers, yarns with elliptical cross-sectional geometry are considered. The studies reported here are generated by imposing a axis ratio $\lambda_e = A/B = L_x/L_y$, where A is the major axis and B is the minor axis of an elliptical fiber.

The square arrays of elliptical yarns are demonstrated in Fig. 5-4 (c), where the yarns contain filaments with square packing (see Fig. 5-5 (c)) or hexagonal packing (see Fig. 5-5 (d)). The weave porosity is accordingly given by:

$$\varepsilon_w = 1 - \frac{\pi AB}{L_x L_y}. \tag{5-20}$$

The side lengths of the representative cell are calculated respectively as:

$$L_x = \sqrt{\lambda AB \frac{\pi}{1-\varepsilon}} \quad \text{and} \quad L_y = \sqrt{\frac{AB}{\lambda} \frac{\pi}{1-\varepsilon}}. \tag{5-21}$$

The half height of channel in this case is $h(x) = L_y - B\sqrt{1 - \frac{x^2}{A^2}}$.

As most of the pressure difference comes from the narrow gap between fibers, the mathematical forms for elliptical yarns is simplified as the circular cases do, i.e. $a = A$:

$$K_{s,e} = \frac{\lambda}{2\int_0^A \frac{1}{\frac{2}{3}\left(\sqrt{\frac{AB}{\lambda}\frac{\pi}{1-\varepsilon}} - B\sqrt{1-\frac{x^2}{A^2}}\right)^3 + 2\left(\sqrt{\frac{AB}{\lambda}\frac{\pi}{1-\varepsilon}} - B\sqrt{1-\frac{x^2}{A^2}}\right)^2 \sqrt{K_p} + \sqrt{\frac{AB}{\lambda}\frac{\pi}{1-\varepsilon}} K_p} dx}. \tag{5-22}$$

D. Elliptical yarns in hexagonal configuration

For hexagonally staggered array of elliptical yarns shown in Fig. 5-4 (d), the weave porosity is given by Eq. (5-20), but the side lengths in x-direction and y-direction respectively of the representative cell are expressed as:

$$L_x = \sqrt{\frac{2\sqrt{3}}{3} \lambda AB \frac{\pi}{1-\varepsilon}}, \tag{5-23}$$

and

$$L_y = \sqrt{\frac{\sqrt{3}}{2}\frac{AB}{\lambda}\frac{\pi}{1-\varepsilon}}. \tag{5-24}$$

One derives the half height of channel according to its structural configuration in Fig. 5-4 (d) as: $h(x) = L_y - B\sqrt{1-\frac{x^2}{A^2}} - B\sqrt{1-\frac{\left(x-\frac{L_x}{2}\right)^2}{A^2}}$.

Finally, the model for elliptical yarns in hexagonal arrangement is obtained:

$$K_h = \frac{\lambda}{2\sqrt{3}\int_{L_x/2-A}^{L_x/4}\left(\begin{array}{l}\frac{2}{3}\left(\sqrt{\frac{\sqrt{3}}{2}\frac{AB}{\lambda}\frac{\pi}{1-\varepsilon}} - B\sqrt{1-\frac{x^2}{A^2}} - B\sqrt{1-\frac{\left(x-\frac{L_x}{2}\right)^2}{A^2}}\right)^3 + \\ 2\left(\sqrt{\frac{\sqrt{3}}{2}\frac{AB}{\lambda}\frac{\pi}{1-\varepsilon}} - B\sqrt{1-\frac{x^2}{A^2}} - B\sqrt{1-\frac{\left(x-\frac{L_x}{2}\right)^2}{A^2}}\right)^2\sqrt{K_p} \\ +\sqrt{\frac{\sqrt{3}}{2}\frac{AB}{\lambda}\frac{\pi}{1-\varepsilon}}K_p\end{array}\right)^{-1} dx}. \tag{5-25}$$

5.2.2. Semi-analytical estimate

The channel close to the narrowest gap between yarns is more or less aligned with the flow direction. The widths of the channel are assumed as parallel walls. As most inter-yarn flow resistances of solid yarns exist near the narrowest gap (Ranganathan et al., 1996, Sobera and Kleijn, 2006) and the intra-yarn permeability is commonly much less than the inter-yarn permeability, the overall permeability may be estimated within the short channel. The intra-yarn permeability K_p is

found to be an additional component of the overall permeability K based on $Q(x)=Q_i(x)+Q_p(x)$ for parallel flows within the fluid/porous layers. Thus, the inter-yarn velocity without the additional term of K_p becomes:

$$u_{inter}=-\left[\frac{h^2(x)}{2}\left(1-\frac{y^2}{h^2(x)}\right)+h(x)\sqrt{K_p}\right]\frac{1}{\mu}\frac{dp}{dx}. \qquad (5\text{-}26)$$

In Eq. (5-26), the term $\frac{h^2(x)}{2}\left(1-\frac{y^2}{h^2(x)}\right)$ accounts for the permeability of impermeable solid yarns. The term $h(x)\sqrt{K_p}$ accounts for the "slip" effect at the interface, which is independent of the former term. Therefore, the overall permeability can be estimated as a sum of inter-yarn permeability for solid yarns, intra-yarn permeability, and "slip" term:

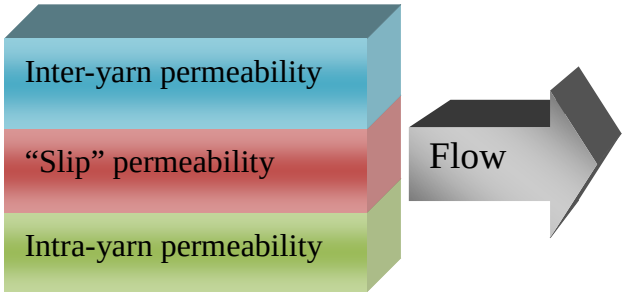

Figure 5-6: Network of inter-yarn, "slip", and intra-yarn permeabilities along the flow direction

$$K=K_i+K_p+jh_{\min}\sqrt{K_p}, \qquad (5\text{-}27)$$

where $h_{\min}$ is the minimum distance between yarns and j is an empirical constant, and K_i represents inter-permeability for solid yarns. $h_{\min}$, close to which flow

velocity varies dramatically, is selected as the characteristic length to satisfy the dimensional equilibrium of Eq. (5-27). For different fibrous arrangements, $h_{\min}$ has different definition as following:

$h_{\min} = \left(\sqrt{\frac{\pi}{1-\varepsilon}} - 2 \right) R$ for square packing circular yarns,

$h_{\min} = \left(\sqrt{\frac{\sqrt{3}\pi}{2(1-\varepsilon)}} - 2 \right) R$ for hexagonal packing circular yarns,

$h_{\min} = \left(\sqrt{\frac{\pi}{1-\varepsilon}} - 2 \right) B$ for square packing elliptical yarns with $\lambda = 2$,

and

$h_{\min} = \left(\sqrt{\frac{2\pi}{\sqrt{3}(1-\varepsilon)}} - 2\sqrt{1 - \frac{\pi}{8\sqrt{3}(1-x)}} \right) B$ for hexagonal packing elliptical yarns

with $\lambda = 2$.

5.2.2. Results and discussion

In this Section, the comparison between the proposed model with those numerical, experimental and analytical results available in the literature is presented. The existing results are generally reported as Darcy permeability, ratio of overall and intra-yarn permeability, flow resistance, and so forth, but most of them are converted to dimensionless permeability against weave porosity for better comparison. Therefore, the permeability K is conducted by dividing square of the yarn radius R^2 for circular yarns or product of semi-major and semi-minor axis AB for ellipses.

Before using the model of Eq. (5-15) to predict permeability of fibrous system, the effective limits of inter-yarn channels are particularly investigated based on Eq. (5-15). It is found that the pressure decreases dramatically near the domain of the smallest distance between fibers and thus a short distance of gap nearby or effective channel length s is only necessarily considered, and the related model is greatly simplified for that (Gebart, 1992). However, this conclusion is questionable when the yarns become porous and permeable. To investigate the effect of the length of the channel (or gap) in the calculation on the predicted permeability, the permeability in x-direction with different chosen length of the channel (or gap) is computed by replacing R with s for circular yarns (see Fig. 5-7) and replacing A with s for elliptical yarns (see Fig. 5-8) based on Eq. (5-15).

(a)

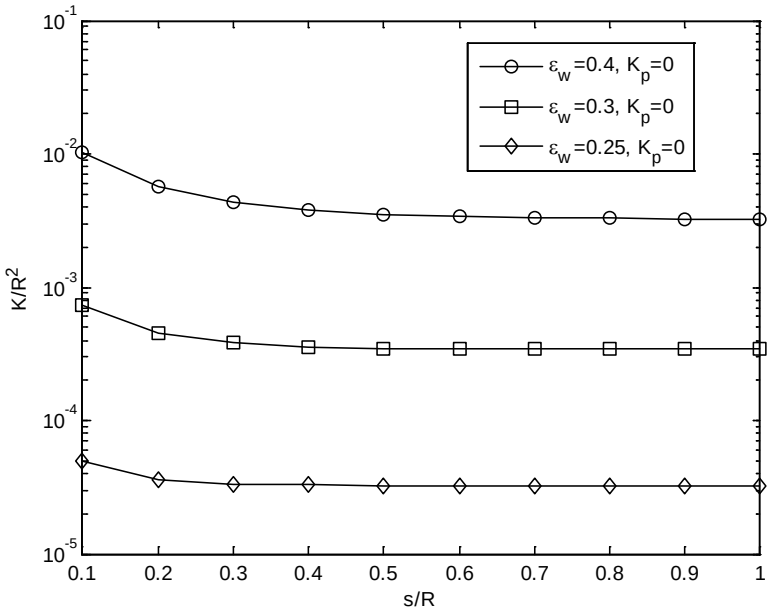

(b)

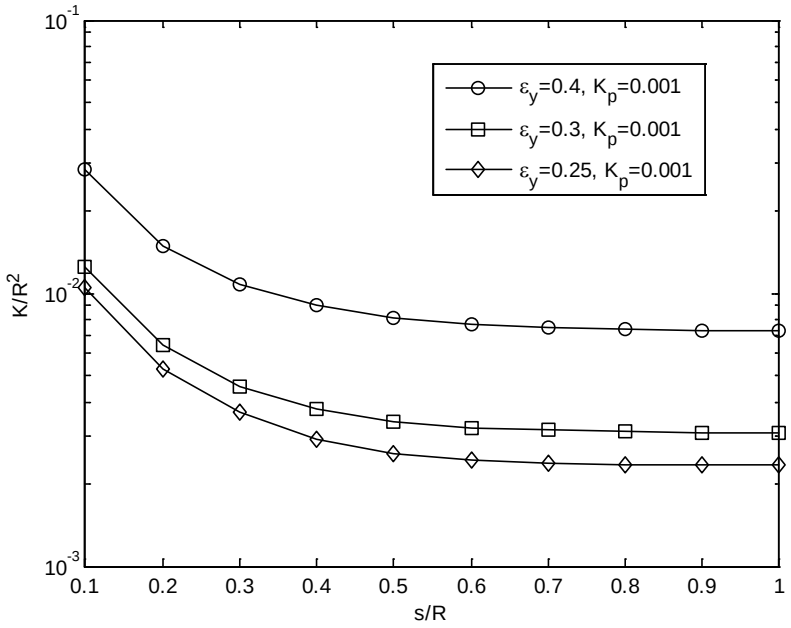

(c)

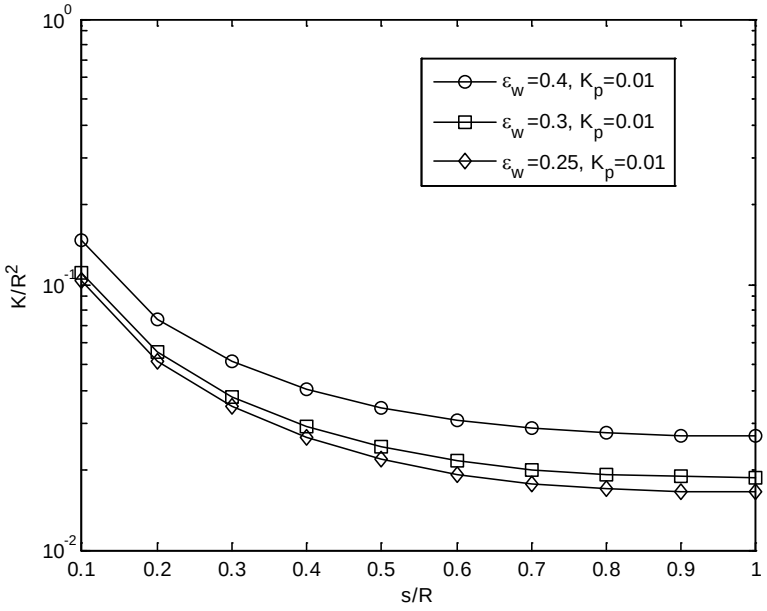

Figure 5-7: Effect of the effective channel length limit (s) on the dimensionless

permeability of the fibrous system. The fibrous systems of circular yarns with weave porosity 0.25, 0.3, and 0.4 have intra-yarn permeability (a) 0; (b) 0.001; (c) 0.01.

(a)

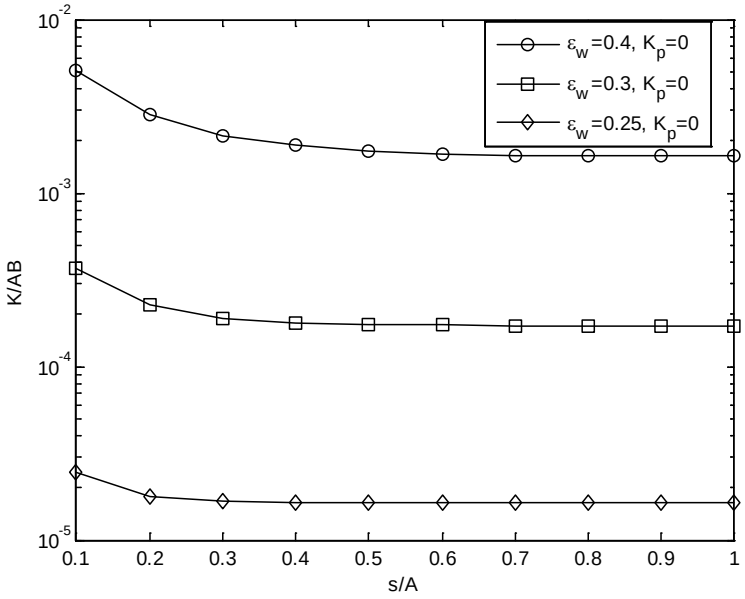

(b)

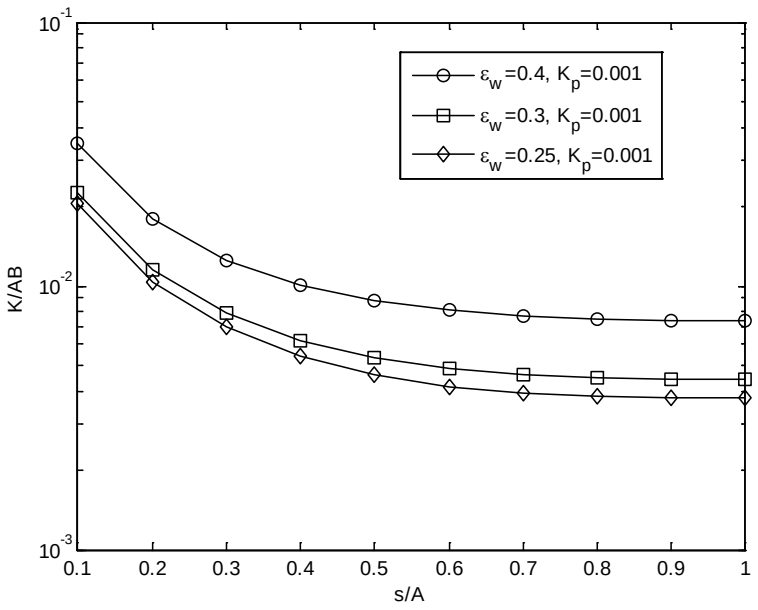

(c)

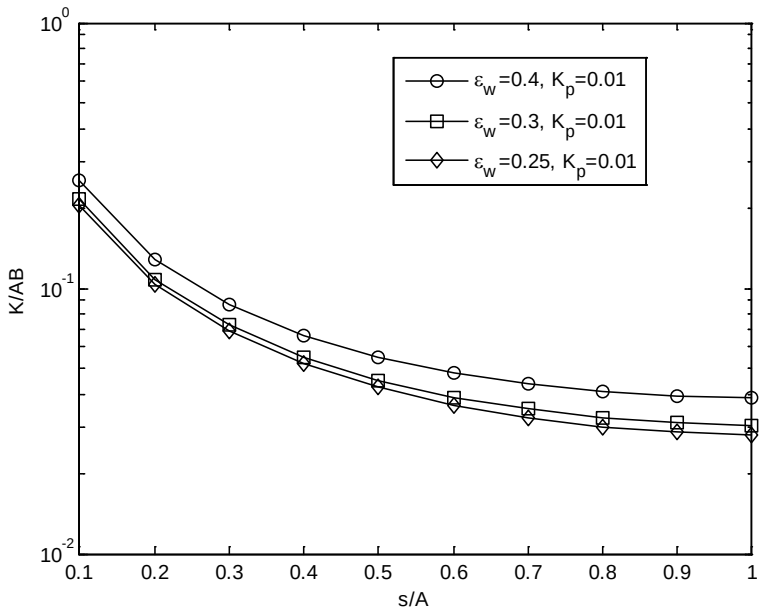

Figure 5-8: Effect of the effective channel length limit (s) on the dimensionless permeability of the fibrous system. The fibrous systems of elliptical yarns of axis ratio 2 with weave porosity 0.25, 0.3, and 0.4 have intra-yarn permeability (a) 0; (b) 0.001; (c) 0.01.

As can be seen, the small domain close to the narrowest gap provides most contribution of fluid flows for the medium with sold yarns and low porosity. To accurately characterize the flow, however, it is important to take into account the full length of the channel (or gap) between the highly porous or elliptical yarns, whose effective channel length increases from Fig. 5-7 and Fig. 5-8. It is found that the lengths of the channel chosen in the calculation, viz. R for circular yarns and A for elliptical yarns, are reasonable without losing accuracy.

The predicted results calculated by employing Eq. (5-16) for square packing pattern, are tested by permeability results of four samples from Sadiq et al.'s (Sadiq

et al., 1995). The squarely packed arrays of yarns have circular cross-sectional shape and are made up of a class of circular nylon filaments (Sadiq et al., 1995). The detailed structural properties of these samples are summarized in Table 5-1. A good agreement between the permeability prediction and the experimental results can be found in Fig. 5-9.

Table 5-1: Darcy permeability and structural parameters of dual-scale fibrous materials of Sadiq et al. (Sadiq et al., 1995)

Sample	ε_w	R (cm)	ε_y	r (cm)	K (m^2)
1	0.60	0.32	0.373	0.036	4.97×10^{-7}
2	0.60	0.32	0.310	0.036	4.76×10^{-7}
3	0.50	0.32	0.247	0.036	1.28×10^{-7}
4	0.49	0.32	0.247	0.036	1.27×10^{-7}

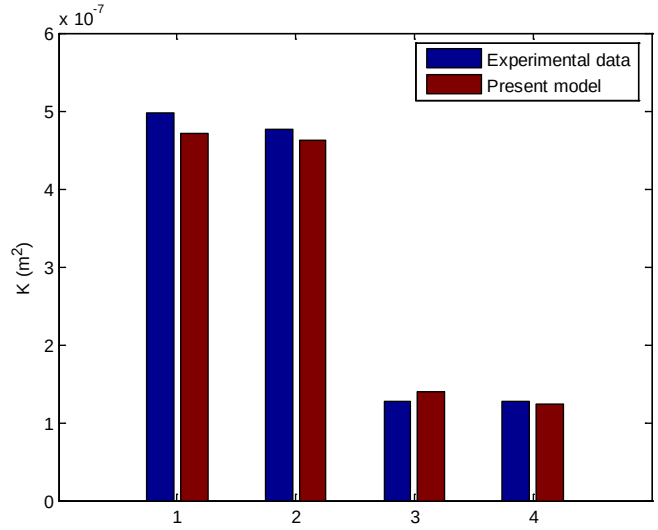

Figure 5-9: Comparison of the model for squarely packed circular yarns with those obtained from experiments by Sadiq et al. (Sadiq et al., 1995).

The dimensionless permeability, calculated by Eq. (5-19), is compared with the numerical values of hexagonal array of circular yarns by Papathanasiou (Papathanasiou, 2001). The yarns were made up of circular filaments in square or hexagonal arrangements. The numerical results were expressed as a function of weave porosity and yarn porosity. In this study, fibrous materials with two different weave porosities as 0.2 and 0.3, and $r = 0.03R$ are considered to evaluate present model. A close agreement between the model and the numerical results for square and hexagonal packing filaments are presented in Fig. 5-10 (a) and Fig. 5-10 (b), respectively. In addition, when the yarn porosity is smaller than 0.6 and the corresponding dimensionless permeability is less than 10^{-5}, the overall permeability is almost not sensitive to the intra-yarn flow. However, when the yarn porosity is greater than 0.6 and the ratio of intra-yarn permeability and inter-yarn permeability becomes larger than 0.01, the overall permeability increases significantly with the increase of intra-yarn permeability.

(a)

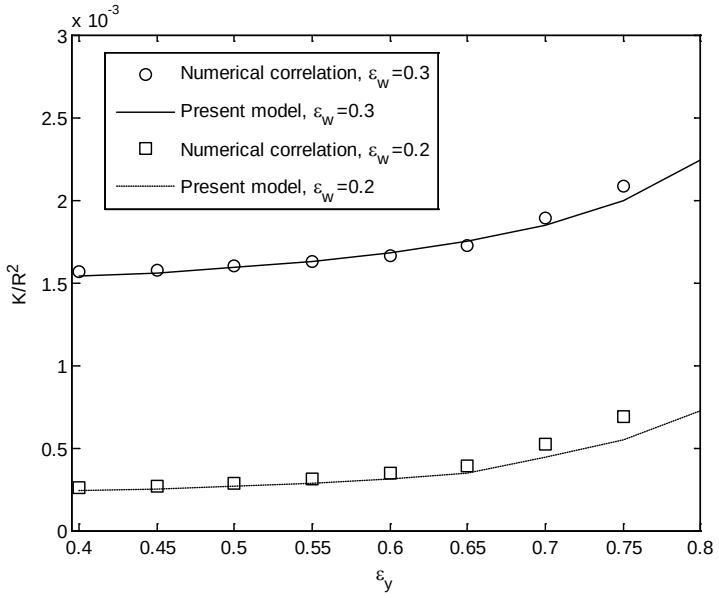

(b)

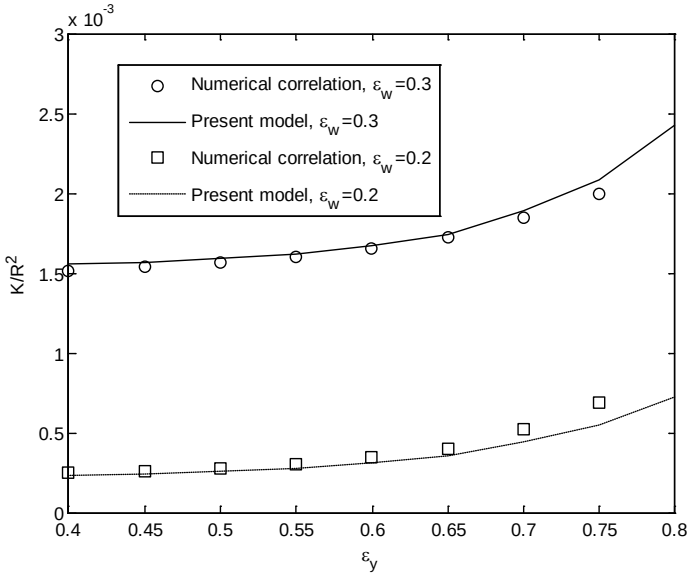

Figure 5-10: Comparison of the model of hexagonally packed circular yarns against numerical results by Papathanasiou (Papathanasiou, 1997). The yarns are made of filaments of (a) square and (b) hexagonal arrangement.

(a)

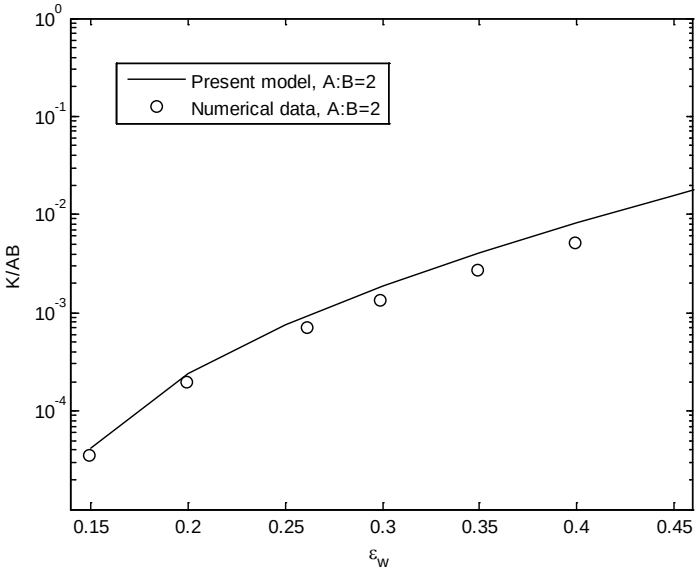

(b)

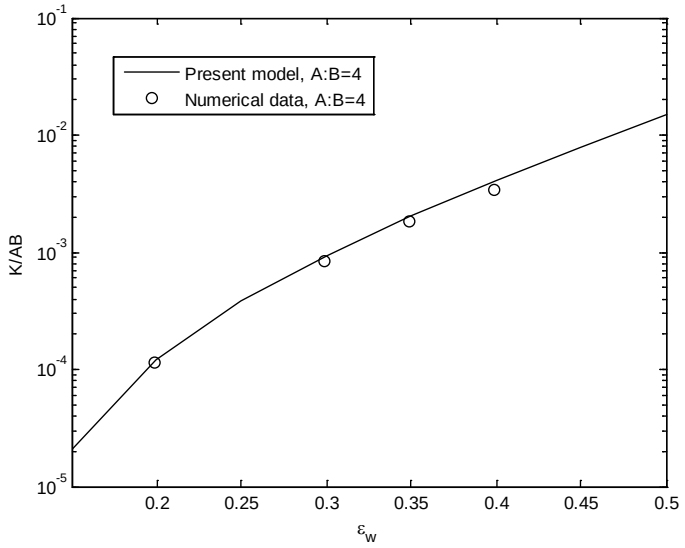

Figure 5-11: Comparison of the model and numerical data (Ranganathan et al., 1996) for hexagonal arrays of solid elliptical yarns with axis ratio (a) 2 and (b) 4.

For yarns of elliptical cross-sectional shape, a computational fluid dynamics package is used by Phelan and Wise (Phelan and Wise, 1996). The yarns are of square packing and a cross-sectional ratio 2. The agreement between the present model of Eq. (5-22) and the numerical data is good for weave porosity 0.25 and 0.3, as shown in Fig. 5-11.

In addition, predicted values of the present model are compared with those computed results by Ranganathan et al. (Ranganathan et al., 1996), who used arrays of hexagonal packed elliptical yarns of axis ratio 2 and 4. It was showed that the small regime close to the smallest gap captures most pressure gradient (Ranganathan et al., 1996). All these numerical values are non-dimensionalized with respect to product of semi-major axis and semi-minor axis. The results shown in Figs. 5-12 (a) and 5-12 (b) indicate good agreement between the proposed model and simulation

results. Moreover, the fibrous material with axis ratio 2 is found to be slightly less permeable than that of ratio 4 when yarns are densely packed. In the other range of porosities, their permeabilities are close to each other, and the effect of cross-sectional shape may be neglected.

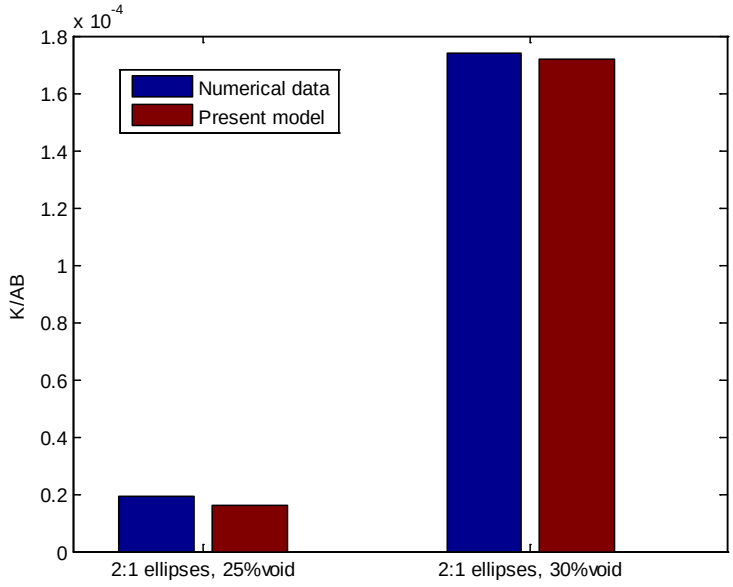

Figure 5-12: Comparison of the model of elliptical yarns of square packing against numerical results by Phelan and Wise (Phelan and Wise, 1996)

The proposed model based on Eq. (5-25) is compared with experimental results of Merhi. et al. (Merhi et al., 2007). In their experiment, the hexagonal arrays of yarns were made up of bundles of glass filaments, with the major axis normal to the flow direction. The circular filaments were found mainly in a hexagonal packing configuration (Merhi et al., 2007). The glass volume fraction in a yarn was about 60% and the all the samples were tested for the same total fiber volume fraction, e.g. 20% (Merhi et al., 2007). The detailed structural properties of these samples are summarized in Table 5-2. Fig. 5-13 reveals a promising agreement between the prediction using the present model and the experimental results.

Table 5-2: Darcy permeability and structural parameters of dual-scale fibrous materials of Merhi et al (Merhi et al., 2007)

Sample	ε_w	$2A(\mu m)$	$2B$ (μm)	ε_y	r (μm)	K (m^2)
1	0.67	700	105	0.4	7.5	2.93×10^{-11}
2	0.67	743	100	0.4	7.5	2.90×10^{-11}
3	0.67	699	93	0.4	7.5	3.45×10^{-11}
4	0.67	782	107	0.4	7.5	4.25×10^{-11}
5	0.67	714	129	0.4	7.5	4.59×10^{-11}

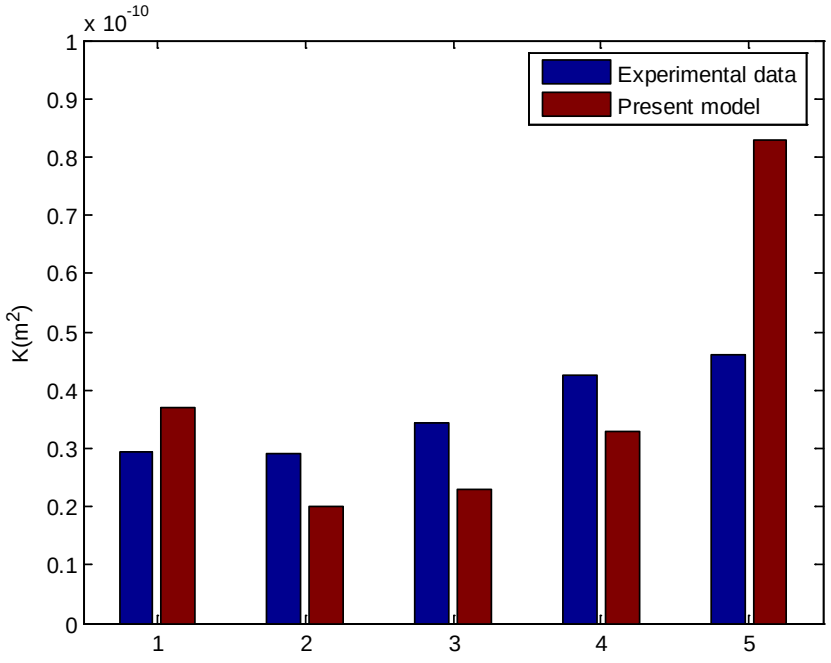

Figure 5-13: Comparison of the model for hexagonal-packed elliptical yarns with those obtained from experiments by Merhi et al. (Merhi et al., 2007)

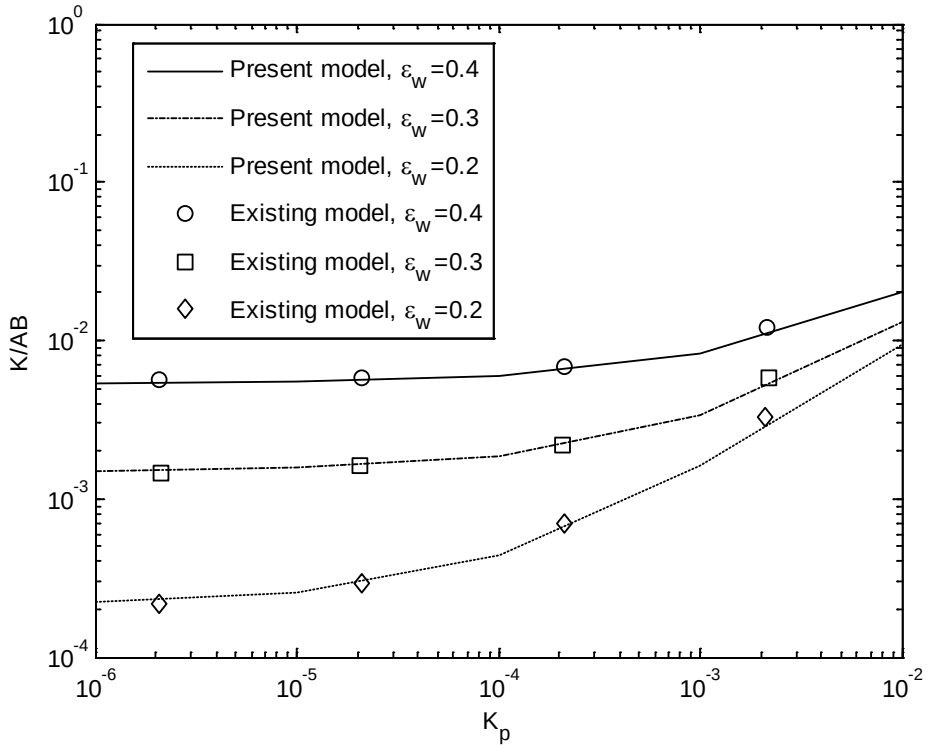

Figure 5-14: Dimensionless permeability of dual-scale fibrous systems as a function of intra-yarn permeability. The model is compared with numerical results of Ranganathan et al. (Ranganathan et al., 1996). The fibrous media are made up of yarns with hexagonal packing at different weave porosity.

Fig. 5-14 presents the dimensionless permeability of hexagonal array of elliptical yarns of axis ratio 2 against intra-yarn permeability based on Eq. (5-26). The fibrous structures with weave porosities of 0.2, 0.3 and 0.4 are studied, and their predicted permeabilities are compared with those predicted using the existing model of Ranganathan et al. (Ranganathan et al., 1996). Ranganthan et al. (Ranganathan et al., 1996) developed a semi-analytical model for staggered elliptical fibrous systems based on solving Stokes equation for external flows and Brinkman law in intra-yarn space. From Fig. 5-14, it can be seen that the prediction of the present model agrees very well with all data of Ranganthan et al. (Ranganathan et al., 1996). Increasing the

weave porosity promotes the overall permeability, but when the intra-yarn permeability is small, the overall permeability keeps being a constant until the intra-yarn permeability reaching a certain value. The intra-yarn permeability increases the overall permeability of dual-scale fibrous materials when the ratio between them is more than 0.01. in addition, for intra-yarn dimensionless permeability around 0.0001, its effect on the overall permeability with a weave porosity of 0.4 is very limited, but it greatly increases the permeability of the structure for a weave porosity of 0.2. It indicates that more fluids have to move through the yarns between yarns when the yarns are densely staggered. On the contrary, when the intra-yarn permeability becomes comparable with or larger than the inter-yarn permeability, the overall permeability increases almost linearly with the intra-yarn permeability. This phenomenon, nevertheless, is not common in reality because the intra-permeabilities in most dual-scale fibrous materials are much lower than the inter-yarn permeabilities.

(a)

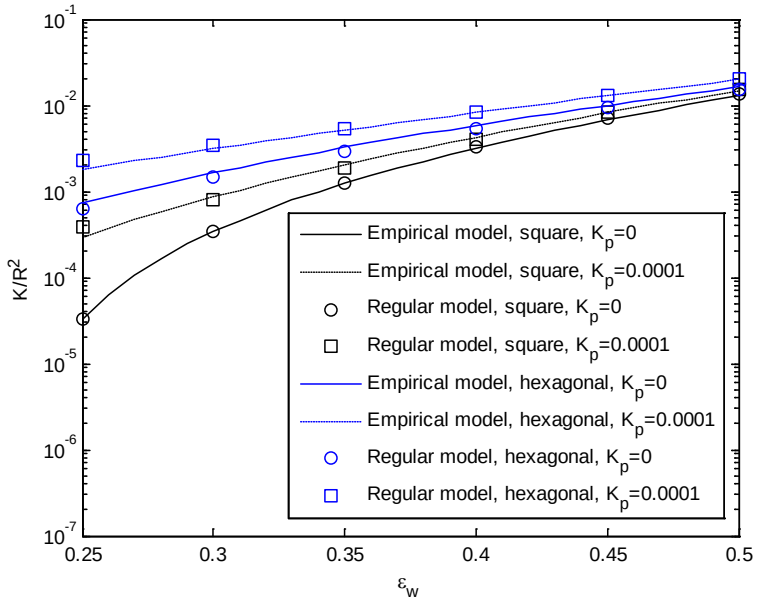

(b)

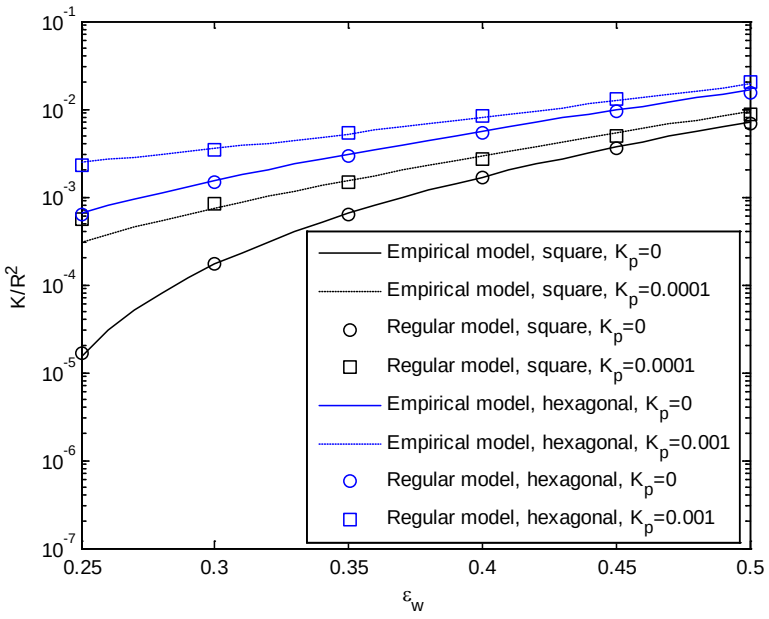

Figure 5-15: Empirical model fitted with the regular model. The yarns are packed squarely and hexagonally with (a) circular cross-section shape and elliptical cross-section shape of axis ratio 2. The black lines represent the square packing, while the blue demons.

As Eq. (5-27) indicates that the permeability coefficient is a combination of solid inter-yarn permeability, "slip" permeability and intra-yarn permeability, the overall permeability is expressed in an empirical form of these contributors. A comparison between the semi-analytical expression of Eq. (5-27) and the regular models based on Eq. (5-13) is conducted in Fig. 5-15 (a) for circular yarns and in Fig, 5-15 (b) for elliptical yarns. For circular yarns, the empirical constant j uses 0.35 for square packing and 0.5 for hexagonal packing, respectively. For elliptical yarns, the empirical constant j is 0.25 for square packing and 0.4 for hexagonal packing, respectively. Excellent fittings are found in Fig. 5-15, which indicates the reliability and predictability of the simple semi-analytical expression.

5.3. 3D woven fabric

The model for the permeability of 3D woven fabric is based on the modified scale estimate method in Chapter 3 with consideration of “slip effect” of intra-yarn permeability.

5.3.1. Model generation

As the model would be compared with the numerical results from Nabovati et al.’s (Nabovati et al., 2010), the same plain bi-axial weave pattern was constructed as shown in Fig. 5-17. The woven fabric is made up of perpendicular yarns along x- and y-directions., and the created yarns have circular cross-sectional shape in the x-z and y-z planes along yarn axes. The distance between two adjacent yarns is S_a.

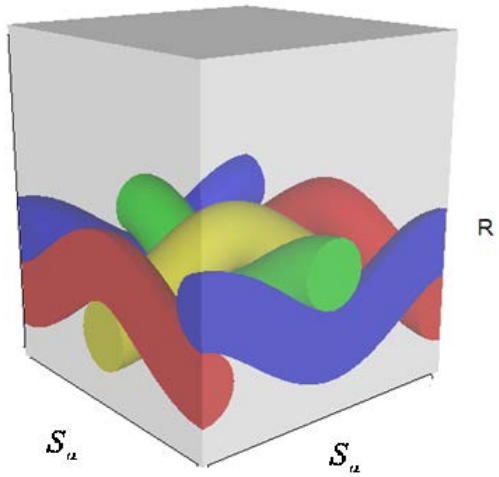

Figure 5-16: Schematic of 3D bi-axial plain woven fabric

Based on the scale estimate method, the minimum distance (or gap) $h(x)$ between two circular yarns parallel with the same plane is selected as the

characteristic length. The pressure gradient of a channel within dx along the x-direction is calculated as:

$$dp = \mu \frac{\langle u \rangle S_a^2}{h^4(z)} dx, \tag{5-6}$$

where, the actual velocity $u(z)$ in the channel between yarns is expressed as $\langle u \rangle S_a^2 / \left[4h^2(z)\right]$ based on conservation of flux, and $\left[4h^2(z)\right] / S_a^2$ is ratio between the minimum to the total frontal areas in z-direction.

Similar to the calculation process of the two scaling models of Eq. (3-43) and (3-45), integrating Eq. (5-28) yields

$$\Delta p = \mu \langle u \rangle S_a^2 \int_0^R \frac{1}{h^4(x)} dx = \mu \langle u \rangle S_a^2 \frac{\sqrt{2Rh_{\min}}}{h_{\min}^{3.5}} \int_0^{\frac{R}{\sqrt{2Rh_{\min}}}} \frac{1}{\left(1+t^2\right)^{3.5}} dt \,. \tag{5-7}$$

Therefore, the dimensionless permeability of 3D woven fabric based on Eq. (5-29) is given by:

$$K_s / R^2 = c h_{\min}^{3.5} \frac{R^{0.5}}{S_a^2}, \tag{5-8}$$

where $S_a = \dfrac{\pi R}{2(1-\varepsilon)}$ and $h_{\min} = \dfrac{\pi R}{2(1-\varepsilon)} - 2R$.

5.3.2. Results and discussion

To our best knowledge, it is the first theoretical attempt to determine

permeability of 3D woven fabric made up of multi-filaments. Fig. 5-17 presents the proposed model as a function of weave porosity, which is compared with numerical results with different yarn porosity from Nabovati et al.'s (Nabovati et al., 2010). For solid yarns, the fitted dimensionless hydraulic permeability is obtained based on Eq. (5-30):

$$K_s / R^2 = 0.46\left(\frac{0.785}{1-\varepsilon}-1\right)^{3.5}\left(1-\varepsilon\right)^{-2}. \tag{5-31}$$

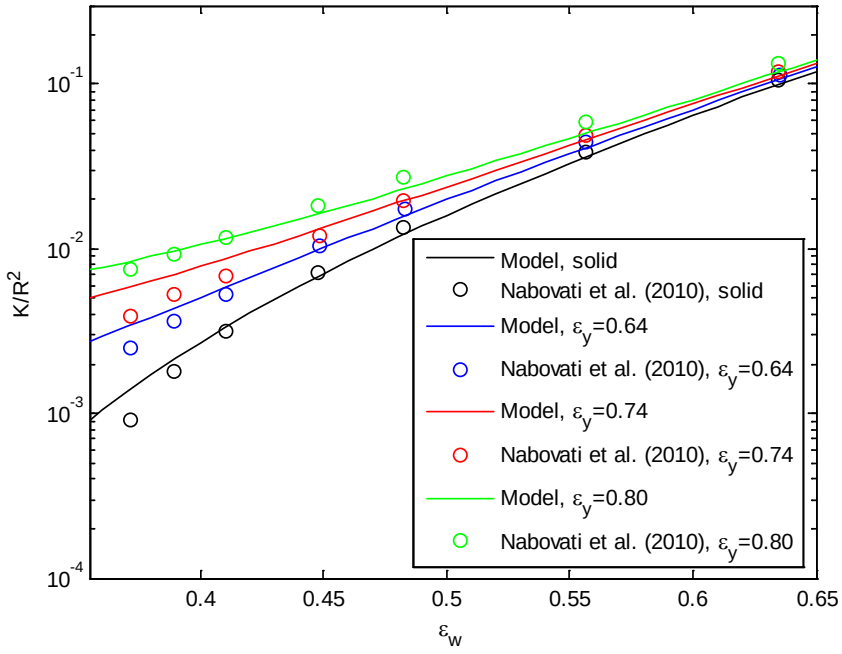

Figure 5-17: Semi-analytical model of 3D woven fabric compares with numerical results by Nabovati et al (Nabovati et al., 2010) with different yarn porosity

For woven fabric of permeable yarns, the empirical constant is selected as $j = 0.7$ after fitting Eq. (5-27) with numerical data. When the yarns in the fabric are densely packed, the present estimates are slightly higher than the numerical results. However, these discrepancies are no more than 50%, and the present correlation

provides the proper trend of permeability over a wide range of weave porosities. Fig. 5-17 also reveals that when the woven fabric becomes loose, the effect of intra-yarn permeability on the overall permeability is limited and eventually negligible.

5.4. Concluding remarks

Transverse flow through fibrous media made up of aligned arrays of permeable yarns has been theoretically investigated. The proposed model was based on a “slip” boundary in intra-yarn regime, which replaced the widely used Brinkman description in previous literature. This model was successfully validated by comparing the model prediction with rigorous numerical calculations and earlier experimental results with different yarn cross-sectional shapes and fiber packing configurations. The intra-yarn permeability increases the overall permeability of fibrous system when the ratio between them is higher than 0.01, and the effect is more significant when fibers are densely packed. It also shows that permeability of aligned yarns with elliptical cross-section is similar to that of aligned yarns with circular cross-section at the same porosity. The present work is also the first analytical attempt to model through-thickness permeability of 3D dual-scale woven fabric..

Chapter 6 Deterministic models for diffusion through fibrous media

6.1. Introduction

Effective Diffusivity of fibrous media is greatly dependent on fibrous architecture. By measuring the drop of the gas concentration and diffusion flux rate, one can determine the gas diffusivity through a testing sample based on Fick's law (Gibson et al., 2001, Huang and Qian, 2007, LaManna and Kandlikar, 2011). Although experimental works are reliable and informative, they are phenomenal and difficult to reveal the underlining physics. Theoretical and numerical studies are therefore essential to better rationalize the relationship between the structural parameters and the resulting gas diffusivity.

Bruggeman model is one of the most widely applied analytical models, but it is modeled for a porous medium composed of a collection of solid spheres (Zamel et al., 2009). Another popular model is derived by solving diffusion equation though periodically and regularly aligned cylinders (Nilsson and Stenstrom, 1995). For more general and realistic fibrous membranes, where fibers are randomly located or orientated, analytical solutions are difficult to find. Numerical techniques allow reconstruction of microstructures of fibrous membranes and simulate molecules diffusion in these structures (Tomadakis and Sotirchos, 1993a). Additionally, bulk diffusion at macro-scale and Knudsen diffusion at nano-scale can be simulated simultaneously in the same fibrous medium with a wide pore size distribution (Tomadakis and Sotirchos, 1993a).

Although many theoretical studies have been conducted to predict gas

diffusivity of fibrous materials based on parallel fibers or layered spheres, they are limited by over-simplified assumptions. Computational technique as well as experimental trials, nevertheless, cannot fully reveal multi-scale mechanisms of gas diffusion, and the analytical relationship between the complex internal structures and the effective diffusivity. Therefore, a theoretical model of gas diffusion through nano- and micro-scale fibrous materials is desirable.

In this chapter, fibers are assumed to distribute randomly to represent the microstructures of realistic fibrous materials. Cell-based method is firstly applied to determine the effective diffusivity of 1D ordered fiber arrays and then the Voronoi Tessellation method is used to model gas diffusion through 1D randomly distributed fiber array. Three mixing laws are adopted to extend the 1D model to 2D and 3D cases.

6.2. Model generation

Here, fibrous media are assumed to be composed of periodical representative unit cells. The assumptions of predicting effective diffusivity of fibrous media are made as follows:

1. The fibrous matrix is made up of straight and circular fibers.

2. All the fibers are impermeable and the gas diffusion takes place only in the void areas between fibers.

3. The fiber radius is much larger than the mean free path of diffusive molecules, and Knudsen diffusion is not considered.

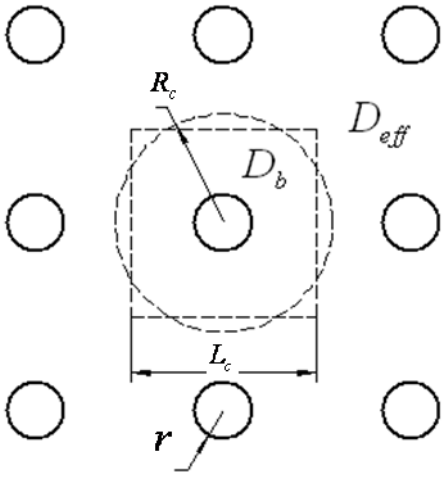

Figure 6-1: A unit cell in regular array of parallel fibers. The square has the same area with the circle in dotted line.

The simplest representative cell for 1D fibrous media is regular array of parallel fibers, as shown in Fig. 6-1. The diffusivity in the open voids of the cell is equal to bulk diffusivity D_b, which characterizes gas diffusion in bulk space without confinement. This representative cell is composed of an impermeable fiber and the gas matrix, surrounded by the effective medium with diffusivity D_{eff}, which is the same with the diffusivity of the whole system. For convenience and without losing generality, the representative cell is assumed to be a circle with the same area of the square containing the fiber. The porosity ε for this arrangement of, both the unit cell and the whole fibrous system can be determined by the following equation:

$$\varepsilon = 1 - \frac{\pi r^2}{S} = 1 - \frac{r^2}{R_c^2}, \tag{6-1}$$

where r is the fiber radius, R_c is the radius of the unit cell, $S = L_c^2$ is the area of

the square or the circular cell.

In a steady state, the gas diffusion across the fiber array is defined by Laplace equation (Nilsson and Stenstrom, 1995):

$$\nabla^2 C(l,\theta) = 0, \tag{6-2}$$

where l and θ are the cylindrical coordinates. The appropriate solution of Eq. (6-2) for gas diffusion normal to a cell containing a fiber is given by (Gueribiz et al., 2009):

$$C(l,\theta) = \begin{cases} A_1 l\cos\theta, \ (0 < l \le r) \\ (A_2 l + \dfrac{A_3}{l})\cos\theta, \ (r < l \le R), \\ A_4 l\cos\theta, \ (R < l) \end{cases} \tag{6-3}$$

where A_1, A_2, A_3, and A_4 are unknown constants arising from boundary conditions.

The continuity of the diffusive gas at the boundary between the impermeable fiber and the voids leads to:

$$C(r,\theta) = A_2 r + \frac{A_3}{r} = A_1 r = 0, \tag{6-4}$$

and there is no gas diffusion flux passing through the boundary of fiber surface, i.e.,

$$\frac{\partial C(r,\theta)}{\partial l} = \left(A_2 - \frac{A_3}{r^2} \right)\sin r = 0. \tag{6-5}$$

The continuity of the diffusive gas at the boundary of the unit cell results in:

$$C(R,\theta) = A_2 R_c + \frac{A_3}{R} = A_4 R, \tag{6-6}$$

and the continuity of gas diffusion rate at the boundary of the unit cell is given by:

$$D_b \left(A_2 - \frac{A_3}{R_c^2} \right) = D_{eff} A_4. \tag{6-7}$$

Solving the equations of (6-4) to (6-7), the effective diffusivity for both the representative cell and the whole 1D regular fibrous system is readily obtained：

$$\frac{D_{eff}}{D_b} = \frac{R_c^2 - r^2}{R_c^2 + r^2}, \tag{6-8}$$

or in terms of porosity ε :

$$\frac{D_{eff}}{D_b} = \frac{\varepsilon}{2 - \varepsilon}. \tag{6-9}$$

Then this study considers the more complicated and realistic structures, in which fibers are placed randomly. Diffusion process through the fibrous system becomes more complex because of the disorder of the fiber arrangement. To describe the randomness of fibers location, the Voronoi Tessellation method is applied (Chen and Hlavacek, 1994). In the fibrous system composed of randomly located fibers, one fiber is assumed to be contained by a polygonal cell whose boundaries are defined by the perpendicular bisectors of the lines joining each fiber with its nearest neighbor, as presented in Fig. 6-2. The polygonal cell is called Voronoi tessellation. Particularly, the areas of the unit cells are found well described by the Gamma distribution (Chen and Hlavacek, 1994).

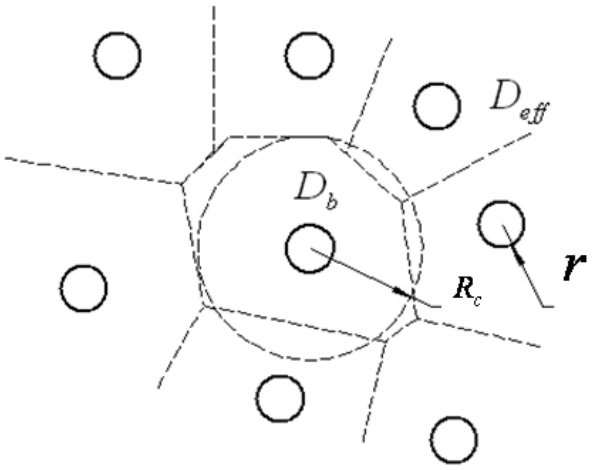

Figure 6-2: A unit cell in randomly distributed array of parallel fibers. The voronoi polygon has the same area with the circle in dotted line.

It is feasible macroscopically to assume the highly porous fibrous system to be homogeneity with a constant concentration gradient. However, the diffusion coefficient and diffusive flux of each cell are different with each other, and thus the effective diffusive flux J_{eff} of the system can be obtained in a volume-averaged form:

$$J_{eff} = \frac{\int J dS}{\int dS} = \frac{\sum J(\Delta S)\Delta S}{\sum \Delta S} = \frac{\sum_{i=0}^{N} J(S_i) S_i}{\sum_{i=0}^{N} S_i}, \tag{6-10}$$

where $J(S_i)$ and S_i is the flux and area of the ith unit cell, respectively, N is the number of the unit cells in the system, and $\langle S \rangle$ is the mean area of the unit cells. As N is very large and S_i is very small comparing with the crossing area of the whole system, the effective diffusive flux J_{eff} can be expressed as a function of

probability density of unit cell area $f(S)$ in an integral form:

$$J_{eff} = \int J(S) f(S) dS. \tag{6-11}$$

Substituting Eq. (6-11) into Eq. (1-4) leads to the effective diffusivity:

$$D_{eff} = \int D(S) f(S) dS. \tag{6-12}$$

Chen and Hlavacek (Chen and Hlavacek, 1994) found that Gamma distribution can properly describe the local void area distribution in the Voronoi Tessellation:

$$f(S_v) = \frac{\beta^{\beta}}{\langle S \rangle^{\beta}} \frac{S^{\beta-1}}{\Gamma(\beta)} e^{-\beta \frac{S}{\langle S \rangle}}, \tag{6-13}$$

where $\Gamma(\alpha)$ is a Gamma distribution, and β is the scale parameter.

It satisfies the following relationship:

$$\int_{\pi r^2}^{\infty} S f(S) dS = \langle S \rangle. \tag{6-14}$$

Here, the diffusivity of the voronoi polygon is approximated to be identical with the overlapped circle with the same area as seen from Fig. 6-2, and this assumption has been successfully used to determine the permeability of more structure-sensitive gas flow in Chapter 3. Substituting Eq. (6-8) and Eq. (6-14) into Eq. (6-12), the dimensionless through-plane effective diffusivity of 1D random fibrous media can be obtained:

$$\frac{D_{eff}}{D_b} = \int_{\pi r^2}^{\infty} \frac{S - \pi r^2}{S + \pi r^2} \frac{\beta^{\beta}}{\Gamma(\beta)} \left(\frac{S}{\langle S \rangle} \right)^{\beta-1} e^{-\beta \frac{S}{\langle S \rangle}} d\left(\frac{S}{\langle S \rangle} \right). \tag{6-15}$$

where $\varepsilon = 1 - \frac{\pi r^2}{\langle S \rangle}$ and $x = \frac{S}{\langle S \rangle}$. The scale parameter is numerically determined as $\beta = 3.61$ (Ferenc and Neda, 2007), which is adopted in this study:

$$\frac{D_{eff}}{D_b} = \int_{1-\varepsilon}^{\infty} 27.4 \frac{x - 1 + \varepsilon}{x + 1 + \varepsilon} x^{3.61} e^{-3.61} dx. \tag{6-16}$$

For gas diffusion parallel with fibers, the tortuosity of the 1D fibrous medium is found to be practically independent of its porosity, and the effective diffusivity for both regular and random 1D fiber beds is:

$$\frac{D_{eff}}{D_b} = \varepsilon. \tag{6-17}$$

The effective diffusivity of 2D randomly layered fibrous structures, which are used widely in GDLs in PEMFC and other fields, will be predicted based on 2D model. The pressure-driven permeability of a porous medium was determined by a function of diffusivity, pore volume, and pore surfaces (Johnson et al., 1986, Tomadakis and Robertson, 2005). The pore volume and pore surfaces keep constant when the in-plane fiber orientation varies from 1D fibers to 2D (Tomadakis and Sotirchos, 1993b). Based on this relationship, it can be safely estimated that the dimensionless diffusivity is not affected by in-plane fiber orientation because the pressure-driven flow permeability is independent of in-plane fiber orientation, as proven both analytically in chapter 3 and numerically (Tahir and Tafreshi, 2009). Indeed, gas diffusion is much less sensitive than gas flow interacting with fibers, so it is reasonable to conclude that the effective diffusivity remains unchanged from 1D to 2D as gas flow does. Therefore, the 2D randomly layered fibrous structure shares the same model with the 1D case as Eq. (6-16).

When the fibers orient more parallel with the total gas diffusion direction, such as gas diffusion through in-plane GDLs or 3D isotropic fibrous media, the exact solutions of gas diffusivity are almost impossible to find. In this study, the system diffusivity is considered as combined local diffusivities of 1D fiber array normal to and parallel with the diffusion direction to estimate the actual diffusivity (see Fig. 6-3). The distribution of fibers is complex, but they can be considered homogeneous at macro-scale. For fibers oriented in different principal directions (x-, y- or z-direction), they share the same average porosity with the whole fibrous system. Three mixing rules, which were proposed for permeability prediction (Mattern and Deen, 2008), are used to determine effective diffusivities in this study based on mathematical analogy between Darcy's law and Fick's law. The three mixing rules based on different approximations and as functions of fiber fraction $\phi = 1-\varepsilon$ are listed as follows:

$$D_{eff}\left(\phi\right) = \frac{\phi_{norm}}{\phi} D_{norm}\left(\phi\right) + \frac{\phi_{par}}{\phi} D_{par}\left(\phi\right), \tag{6-18}$$

$$D_{eff}\left(\phi\right) = \left[\frac{\phi_{norm}}{\phi} D_{norm}^{-1}\left(\phi\right) + \frac{\phi_{par}}{\phi} D_{par}^{-1}\left(\phi\right)\right]^{-1}, \tag{6-19}$$

$$D_{eff}\left(\phi\right) = \left[D_{norm}\left(\phi\right)\right]^{\frac{\phi_{norm}}{\phi}} \left[D_{par}\left(\phi\right)\right]^{\frac{\phi_{par}}{\phi}}, \tag{6-20}$$

where, norm and par mean normal to and parallel with the flux direction, respectively. In Eq. (6-18), the volume-weighted diffusivity assumes each fiber type as parallel resistors. The volume-weighted resistivity regards diffusive resistors as series in Eq. (6-19). In Eq. (6-20), the geometric mean is a mathematical blend.

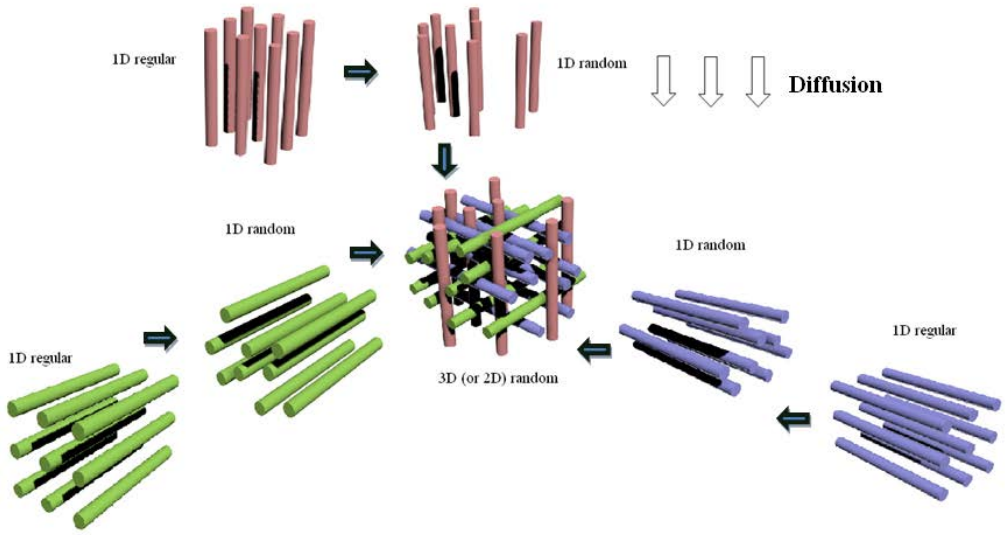

Figure 6-3: Illustration of 3D or 2D fibrous media composed of 1D fiber arrays

6.3. Results and discussion

In this section, the proposed model is compared with numerical, experimental and analytical results available in the literature. However, the collected data were reported in terms of tortuosity, equivalent diffusivity, diffusive resistance, or related parameters. In order to directly compare them with the present predictions, they are converted to dimensionless effective diffusivity against porosity. For in-plane gas diffusion of 2D fibrous media, $\phi_{norm} = \phi_{para}$, and for through-plane gas diffusion of 3D fibrous media, $\phi_{norm} = 2/3$, and $\phi_{para} = 1/3$.

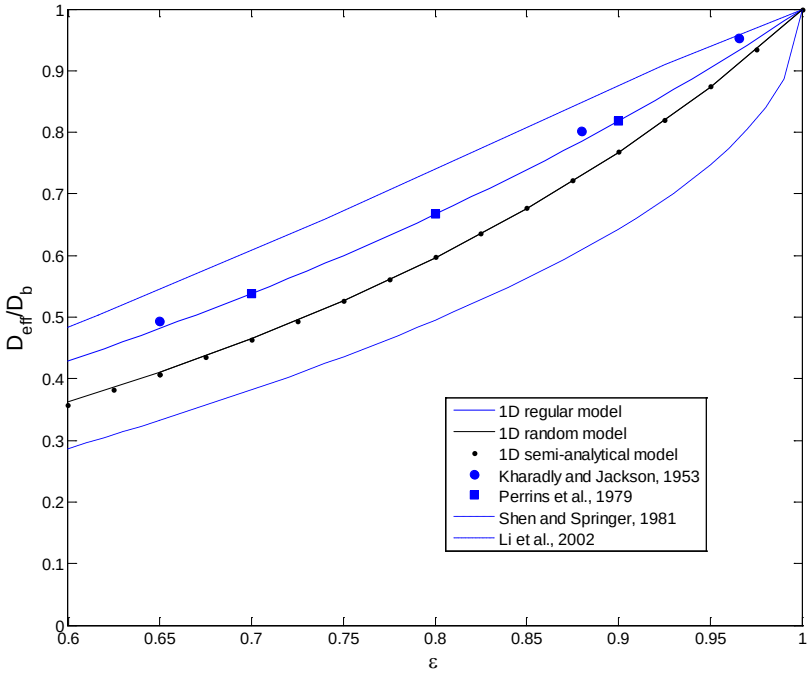

Figure 6-4: Comparison of the model of 1D fibrous media with experimental, numerical, and analytical results. The blue line and the black line are present models of through-plane diffusion in 1D regular and 1D random structure, respectively.

The dimensionless through-plane effective diffusivity, which is calculated for a periodic array of fibers for both regular and random packing, is presented in Fig. 6-4. For regular case, the results of the present model match perfectly with numerical results of Perrins at al. (Perrins et al., 1979) and experimental data by Kharadly and Jackson (Kharadly and Jackson, 1953). However, the trend of the model is considerably different from Shen and Springer's model (Shen and Springer, 1981), who did not consider the shape variation of void gap between fibers. The prediction of Li et al. (Li et al., 2002) is a little higher than the present model, which may arise from their over-idealized assumption that gas concentration is uniform at any cross-section of the void channel. Fig. 6-4 shows that the through-plane effective diffusivity of 1D random structure slightly lower than 1D regular case, which may be

due to that more random and disorder structures increases tortuosity. It should be noted that for viscous flow though fibrous media, hydraulic permeability increases with increasing degrees of randomness, where the trend can be ascribed to the increased mean pore size for random structure (Sobera and Kleijn, 2006). Therefore, when the fibers are more randomly located, the fibrous structures will have lower hydraulic permeability, but higher vapor diffusivity, making them good candidates of breathable materials.

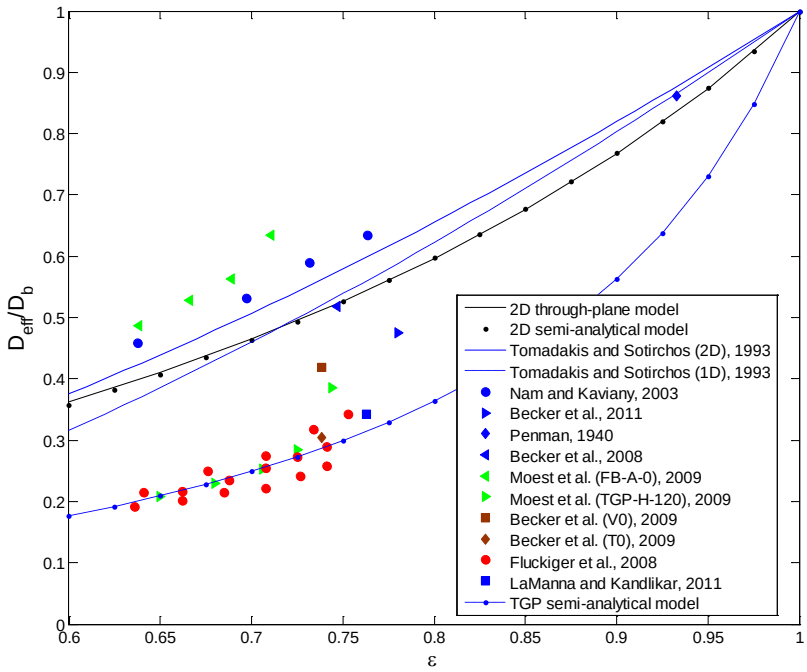

Figure 6-5: Comparison of the model of through-plane diffusion in 2D fibrous media with experimental and numerical results

According to Eq. (6-9) and Eq. (14), the tortuosity of the present model for 1D regular structure is equal to $(2-\varepsilon)$. It can be expressed as

$$\tau = 1+\phi. \tag{6-21}$$

In analogy to the widely used equation for tortuosity of porous media (Koponen et al., 1996), $\tau = 1+0.8\phi$, Eq. (6-21) is extended to estimate the tortuosity of randomly

located fibers by:

$$\tau = 1 + \phi_e, \tag{6-22}$$

where, $\phi_e = k\phi$ is the equivalent fiber fraction for the random structure and k is a geometrical factor. It can be seen in Fig. 4 that the semi-analytical model based on Eq. (6-22) matches perfectly with the 1D random model of Eq. (14) when $k = 1.7$. The semi-analytical model can therefore be expressed in the following form:

$$\frac{D_{eff}}{D_b} = \frac{\varepsilon}{2.7 - 1.7\varepsilon}. \tag{6-23}$$

In order to validate the present model, past numerical and experimental results of GDLs are plotted and compared with the prediction of the present model in Fig. 6-5. Tomadakis and Sotirchos (Tomadakis and Sotirchos, 1993b) investigated the diffusivities through 1D and 2D randomly located fiber assembles using Monte Carlo simulation and found that 1D and 2D through-plane diffusivities are similar. As can be seen from Fig. 6, both 1D and 2D through-plane diffusivities from Tomadakis and Sotirchos (Tomadakis and Sotirchos, 1993b) are close to our 2D (1D) through-plane model, which shows that 1D and 2D through-plane diffusivities are approximately independent of in-plane fiber orientation. It can be seen from the figure that this model prediction agrees well with the experimental data from Penman (Penman, 1940) and Moest et al. (Moest et al., 2009) and numerical results by Nam and Kaviany [21] and by Becker et al. (Becker et al., 2011, Becker et al., 2008). Nevertheless, it should be noted this model prediction deviates greatly from some experimental data in literature. This is due to the fact that chemical binders were applied in the samples of these experiments, but not considered in our model. The binder is used to bind carbon fibers together, can fill the voids between the fibers (see Fig. 7 from Ref. (Flueckiger et al., 2008)). Therefore, the effective diffusivities measured in these experiments (e.g. the experimental results of Toray TGP-060

carbon fibers by Flueckiger at al. (Flueckiger et al., 2008) and Toray TGP-120 carbon fibers by Moest et al. (Moest et al., 2009) and LaManna and Kandlikar (LaManna and Kandlikar, 2011) are significantly lower than the model prediction. Moest et al. (Moest et al., 2009) also measured effective diffusivity of Freudenberg FB-A-0 carbon fiber layers, which are bonded mechanically without chemical binder, and the experimental data are in agreement with the present model of Eq. (6-23). In addition, numerical simulations by Becker et al. (Becker et al., 2009) show that the virtually created GDL with binder converged on the fiber contacting area (V0) has higher diffusivity than the reconstructed GDL based on the tomographic image of real TGP-060 paper (T0). Therefore, high performance of PEMFCs with higher gas diffusivity can be achieved with lower binder used or less binder distributed in void pores between fibers. We also provide a semi-analytical model fitted by the diffusivities of existing TGP carbon fibers based on Eq. (6-22):

$$\frac{D_{eff}}{D_b} = \frac{\varepsilon}{7-6\varepsilon}. \tag{6-24}$$

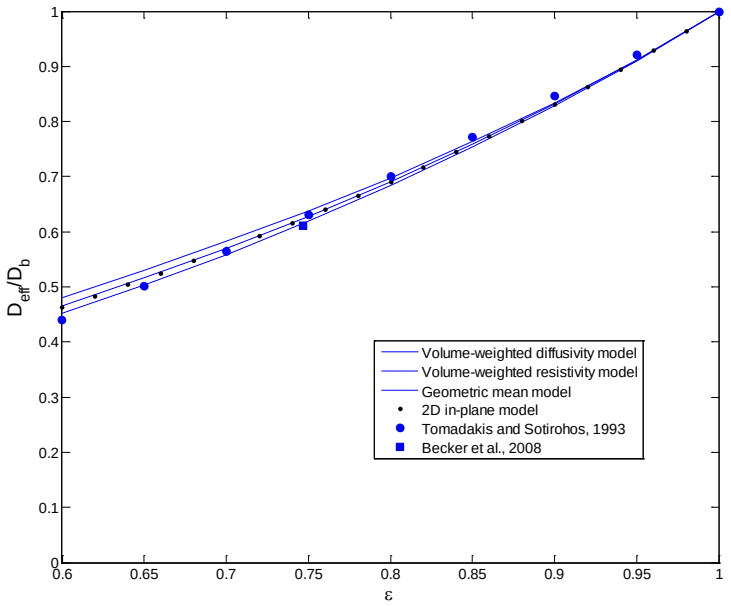

Figure 6-6: Comparison of the mixing laws of in-plane diffusion through 2D

fibrous media with numerical results

In Fig. 6-6, the diffusivity of a fibrous material, consisting of 1D random fibers half parallel and half normal to flux direction, predicted by the present model using three different mixing rules, is compared with the numerical results from Tomadakis and Sotirchos (Tomadakis and Sotirchos, 1993b) and Becker et al. (Becker et al., 2008). It is interesting to see that there is only very small difference between the three mixing rules, and the model prediction using either of the mixing rules agree well with the numerical results. The volume-averaged diffusivity model and the volume-averaged resistance model are the upper and lower limits of diffusivity estimates, respectively (see Fig. 6-7), while the geometric mean is merely a mathematical estimate without physical meaning. Therefore, a better estimate would be the average of volume-averaged diffusivity model and volume-averaged resistance model, which is adopted in this study and is plotted in Fig. 6-6:

$$D_{eff}(\phi)=\frac{1}{2}\left[\frac{\phi_{norm}}{\phi}D_{norm}(\phi)+\frac{\phi_{par}}{\phi}D_{par}(\phi)\right] + \frac{1}{2}\left[\frac{\phi_{norm}}{\phi}D_{norm}^{-1}(\phi)+\frac{\phi_{par}}{\phi}D_{par}^{-1}(\phi)\right]^{-1}. \tag{6-25}$$

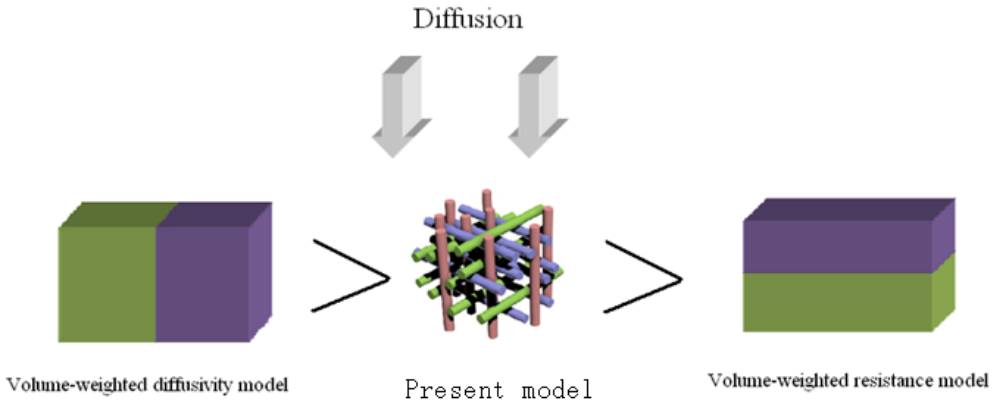

Figure 6-7: Relationship between the realistic model, volume-averaged diffusivity model, and volume-averaged resistance model

Based on Eq. (6-17), Eq. (6-23) and Eq. (6-25) the 2D in-plane diffusivity model can be expressed as:

$$\frac{D_{eff}}{D_b} = \frac{\varepsilon}{4}\left(\frac{3.7-1.7\varepsilon}{2.7-1.7\varepsilon} + \frac{4}{3.7-1.7\varepsilon}\right). \tag{6-26}$$

Likewise, comparison of three different mixing rules is carried out for 3D fibrous structures in Fig. 6-8. The prediction of this model for the 3D fibrous structure, as assuming it consists of 1D random fibers with 1/3 parallel and 2/3 normal to flux direction, agrees well with the numerical data by Tomadakis and Sotirchos (Tomadakis and Sotirchos, 1993b). Based on Eq. (6-17), Eq. (6-23) and Eq. (6-25), we can derive a semi-analytical model for 3D fibrous structure:

$$\frac{D_{eff}}{D_b} = \frac{\varepsilon}{6}\left(\frac{4.7-1.7\varepsilon}{2.7-1.7\varepsilon} + \frac{9}{6.4-3.4\varepsilon}\right). \tag{6-27}$$

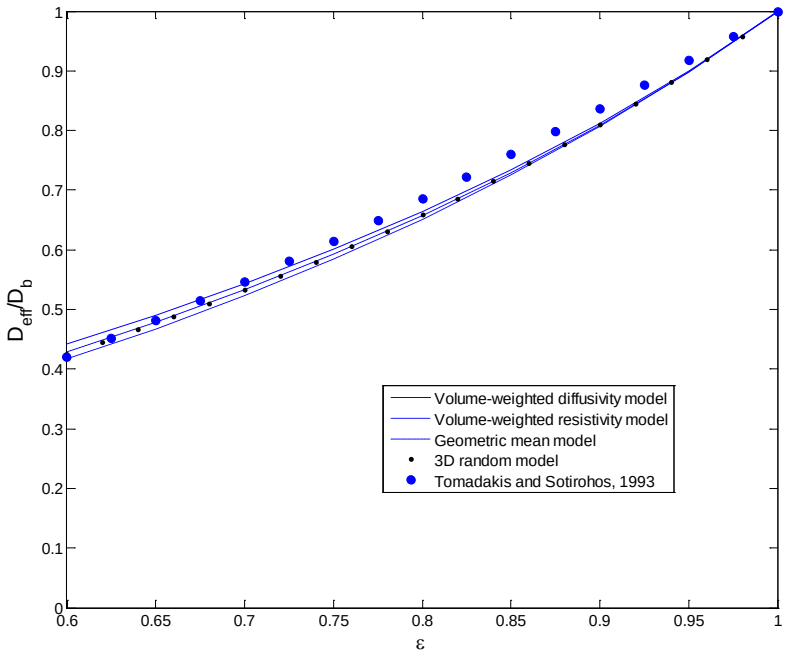

Figure 6-8: Comparison of the mixing laws of 3D fibrous media with numerical results

For the three types of random fiber mats, the effective diffusivity of this model increases with growing porosity and increasing orientation preference of fibers normal to diffusion direction, which has the same tendency with the effective permeability caused by viscous flow, as revealed in Chapter 3.

6.4. Concluding remarks

Theoretical models with semi-analytical forms have been proposed to predict the effective diffusivities of 1D, 2D, and 3D randomly distributed fiber assembles, which are widely used as GDLs in PEMFCs. The predicted effective diffusivities agree well with those of experimental measurements and past numerical simulations. It is particularly found that randomly distributed fibers have lower diffusivities than those ordered distributed. In addition, effective diffusivity is not sensitive with in-plane orientation, but positively increasing with increasing through-plane orientation. Using less binder or properly filling binder in GDLs can increases their effective diffusivities. This work provides an in-depth understanding of diffusion mechanisms in fibrous media and can simplify the process of design and optimization for GDLs and other applications.

Chapter 7 Statistical models for diffusion through fibrous media

7.1. Introduction

Modeling gas diffusion in nanofiber layers is challenging. In such media, the disordered nature of pore structures is difficult to describe, and further complexities are introduced as multiple mechanisms of gas diffusion exist simultaneously. In this work, an analytical model is proposed to study gas diffusion across nanofiber layers based on fractal theory. The fractal model is expressed in terms of pore area and tortuosity fractal dimensions, which enable to statistically characterize the internal geometric structures of nano-fibrous media. Knudsen diffusion in nano-scale channels is considered, and the Knudsen tortuosity factor is redefined to make it independent of diffusion mechanism. Thereafter, experiments of measuring the effective diffusivity of electrospun nano-fibrous mats and commercial nonwoven webs by the inverted-cup test method are conducted. Finally, the proposed model is compared with experimental results, and the influences of structural parameters are analyzed.

7.2. Model generation

Before development of the effective gas diffusivity of nanofiber layers, the following assumptions are made: (1) fibrous media are regarded as a collection of bundles of tortuous open channels; (2) all the fibers are impermeable; (3) all the fibers have the uniform radius; (4) gas diffusion is in steady state.

For a fractal object, the following statistical relationship exists (Mandelbrot,

1982):

$$M\left(L\right) \propto L^{D_0}, \tag{7-1}$$

where, D_0 is the fractal dimension, $M\left(L\right)$ can be a quality, such as length, volume, or area, and L is the length scale. It is also shown that the pore number in the realistic fibrous porous media follows the fractal power law (Yu and Li, 2001):

$$N(L \geq R) = (R_{\max} / R_p)^{D_f}, \tag{7-2}$$

where, D_f is the pore area fractal dimension with $0 < D_f < 2$ in two dimensions, and R_p and $R_{\max}$ is the pore radius and maximum pore radius, respectively. The total number of pores N_t, from the minimum pore radius $R_{\min}$ to maximum pore radius $R_{\max}$, is therefore given by $(R_{\max} / R_{\min})^{D_f}$. Additionally, the pore number with radius between R_p and $R_p + dR_p$ can be obtained:

$$dN = -D_f R_{\max}^{D_f} R_p^{-D_f - 1} dR_p. \tag{7-3}$$

Hence, the total fluxes of gas diffusion Q_d can be obtained by integrating the individual diffusion flux $q_d(R)$ using Eq. (7-3):

$$Q_d = \int_{R_{\min}}^{R_{\max}} q(R_p) dN. \tag{7-4}$$

where, $q_d(R_p) = j(R_p) A(R_p)$, $j(R_p)$ is the diffusion rate of a single channel, and $A(R_p) = \pi R_p^2$ is the crossing area of a single pore. Similarly, the total crossing area

of pores A_p is obtained by integration:

$$A_p = \int_{R_{\min}}^{R_{\max}} A(R_p) dN. \tag{7-5}$$

And the total cross-sectional area A_t is derived by the definition of the system porosity (Yu, 2008):

$$A_t = \frac{A_p}{\varepsilon}. \tag{7-6}$$

Gas diffusion rate $j(R_p)$ can be described by the following expression:

$$j(R_p) = D_{equ}\left(R_p\right)\frac{\triangle C}{L\left(R_p\right)}, \tag{7-7}$$

where, $D_{equ}\left(R\right)$ is the equivalent diffusivity of a channel based on Eq. (2-15):

$$D_{equ} = \frac{u}{3}\left(\frac{1}{2R_p} + \frac{1}{\lambda}\right)^{-1} = \frac{1}{1+Kn} D_b. \tag{7-8}$$

when pore size is much larger than mean free path of molecules, $D_{equ} \to D_b$; when pore size is much smaller than mean free path of molecules, $D_{equ} \to D_{Kn}$. Therefore, the equivalent diffusion captures the diffusive mechanisms through all range of pore length scales. And $L\left(R\right)$ is the tortuous length of a channel seen in Fig. 7-1, which is related with pore radius (Yu, 2008):

$$H\left(R_p\right) = H_0 \tau(R_p) = H_0^{D_t}\left(2R_p\right)^{1-Dt}, \tag{7-9}$$

where D_t is the tortuosity fractal dimension, and H_0 is the straight length of a channel, which is equal to the thickness of the medium.

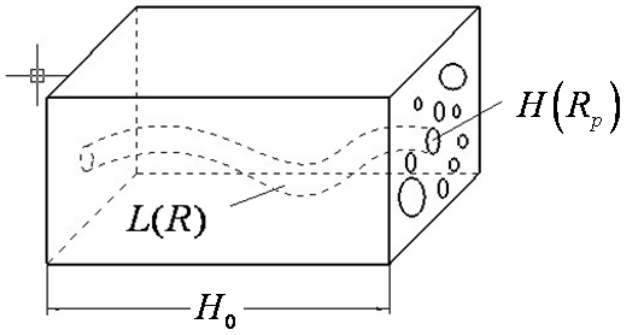

Figure 7-1: Schematic of fibrous media composed of tortuous channels

As the tortuosity defined and calculated above is solely determined by the geometric details of porous media, it should be independent of diffusive mechanisms. However, Knudsen tortuosity τ_{Kn} is found to be greater than geometric tortuosity in bulk regime τ experimentally by Papadopoulos et al. (Papadopoulos et al., 2007), and numerically and theoretically by Zalc et al. (Zalc et al., 2004). The mechanism-dependent tortuosity in Knudsen regime is due to different path distributions and wall reflections of gas molecules from that in bulk regime, and interested readers are referred to Zalc et al.'s work (Zalc et al., 2004). The modified tortuosity independent of diffusion mechanism can be obtained by a proper definition.It is particularly found $\tau_{Kn} = 3\tau$ in a single cylindrical tube (Zalc et al., 2004), so the modified tortuosity can be expressed as $\tau_M = \frac{\tau + \tau_{Kn} Kn}{1 + Kn}$. Thus, the modified length of a tortuous channel is given by:

$$H\left(R_p\right)=H_0\frac{\tau+\tau_{Kn}Kn}{1+Kn}=\frac{1+3Kn}{1+Kn}H_0^{D_t}\left(2R_p\right)^{1-Dt}. \tag{7-10}$$

Substituting Eqs. (7-5 to 7-10) into Eq. (7-4), a compact fractal model of dimensionless diffusivity is obtained, viz.,

$$\frac{D_{eff}}{D_b}=\frac{\varepsilon L_0^{D_t-1}\left(2-D_f\right)\int_{R_{\min}}^{R_{\max}}\frac{\left(2R\right)^{Dt+1-D_f}}{2R+3\lambda}dR_p}{\left(1-\left(\frac{R_{\min}}{R_{\max}}\right)^{2-D_f}\right)R_{\max}^{2-D_f}} \tag{7-11}$$

In Eq. (7-11), all the parameters have clear physical meanings and no empirical constants exist. This model can be particularly used to calculate effective diffusivity of nanofiber layers, and can be also applied to general porous media.

The pore size of fibrous media is difficult to measure, but it can be estimated from fiber radius. The relationship between the mean pore size and fiber radius in fibrous media is given by (Tomadakis and Robertson, 2005, Tomadakis and Sotirchos, 1991):

$$\left\langle R_p\right\rangle=\frac{\varepsilon}{1-\varepsilon}r, \tag{7-12}$$

where $\left\langle R\right\rangle$ is the mean pore radius and r is fiber radius. In addition, the mean pore radius can be computed as:

$$\left\langle R_p\right\rangle=\int_{R_{\min}}^{R_{\max}}Rf\left(R_p\right)dR_p=\frac{D_f}{D_f-1}R_{\min.} \tag{7-13}$$

Based on Eq. (7-12) and Eq. (7-13), the minimum pore radius is given by $R_{\min}=\frac{D_f-1}{D_f}\frac{\varepsilon}{1-\varepsilon}r$. It is set that $R_{\max}=R_{\min}/k$, where k is the ratio between

maximum and minimum pore radius. Therefore, the dimensionless diffusivity in terms of fiber radius and fractal dimensions can be easily obtained:

$$\frac{D_{eff}}{D_b} = \frac{\varepsilon H_0^{D_t-1}\left(2-D_f\right)\int_{\frac{D_f-1}{kD_f}\frac{\varepsilon}{1-\varepsilon}r}^{\frac{D_f-1}{D_f}\frac{\varepsilon}{1-\varepsilon}r} \frac{2R_p^{D_t+1-D_f}}{2R_p+3\lambda}dR_p}{\left(1-(k)^{2-D_f}\right)\left(\frac{D_f-1}{kD_f}\frac{\varepsilon}{1-\varepsilon}r\right)^{2-D_f}}. \tag{7-14}$$

7.3. Experimental

The electrospinning set-up is shown in Fig. 7-2. The polymer solution was pushed out of the needle by a controlled syringe pump. The applied positive voltage was supplied to the metal tip of the needle via a copper wire from a DC high-voltage generator.

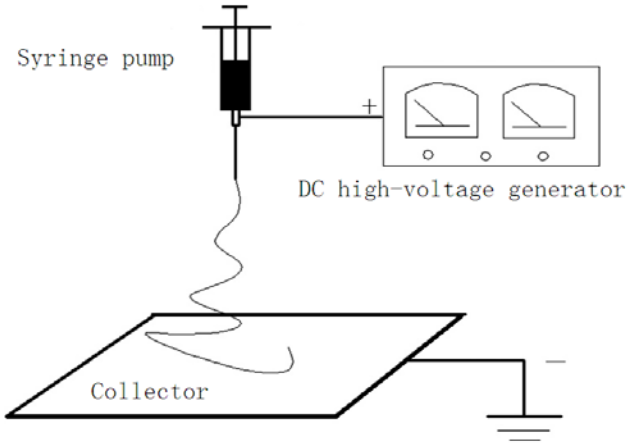

Figure 7-2: Electrospinning set-up

The nylon 6 particles were dissolved in formic acid with 20 wt% concentration at room temperature by continuous stirring for 24 hours. The potential differences between the needle tip and the counter electrode (collector) were controlled at 25 kV.

A rotating mental drum covered with aluminum foil, placed 15 cm away from the needle tip, was used to collect the electrospun nanofibers. The typical ejection rate of the solution was 0.3 mL/h. The electrospinning process was conducted in the fume cupboard.

The porosities of electrospun fiber web are calculated by the following equation:

$$\varepsilon = 1 - \frac{\rho_{media}}{\rho_{nylon}}, \tag{7-15}$$

where, ε is the porosity of the electrospun web, ρ_{media} is the density of fibrous media, and ρ_{nylon} is the density of solid nylon 6.

(a) 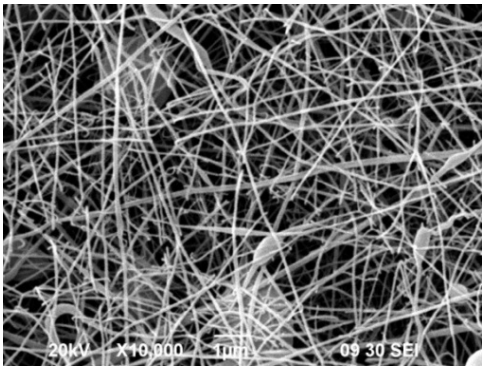

(b) 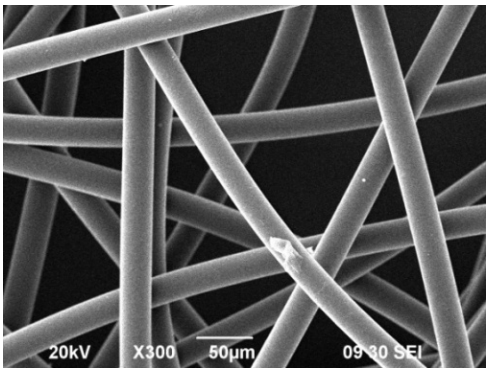

Figure 7-3: SEM images of (a) Nylon 6 electrospun fibrous medium and (b) conventional nonwoven

A FEI Sirion 200 field emission scanning electron microscope (FESEM) was used to image electrospun samples. An example is shown in Fig. 7-2, and a sample of conventional nonwoven was also added for comparison. Samples were coated with Au/Pd using a Polaron Range sputter coater prior to imaging. The thickness of

electrospun nanofibers collected in this experiment is between 100 and 200 microns. ImageJ was used to measure individual fiber radius in each SEM micrograph. On average, 40 measurements were conducted on each sample to determine the average fiber radius.

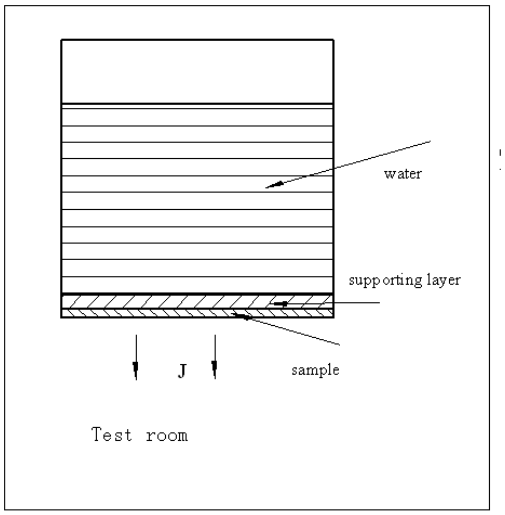

Figure 7-4: Inverted cup test set-up

The moisture vapor diffusivity was measured using inverted-cup test method, seen as in Fig. 7-4. A cup with water was invertedly put in a test room with strictly constant temperature and humidity. To prevent the water in the cup from wetting and pressing the sample, a breathable hydrophobic PTFE membrane was covering the opening of the cup. Moisture vapor diffused from the liquid water in the cup (high concentration of vapor) to air out of the cup (low concentration of vapor) through fibrous samples. The cup assembly was weighed periodically every hour. The water closely next to the PTFE membrane avoids the additional time-dependent diffusive resistance of internal air between the layers and water.

In the test room, the inverted cup test was conducted at an air temperature of 20± 0.5°C and a relative humidity of 62 ± 1%. The diffusion coefficient of moisture

vapor in air D_b is $2.45\times10^{-5}\mathrm{m}^2/\mathrm{s}$ and the density of saturation vapor ρ_v in air is $17.3\mathrm{g/m}^3$ (Bolz and Tuve, 1976), and the mean free path of vapor molecules λ is about $0.1\ \mu\mathrm{m}$ (Phattaranawik et al., 2003). The diffusivity can be averaged based on the following form:

$$D_{eff} = \frac{h_i}{\frac{\Delta C}{J_i} - \frac{\Delta C}{J_0}}, \tag{7-16}$$

where, ΔC is the concentration difference, J_0 is the diffusion rate of a layer of PTFE membrane, and J_i is the diffusion rate of PTFE membrane and sample layers with total thickness h_i. Diffusion rates with 0, 1, 2, and 3 layers of samples were measured, and the effective diffusivity was obtained based on Eq. (7-16).

7.4. Results and discussion

In this section, the proposed model is compared with experimental results, and the structural parameters of effective diffusivity in nanofiber media are analyzed. To calculate effective diffusivity using Eq. (7-14), the area fractal dimension D_f for layered fibrous membrane is necessarily determined, which is given by (Yu and Li, 2001):

$$D_f = 2 + \frac{\ln \varepsilon}{\ln\left(R_{\max}/R_{\min}\right)} \tag{7-17}$$

and the tortuosity fractal dimension is given by (Yu, 2005):

$$D_t = 1 + \ln\langle\tau\rangle / \ln\frac{H_0}{\langle 2R_p\rangle}, \tag{7-18}$$

where, the average tortuosity for the layered random fibrous porous media can be estimated by (Tomadakis and Robertson, 2005, Tomadakis and Sotirchos, 1991): $\langle\tau\rangle = (\frac{0.89}{\varepsilon - 0.11})^{0.785}$.

The fiber radius of the electrospun nanofiber in the present experiments is around $50nm$, and the fiber radius of the conventional fibrous samples is $15\mu m$. Vapor diffusion through electrospun nanofiber media is affected by both Knudsen diffusion and bulk diffusion due to their wide pore size distribution from nano-scale to macro-scale, but only bulk diffusion exists in the conventional nonwoven media for their internal pores much larger than mean free path of vapor molecules. For an electrospun web with porosity 0.9, as seen in Fig. 7-3 (a), the maximum pore radius is $5\mu m$ based on that the entire disordered pores in fibrous media are converted to area-equivalent circulars by ImageJ. The radius is comparable with the predicted value $2.1\mu m$, which is calculated using the formula $R_{\max} = \frac{4\sqrt{\varepsilon}}{1-\sqrt{\varepsilon}}\frac{r}{\sqrt{\pi}}$ (He et al., 2007). Determination of minimum pore radius $R_{\min}$ in fibrous assemblies is difficult to conduct. Fortunately, the mean pore radius, as a function of minimum pore radius and area fractal dimension, can be used to determine the minimum pore radius with the help of Eq. (7-13). With maximum pore radius $5\mu m$ and $2.1\mu m$, the corresponding dimensionless effective diffusivities were calculated as 0.67 and 0.70, respectively, based on Eq. (7-14). The two diffusivities are indeed close to each other. Therefore, a reasonable estimate of ratio of minimum and maximum radius, $k = 0.05$, with maximum pore radius equal to $4.4\mu m$ (between predicted $2.1\mu m$ and measured $5\mu m$) in this case, is chosen in this study. Moreover, the

fractal theory holds because the probability density function satisfies that $\int_{-\infty}^{+\infty} f(R)dR = \int_{-\infty}^{+\infty} \frac{1}{N_t} dN = 99.72\% \approx 1$. The comparison between measured vapor diffusivities of electrospun nanofibers and two conventional nonwovens with predicted values shows a close agreement, which is seen in Fig. 7-5.

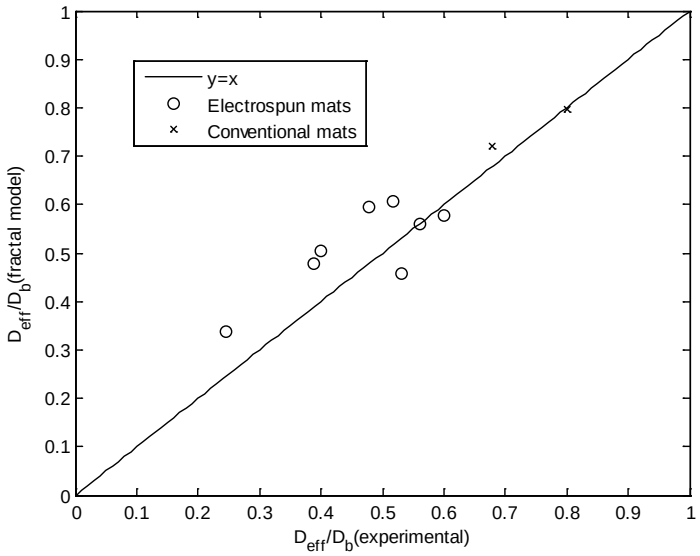

Figure 7-5: Comparison of fractal model and experimental results

The proposed model, which is based on Eq. (7-11) for general porous media, is also compared with the experimental data reported by Baker et al. (Baker et al., 2006), who used a diffusion cell to measure the through-thickness water vapor diffusion rate in untreated TGP-H-060 carbon paper, and by Flueckiger et al. (Flueckiger et al., 2008), who obtained effective diffusivity of TGP-H-060 carbon paper by an electrochemical diffusimetry. The geometric parameters of TGP-H-060 mat are listed in Table 1. In their experiments, TGP-H-060 mat was compressed to make variation of the mat porosity. Therefore, the thickness of compressed mat becomes $0.22/(1-\varepsilon)H_0$, and the mean tortuosity becomes $(1-\varepsilon)/0.22\tau_0$ assuming the tortuous diffusive distance unchanged during compression, based on

$\tau_0 = 3.2$ when $\varepsilon = 0.78$ from Eq. (7-18). As the pore size changes approximately proportionally and k is a constant accordingly, the maximum pore radius can obtained based on Eq. (7-13). Fig. 7-6 shows that the predictions of vapor diffusivity agree well with those experimental results.

The effects of different geometric parameters on effective diffusivities of fibrous media are also analyzed. As shown in Fig. 7-7, the dimensionless diffusivity increases monotonously with the increase of porosity and fiber radius, and the resistance of Knudsen effect becomes important when the fiber radius is smaller than $500\ nm$. The effective diffusivity is independent of fiber radius when fiber radius is much larger than mean free path of diffusive molecules, i.e. around 0.1 μm. According to the results plotted in Fig. 7-5 and Fig. 7-7, the effective diffusivity of layered electrospun nano-fibrous webs is smaller than conventional fibrous webs, but they are still in the same order. Therefore, electrospun nano-fibrous webs are potential candidates of breathable materials with their commonly thin thickness.

Table 7-1: Structural parameters of TGP-H-060 carbon fiber mat (Shi et al., 2006)

Parameter	Value
$R_{\max}$	$4\times10^{-5} m$
$R_{\max}$	$1.54\times10^{-8} m$
ε	0.78
H_0	$1.9\times10^{-4} m$
D_f	1.9669
D_t	1.1447

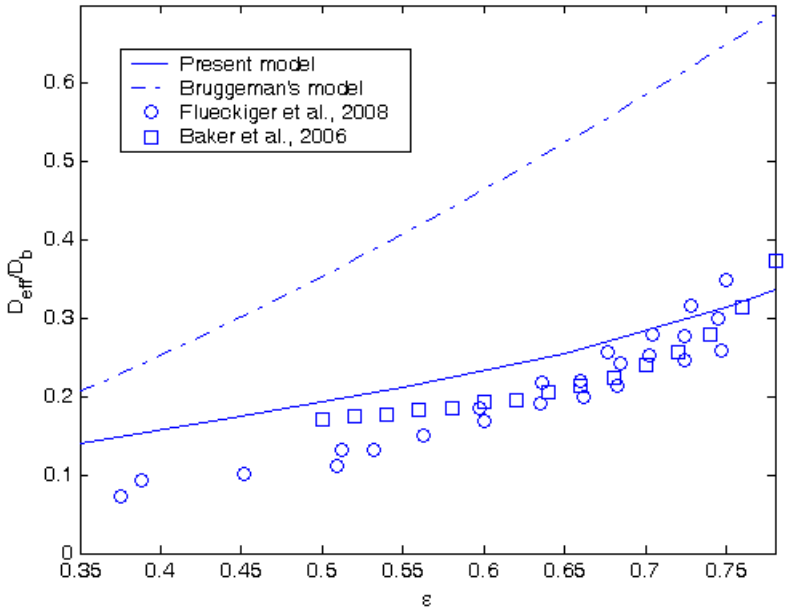

Figure 7-6: Comparison of the present model with previous model and experimental data from literature

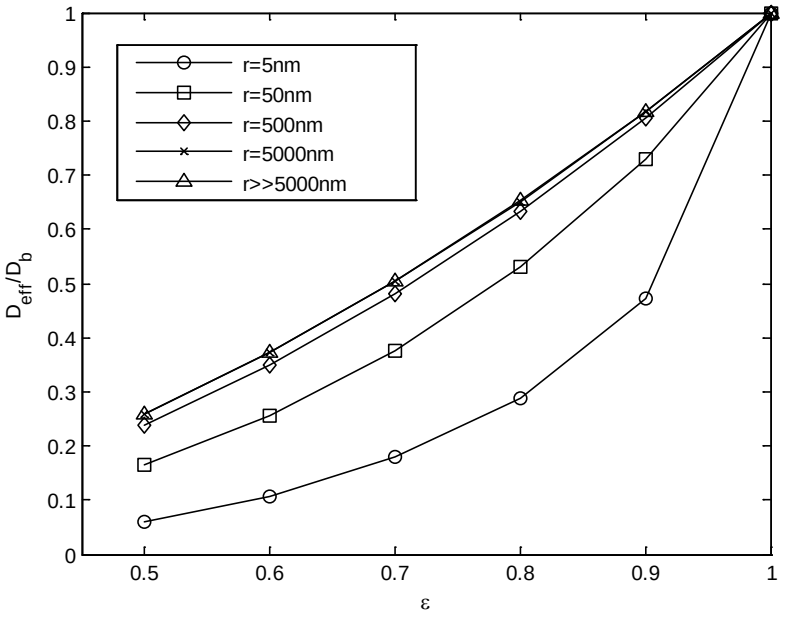

Figure 7-7: Effect of the fiber radius on effective diffusivity versus porosity

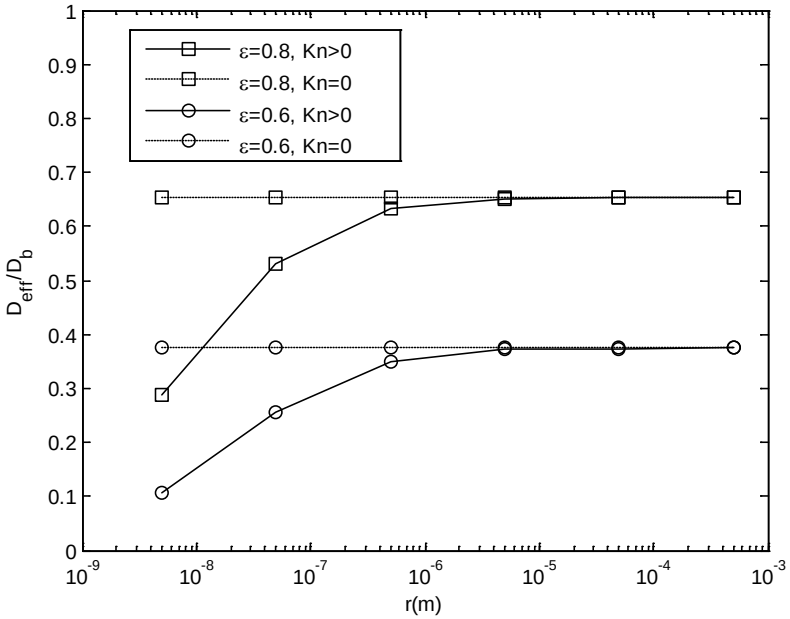

Figure 7-8: Effect of the porosity on effective diffusivity versus fiber radius

The effective diffusivities of fibrous webs with $\varepsilon = 0.6$ and $\varepsilon = 0.8$ are compared in Fig. 7-8, which indicates that fibrous media with higher porosity have higher diffusivity, but Knudsen effect reduces diffusivities more significantly at low porosity range.

Fig. 7-9 shows the influence of thickness of the fibrous medium on effective diffusivity when $\varepsilon = 0.8$ and $Kn = 0$. When the thickness is much larger than the pore size, the effective diffusivity is independent of thickness. When thickness is comparable with pore size, the effective diffusivity becomes sensitive to thickness and increases with decreasing thickness.

Fig. 7-10 plots the effective diffusivity versus porosity ε at different ratios of minimum and maximum pore radius k by setting $r = 50\text{nm}$. It can be seen that the effective diffusivity increases with the increasing k, which may be attributed to the fact that when the ratio k with given porosity becomes larger, more

opportunities are created for gas molecules to diffuse through the larger pores with less resistances or Knudsen effect. This trend is similar with viscous gas flow through fractal porous media reported in the literature (Shi et al., 2006).

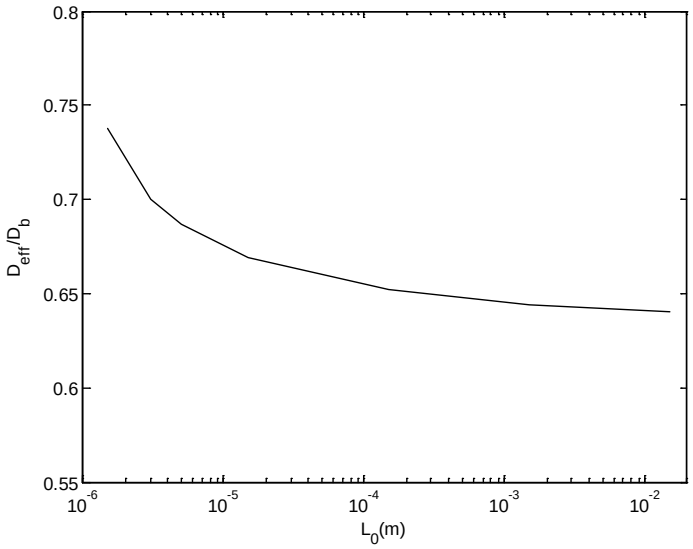

Figure 7-9: Effect of the thickness on dimensionless effective diffusivity

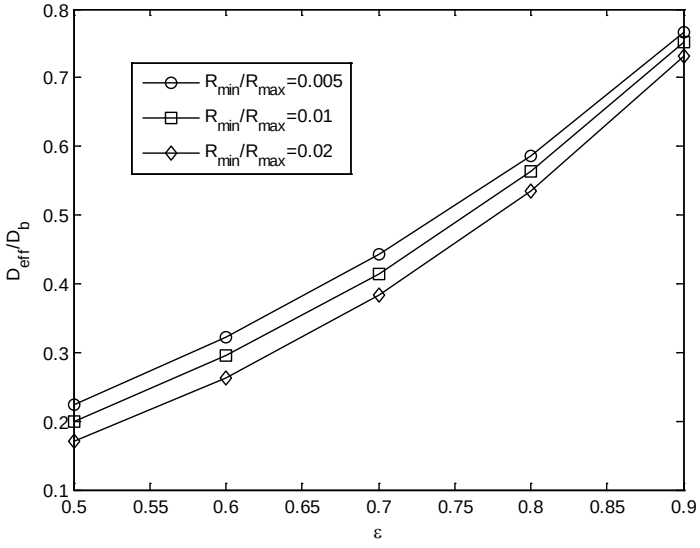

Figure 7-10: Effect of ratio of $R_{\min} / R_{\max}$ on dimensionless effective diffusivity

7.5. Concluding remarks

A fractal approach was applied to model gas diffusion through nano- and micro-fibrous porous media considering Knudsen effect. This fractal model is expressed as an analytical function of porosity, fiber/pore radius and fractal dimensions. The prediction of the model shows good agreement with experimental data. It demonstrates that the effective diffusivity is reduced owing to Knudsen effect in nano-scale fibrous webs. In addition, the theoretical analysis illustrates that electrospun fibers are good candidates of breathable materials, because although their diffusivity is decreased due to Knudsen effect, but they have very small diffusion resistances considering their extremely thin thickness. The effective diffusivity is found to be almost independent of the thickness of the fibrous media when the thickness is far greater than the pore size, but is inversely related to web thickness when it is comparable with the pore size. The model also indicates that the effective diffusivity of the fibrous media increases slightly with the increasing ratio of minimum and maximum pore radius, when fiber radius is comparable with mean free path of diffusive molecules.

Chapter 8 Summary and future work

In this thesis, gas permeability and vapor diffusivity of nano- and micro-fibrous materials were analytically studied based on deterministic and statistical methods. The thesis was first focused on modeling viscous gas flow though single-scale and dual-scale fibrous materials with structural analysis, and then investigating vapor diffusion in fibrous media theoretically and experimentally. The obtained models were compared with experimental, numerical, and analytical results obtained from literature over last decades and superior accuracy was observed. However, future work is still desirable, particularly in applications of the models and design of optimized fibrous structures.

8.1. Summary

The conclusive contributions of this thesis can be summarized as follows:

Deterministic models were established to predict gas permeability from simplified structures to realistic fibrous materials in high porosity range ($\varepsilon > 0.7$). It is shown that gas permeability increases with increasing degree of randomness of fiber distribution, and is not sensitive to in-plane fiber orientation, but increases with increasing through-plane fiber orientation. The slip effect on increasing longitudinal permeability is higher than transverse permeability in 1D fiber beds.

Gas permeability of fiber assembles was also studied at relatively low porosity range ($\varepsilon < 0.6$). The model considered the minimum distance (or gap) and the inscribed radius between fibers as the most critical parameter for transverse

permeability and longitudinal permeability, respectively. Permeability prediction by this model is in excellent agreement with experimental, numerical and analytical results collected from literature. It is also shown that permeability of elliptical fibers is similar to that of circular fibers in a wide range of porosities, but more permeable at the low porosity limit. Hexagonally packed fiber arrays are more transversely permeable than the squarely located fibers, while the relationship is opposite for longitudinal permeability.

Meanwhile, a statistical model was presented to determine the permeability of fibrous layers based on fractal theory. The model is a function of porosity and fractal dimension, which is validated by the collected experimental results throughout the porosity range. In addition, the overall permeability is found to be greatly sensitive with increasing maximum pore size of the fibrous system.

Calculation cost of computing permeability of dual-scale fibrous materials was reduced by applying a “slip” velocity at the interface between porous yarns and open channels between yarns. Based on that, the permeability models of 1D aligned yarns and 3D woven were successfully validated by comparing the model predictions with numerical calculations and experimental results. Particularly, it is found that the intra-yarn permeability has great influence on the overall permeability, especially for those with high degrees of packing. A semi-analytical expression for easy use was also proposed by fitting the numerical data.

The predicted effective diffusivities agree very well with experimental measurements and numerical simulations. In addition, in-plane orientation is found to not affect the effective diffusivity, but increasing through-plane orientation reduces the diffusion resistance. Particularly, randomly located fibers have lower diffusivity than those ordered distributed fibers.

A fractal approach was applied to determine vapor diffusivities of nano- and micro-fibrous porous layers. The model is expressed in terms of porosity, fiber radius, and fractal dimensions. The prediction of the model shows good agreement with the measured diffusivities of nylon 6 electrospun layers by an inverted-cup test. The experimental and theoretical studies suggested that electrospun nanofibers are good candidates as breathable materials. It is also found that effective diffusivity is reduced owing to Knudsen effect in nano- and micro- fibrous web. Besides, effective diffusivity is not sensitive with the thickness of the fiber layer when the thickness is larger than its pore size. The model also indicates that the effective diffusivity increases slowly with increasing the ratio of minimum and maximum pore radius.

8.2. Recommendations for future work

Based on the progress achieved through the present study, the following further work is suggested:

1. Apply present models to engineering problems such as clothing, filtration, fuel cells, resin molding transfer, and tissue engineering. Additionally, design optimal fibrous structures with required or max/min permeability, diffusivity, or production expense. Structural parameters, such as porosity, thickness, fiber size, fiber distribution, scale hierarchy, and layer arrangement, can be optimized based on the specific requirement.

2. With the analogy theory, apply the models of effective permeability and diffusivity to heat transfer, electrical conduction, elastic, and so forth. In addition, extend the present models to investigate dynamic transport behaviors and transport properties in deformed fibrous structures.

3. Perform numerical simulations of coupled transport properties in complex fibrous structures from nano-scale to macro-scale and develop easy-to-use software to describe the complex transport phenomena. Computational cost of transport behaviors in realistic and complicated fibrous structures will be greatly reduced based on present models.

4. Study additional structural parameters of fibrous systems on transport properties, including surface roughness, layer distribution, edge effect, inclusion influence and so forth.

5. Explore the mechanism of generation of fibrous structures, which enables to better characterize fibrous structures and transport behaviors.

References

AHMADI, M. M., MOHAMMADI, S. & HAYATI, A. N. (2011) Analytical derivation of tortuosity and permeability of monosized spheres: A volume averaging approach. *Physical Review E,* 83**,** 026312.

AHN, K. J., SEFERIS, J. C. & BERG, J. C. (1991) SIMULTANEOUS MEASUREMENTS OF PERMEABILITY AND CAPILLARY-PRESSURE OF THERMOSETTING MATRICES IN WOVEN FABRIC REINFORCEMENTS. *Polymer Composites,* 12**,** 146-152.

ALAVUDEEN, A., THIRUCHITRAMBALAM, M., VENKATESHWARAN, N. & ATHIJAYAMANI, A. (2011) REVIEW OF NATURAL FIBER REINFORCED WOVEN COMPOSITE. *Reviews on Advanced Materials Science,* 27**,** 146-150.

ALAZMI, B. & VAFAI, K. (2001) Analysis of fluid flow and heat transfer interfacial conditions between a porous medium and a fluid layer. *International Journal of Heat and Mass Transfer,* 44**,** 1735-1749.

ALVAREZRAMIREZ, J., NIEVESMENDOZA, S. & GONZALEZTREJO, J. (1996) Calculation of the effective diffusivity of heterogeneous media using the lattice-Boltzmann method. *Physical Review E,* 53**,** 2298-2303.

AMSC, N. & CMPS, A. A. (2002) COMPOSITE MATERIALS HANDBOOK.

ANDERSON, J. D. (2001) *Fundamentals of aerodynamics,* McGraw-Hill New York.

ARMOUR, J. C. & CANNON, J. N. (1968) Fluid flow through woven screens. *Aiche journal,* 14**,** 415-420.

BAKER, D. R., WIESER, C., NEYERLIN, K. C. & MURPHY, M. W. (2006) The Use of Limiting Current to Determine Transport Resistance in PEM Fuel Cells. *ECS Trans,* 3**,** 989-999.

BATEMAN, B., WAY, J. & LARSON, K. (1984) AN APPARATUS FOR THE

MEASUREMENT OF GAS FLUXES THROUGH IMMOBILIZED LIQUID MEMBRANES. *Separation Science and Technology,* 19**,** 21-32.

BAZBOUZ, M. B. & STYLIOS, G. K. (2008) Novel mechanism for spinning continuous twisted composite nanofiber yarns. *European Polymer Journal,* 44**,** 1-12.

BEAR, J. & BACHMAT, Y. (1990) *Introduction to modeling of transport phenomena in porous media,* Springer.

BEAVERS, G. S. & JOSEPH, D. D. (1967) BOUNDARY CONDITIONS AT A NATURALLY PERMEABLE WALL. *Journal of Fluid Mechanics,* 30**,** 197-207.

BECKER, J., FLUECKIGER, R., REUM, M., BUECHI, F. N., MARONE, F. & STAMPANONI, M. (2009) Determination of Material Properties of Gas Diffusion Layers: Experiments and Simulations Using Phase Contrast Tomographic Microscopy. *Journal of the Electrochemical Society,* 156**,** B1175-B1181.

BECKER, J., SCHULZ, V. & WIEGMANN, A. (2008) Numerical determination of two-phase material parameters of a gas diffusion layer using tomography images. *Journal of Fuel Cell Science and Technology,* 5**,** 021006.

BECKER, J., WIESER, C., FELL, S. & STEINER, K. (2011) A multi-scale approach to material modeling of fuel cell diffusion media. *International Journal of Heat and Mass Transfer,* 54**,** 1360-1368.

BERGELIN, O. P., BROWN, G. A., HULL, H. L. & SULLIVAN, F. W. (1950) Heat transfer and fluid friction during viscous flow across banks of tubes. III. A study of spacing and tube size. *TRANSACTIONS OF THE ASME Journal,* 72**,** 881-888.

BOLZ, R. & TUVE, G. (1976) *Handbook of tables for applied engineering science. (2nd ed.),* Cleveland, CRC Press.

BOSANQUET, C. H. (1944) British TA Report BR-507.

BRINKMAN, H. C. (1947) A CALCULATION OF THE VISCOUS FORCE EXERTED BY A FLOWING FLUID ON A DENSE SWARM OF PARTICLES. *Applied Scientific Research Section a-Mechanics Heat Chemical Engineering Mathematical Methods,* 1**,** 27-34.

BROWN JR., J. C. (1950) Determination of the Exposed Specific Surface of Pulp Fibers from Air Permeability Measurements. *TAPPI,* 33**,** 130-137.

BROWN, R. C. (1993) *Air filtration: an integrated approach to the theory and application of fibrous filters,* Oxford, Pergamon Press.

BRUSCHKE, M. V. & ADVANI, S. G. (1993) FLOW OF GENERALIZED NEWTONIAN FLUIDS ACROSS A PERIODIC ARRAY OF CYLINDERS. *Journal of Rheology,* 37**,** 479-498.

CARMAN, P. C. (1938) The Determination of the Specific Surface of Powders. *Transactions, Journal of the Society of Chemical Industries,* 57**,** 225-234.

CHAE, H. S., SONG, Y. S. & YOUN, J. R. (2007) Transverse permeability measurement of a circular braided preform in liquid composite molding. *Korea-Australia Rheology Journal,* 19**,** 17-25.

CHAI, Z. H., LU, J. H., SHI, B. C. & GUO, Z. L. (2011) Gas slippage effect on the permeability of circular cylinders in a square array. *International Journal of Heat and Mass Transfer,* 54**,** 3009-3014.

CHAN, D. Y. C., HUGHES, B. D. & PATERSON, L. (1988) FLUID CAPACITY DISTRIBUTIONS OF RANDOM POROUS-MEDIA. *Transport in Porous Media,* 3**,** 81-94.

CHEN, V. & HLAVACEK, M. (1994) APPLICATION OF VORONOI TESSELLATION FOR MODELING RANDOMLY PACKED HOLLOW-FIBER BUNDLES. *Aiche Journal,* 40**,** 606-612.

CHEN, Y. S., FAN, J. T., QIAN, X. & ZHANG, W. (2004) Effect of garment fit on

thermal insulation and evaporative resistance. *Textile Research Journal,* 74**,** 742-748.

CHEN, Z.-R., YE, L. & KRUCKENBERG, T. (2006) A micromechanical compaction model for woven fabric preforms. Part I: Single layer. *Composites Science and Technology,* 66**,** 3254-3262.

CHEN, Z.-R., YE, L. & LU, M. (2010) Permeability Predictions for Woven Fabric Preforms. *Journal of Composite Materials,* 44**,** 1569-1586.

CLAGUE, D. S., KANDHAI, B. D., ZHANG, R. & SLOOT, P. M. A. (2000) Hydraulic permeability of (un)bounded fibrous media using the lattice Boltzmann method. *Physical Review E,* 61**,** 616-625.

CLAGUE, D. S. & PHILLIPS, R. J. (1997) A numerical calculation of the hydraulic permeability of three-dimensional disordered fibrous media. *Physics of Fluids,* 9**,** 1562-1572.

CLIFFORD, S. M. & HILLEL, D. (1986) KNUDSEN DIFFUSION - THE EFFECT OF SMALL PORE-SIZE AND LOW GAS-PRESSURE ON GASEOUS TRANSPORT IN SOIL. *Soil Science,* 141**,** 289-297.

DARCY, H. (1856) Les fontaines publiques de la ville de Dijon. *Dalmont, Paris*.

DAVIES, C. N. (1952) The Separation of Airborne Dust and Particles. *Proceedings of the Institution of Mechanical Engineers,* B1**,** 185-213.

DENN, M. M. (1980) *Process Fluid Mechanics,* NJ, Prentice Hall.

DRUMMOND, J. E. & TAHIR, M. I. (1984) LAMINAR VISCOUS-FLOW THROUGH REGULAR ARRAYS OF PARALLEL SOLID CYLINDERS. *International Journal of Multiphase Flow,* 10**,** 515-540.

DU PLESSIS, E., WOUDBERG, S. & DU PLESSIS, J. P. (2010) Pore-scale modelling of diffusion in unconsolidated porous structures. *Chemical Engineering Science,* 65**,** 2541-2551.

EICHHORN, S. J. & SAMPSON, W. W. (2005) Statistical geometry of pores and

statistics of porous nanofibrous assemblies. *Journal of the Royal Society Interface,* 2**,** 309-318.

FAESSEL, M., DELISEE, C., BOS, F. & CASTERA, P. (2005) 3D Modelling of random cellulosic fibrous networks based on X-ray tomography and image analysis. *Composites Science and Technology,* 65**,** 1931-1940.

FAN, J. T. & CHEN, Y. S. (2002) Measurement of clothing thermal insulation and moisture vapour resistance using a novel perspiring fabric thermal manikin. *Measurement Science & Technology,* 13**,** 1115-1123.

FAN, J. T., LUO, Z. X. & LI, Y. (2000) Heat and moisture transfer with sorption and condensation in porous clothing assemblies and numerical simulation. *International Journal of Heat and Mass Transfer,* 43**,** 2989-3000.

FERENC, J. S. & NEDA, Z. (2007) On the size distribution of Poisson Voronoi cells. *Physica a-Statistical Mechanics and Its Applications,* 385**,** 518-526.

FLUECKIGER, R., FREUNBERGER, S. A., KRAMER, D., WOKAUN, A., SCHERER, G. G. & BUECHI, F. N. (2008) Anisotropic, effective diffusivity of porous gas diffusion layer materials for PEFC. *Electrochimica Acta,* 54**,** 551-559.

GEBART, B. R. (1992) PERMEABILITY OF UNIDIRECTIONAL REINFORCEMENTS FOR RTM. *Journal of Composite Materials,* 26**,** 1100-1133.

GENTLEMAN, E., NAUMAN, E., DEE, K. & LIVESAY, G. (2004) Short collagen fibers provide control of contraction and permeability in fibroblast-seeded collagen gels. *Tissue engineering,* 10**,** 421-427.

GIBSON, P. & CHARMCHI, M. (1997) The use of volume-averaging techniques to predict temperature transients due to water vapor sorption in hygroscopic porous polymer materials. *Journal of Applied Polymer Science,* 64**,** 493-505.

GIBSON, P., SCHREUDER-GIBSON, H. & RIVIN, D. (2001) Transport properties

of porous membranes based on electrospun nanofibers. *Colloids and Surfaces a-Physicochemical and Engineering Aspects,* 187**,** 469-481.

GOOIJER, H., WARMOESKERKEN, M. & WASSINK, J. G. (2003) Flow resistance of textile materials - Part I: Monofilament fabrics. *Textile Research Journal,* 73**,** 437-443.

GOSTICK, J. T., FOWLER, M. W., IOANNIDIS, M. A., PRITZKER, M. D., VOLFKOVICH, Y. M. & SAKARS, A. (2006a) Capillary pressure and hydrophilic porosity in gas diffusion layers for polymer electrolyte fuel cells. *Journal of Power Sources,* 156**,** 375-387.

GOSTICK, J. T., FOWLER, M. W., PRITZKER, M. D., IOANNIDIS, M. A. & BEHRA, L. M. (2006b) In-plane and through-plane gas permeability of carbon fiber electrode backing layers. *Journal of Power Sources,* 162**,** 228-238.

GOSTICK, J. T., IOANNIDIS, M. A., FOWLER, M. W. & PRITZKER, M. D. (2007) Pore network modeling of fibrous gas diffusion layers for polymer electrolyte membrane fuel cells. *Journal of Power Sources,* 173**,** 277-290.

GOYEAU, B., LHUILLIER, D., GOBIN, D. & VELARDE, M. G. (2003) Momentum transport at a fluid-porous interface. *International Journal of Heat and Mass Transfer,* 46**,** 4071-4081.

GRUJICIC, M., CHITTAJALLU, K. M. & WALSH, S. (2004) Effect of shear, compaction and nesting on permeability of the orthogonal plain-weave fabric preforms. *Materials Chemistry and Physics,* 86**,** 358-369.

GUERIBIZ, D., RAHMANI, M., JACQUEMIN, F., FREOUR, S., GUILLEN, R. & LOUCIF, K. (2009) Homogenization of Moisture Diffusing Behavior of Composite Materials with Impermeable or Permeable Fibers - Application to Porous Composite Materials. *Journal of Composite Materials,* 43**,** 1391-1408.

HAO, L. & CHENG, P. (2009) Lattice Boltzmann simulations of anisotropic permeabilities in carbon paper gas diffusion layers. *Journal of Power Sources,* 186**,** 104-114.

HAPPEL, J. (1959) VISCOUS FLOW RELATIVE TO ARRAYS OF CYLINDERS. *Aiche Journal,* 5**,** 174-177.

HE, G. L., ZHAO, Z. C., MING, P. W., ABULITI, A. & YIN, C. Y. (2007) A fractal model for predicting permeability and liquid water relative permeability in the gas diffusion layer (GDL) of PEMFCs. *Journal of Power Sources,* 163**,** 846-852.

HEARLE, J. W. S., GROSBERG, P. & BACKER, S. (1969) *Structural mechanics of fibers, yarns, and fabrics,* Wiley-interscience New York.

HENRY, R. S. H. (1939) Diffusion in Absorbing Media. *Proceedings of the Royal Society of London Series a-Mathematical Physical and Engineering Sciences,* 171**,** 215-241.

HIGDON, J. J. L. & FORD, G. D. (1996) Permeability of three-dimensional models of fibrous porous media. *Journal of Fluid Mechanics,* 308**,** 341-361.

HOSSEINI, S. A. & TAFRESHI, H. V. (2010) Modeling permeability of 3-D nanofiber media in slip flow regime. *Chemical Engineering Science,* 65**,** 2249-2254.

HOUST, Y. F. & WITTMANN, F. H. (1994) INFLUENCE OF POROSITY AND WATER-CONTENT ON THE DIFFUSIVITY OF CO2 AND O2 THROUGH HYDRATED CEMENT PASTE. *Cement and Concrete Research,* 24**,** 1165-1176.

HUANG, H., LEE, T. S. & SHU, C. (2007) Lattice Boltzmann method simulation gas slip flow in long microtubes. *International Journal of Numerical Methods for Heat & Fluid Flow,* 17**,** 587-607.

HUANG, J. H. & QIAN, X. M. (2007) A new test method for measuring the water

vapour permeability of fabrics. *Measurement Science & Technology,* 18**,** 3043-3047.

INGMANSON, W. L., ANDREWS, B. D. & JOHNSON, R. C. (1959) Internal Pressure Distributions in Compressible Mats under Fluid Stress. *TAPPI,* 42**,** 840-849.

J RVINEN, K. (2007) Development of filter media treatments for liquid filtration. *Acta Universitatis Lappeenrantaensis.*

JACKSON, G. W. & JAMES, D. F. (1986) THE PERMEABILITY OF FIBROUS POROUS-MEDIA. *Canadian Journal of Chemical Engineering,* 64**,** 364-374.

JIA, P., DONG, M. Z., DAI, L. M. & YAO, J. (2008) Slow viscous flow through arbitrary triangular tubes and its application in modelling porous media flows. *Transport in Porous Media,* 74**,** 153-167.

JOHNSON, D. L., KOPLIK, J. & SCHWARTZ, L. M. (1986) NEW PORE-SIZE PARAMETER CHARACTERIZING TRANSPORT IN POROUS-MEDIA. *Physical Review Letters,* 57**,** 2564-2567.

JOHNSON, E. M., BERK, D. A., JAIN, R. K. & DEEN, W. M. (1996) Hindered diffusion in agarose gels: Test of effective medium model. *Biophysical Journal,* 70**,** 1017-1023.

JOHNSTON, P. R. (1998) Revisiting the most probable pore-size distribution in filter media: The gamma distribution. *Filtration & Separation,* 35**,** 287-292.

KELLER, J. B. (1964) VISCOUS FLOW THROUGH A GRATING OR LATTICE OF CYLINDERS. *Journal of Fluid Mechanics,* 18**,** 94-96.

KHARADLY, M. M. Z. & JACKSON, W. (1953) THE PROPERTIES OF ARTIFICIAL DIELECTRICS COMPRISING ARRAYS OF CONDUCTING ELEMENTS. *Proceedings of the Institution of Electrical Engineers-London,* 100**,** 199-212.

KHOMAMI, B. & MORENO, L. D. (1997) Stability of viscoelastic flow around periodic arrays of cylinders. *Rheologica Acta,* 36**,** 367-383.

KIM, J. S. & RENEKER, D. H. (1999) Mechanical properties of composites using ultrafine electrospun fibers. *Polymer Composites,* 20**,** 124-131.

KIRSCH, A. & FUCHS, N. (1967) Studies on Fibrous Aerosol Filters—II. Pressure Drops in Systems of Parallel Cylinders. *Annals of Occupational Hygiene,* 10**,** 23-30.

KOPONEN, A., KANDHAI, D., HELLEN, E., ALAVA, M., HOEKSTRA, A., KATAJA, M., NISKANEN, K., SLOOT, P. & TIMONEN, J. (1998) Permeability of three-dimensional random fiber webs. *Physical Review Letters,* 80**,** 716-719.

KOPONEN, A., KATAJA, M. & TIMONEN, J. (1996) Tortuous flow in porous media. *Physical Review E,* 54**,** 406-410.

KOSTORNOV, A. & SHEVCHUK, M. (1977) Hydraulic characteristics and structure of porous metal fiber materials. *Powder Metallurgy and Metal Ceramics,* 16**,** 694-699.

KOSTORNOV, A. & SHEVCHUK, M. S. (1973) Hydraulic characteristics and structure of porous metal fiber materials. *Powder Metallurgy and Metal Ceramics,* 12**,** 752-756.

KUWABARA, S. (1959) THE FORCES EXPERIENCED BY RANDOMLY DISTRIBUTED PARELLEL CIRCULAR CYLINDERS OR SPHERES IN A VISCOUS FLOW AT SMALL REYNOLDS NUMBERS. *Journal of the Physical Society of Japan,* 14**,** 527-532.

LABRECQUE, R. P. (1968) The Effects of Fiber Cross-Sectional Shape on the Resistance to the Flow of Fluids through Fiber Mats. *TAPPI,* 51**,** 8-15.

LAMANNA, J. M. & KANDLIKAR, S. G. (2011) Determination of effective water vapor diffusion coefficient in pemfc gas diffusion layers. *International*

Journal of Hydrogen Energy, 36**,** 5021-5029.

LI, D. & XIA, Y. N. (2004) Electrospinning of nanofibers: Reinventing the wheel? *Advanced Materials,* 16**,** 1151-1170.

LI, S. J., LEE, L. J. & CASTRO, J. (2002) Effective mass diffusivity in composites. *Journal of Composite Materials,* 36**,** 1709-1724.

LI, Y. & ZHU, Q. Y. (2003) Simultaneous heat and moisture transfer with moisture sorption, condensation, and capillary liquid diffusion in porous textiles. *Textile Research Journal,* 73**,** 515-524.

LIFSHUTZ, N. (2005) On the 'Mean Flow' Pore Size Distribution of Microfiber and Nanofiber Webs. *INJ Spring***,** 18-24.

LITSTER, S. & MCLEAN, G. (2004) PEM fuel cell electrodes. *Journal of Power Sources,* 130**,** 61-76.

LORD, E. (1955) Air Flow through Plugs of Textile Fibres: Part I – General Flow Relations. *Journal of the Textile Institute,* 46**,** T191-T213.

LU, W. M., TUNG, K. L. & HWANG, K. J. (1996) Fluid flow through basic weaves of monofilament filter cloth. *Textile Research Journal,* 66**,** 311-323.

MANDELBROT, B. B. (1982) *The fractal geometry of nature,* New York, W. H. Freeman.

MARIATTI, M., NASIR, M. & ISMAIL, H. (2000) Effect of sample cutting direction on mechanical properties of woven thermoplastic prepreg. *Polymer Testing,* 19**,** 617-624.

MATTERN, K. J. & DEEN, W. M. (2008) "Mixing Rules" for estimating the hydraulic permeability of fiber mixtures. *Aiche Journal,* 54**,** 32-41.

MERHI, D., MICHAUD, V., KAMPFER, L., VUILLIOMENET, P. & MANSON, J. A. E. (2007) Transverse permeability of chopped fibre bundle beds. *Composites Part a-Applied Science and Manufacturing,* 38**,** 739-746.

MEZEDUR, M. M., KAVIANY, M. & MOORE, W. (2002) Effect of pore structure,

randomness sand size on effective mass diffusivity. *Aiche Journal,* 48**,** 15-24.

MICROFIBER.COM (2012). http://microfiber.com.

MOEST, M., RZEPKA, M. & STIMMING, U. (2009) Analysis of the diffusive mass transport in the anode side porous backing layer of a direct methanol fuel cell. *Journal of Power Sources,* 191**,** 456-464.

MORINI, G. L., SPIGA, M. & TARTARINI, P. (2004) The rarefaction effect on the friction factor of gas flow in microchannels. *Superlattices and Microstructures,* 35**,** 587-599.

MOTAKEF, S. & ELMASRI, M. A. (1986) SIMULTANEOUS HEAT AND MASS-TRANSFER WITH PHASE-CHANGE IN A POROUS SLAB. *International Journal of Heat and Mass Transfer,* 29**,** 1503-1512.

MU, D., LIU, Z.-S., HUANG, C. & DJILALI, N. (2008) Determination of the effective diffusion coefficient in porous media including Knudsen effects. *Microfluidics and Nanofluidics,* 4**,** 257-260.

NABOVATI, A., LLEWELLIN, E. W. & SOUSA, A. C. M. (2009) A general model for the permeability of fibrous porous media based on fluid flow simulations using the lattice Boltzmann method. *Composites Part a-Applied Science and Manufacturing,* 40**,** 860-869.

NABOVATI, A., LLEWELLIN, E. W. & SOUSA, A. C. M. (2010) Through-thickness permeability prediction of three-dimensional multifilament woven fabrics. *Composites Part a-Applied Science and Manufacturing,* 41**,** 453-463.

NAM, J. H. & KAVIANY, M. (2003) Effective diffusivity and water-saturation distribution in single- and two-layer PEMFC diffusion medium. *International Journal of Heat and Mass Transfer,* 46**,** 4595-4611.

NEALE, G. & NADER, W. (1974) PRACTICAL SIGNIFICANCE OF BRINKMANS EXTENSION OF DARCYS LAW - COUPLED PARALLEL

FLOWS WITHIN A CHANNEL AND A BOUNDING POROUS-MEDIUM. *Canadian Journal of Chemical Engineering,* 52**,** 475-478.

NGO, N. & TAMMA, K. K. (2001) Microscale permeability predictions of porous fibrous media. *International Journal of Heat and Mass Transfer,* 44**,** 3135-3145.

NILSSON, L. & STENSTROM, S. (1995) GAS-DIFFUSION THROUGH SHEETS OF FIBROUS POROUS-MEDIA. *Chemical Engineering Science,* 50**,** 361-371.

OCHOATAPIA, J. A. & WHITAKER, S. (1995) MOMENTUM-TRANSFER AT THE BOUNDARY BETWEEN A POROUS-MEDIUM AND A HOMOGENEOUS FLUID .1. THEORETICAL DEVELOPMENT. *International Journal of Heat and Mass Transfer,* 38**,** 2635-2646.

OGI, K. & TAKEDA, N. (1997) Effects of moisture content on nonlinear deformation behavior of CF/epoxy composites. *Journal of Composite Materials,* 31**,** 530-551.

PAN, N. & GIBSON, P. (2006) *Thermal and moisture transport in fibrous materials*, Woodhead Pub Ltd.

PAPADOPOULOS, G. K., THEODOROU, D. N., VASENKOV, S. & KARGER, J. (2007) Mesoscopic simulations of the diffusivity of ethane in beds of NaX zeolite crystals: Comparison with pulsed field gradient NMR measurements. *Journal of Chemical Physics,* 126**,** 094702.

PAPATHANASIOU, T. D. (1997) On the effective permeability of square arrays of permeable fiber tows. *International Journal of Multiphase Flow,* 23**,** 81-92.

PAPATHANASIOU, T. D. (2001) Flow across structured fiber bundles: a dimensionless correlation. *International Journal of Multiphase Flow,* 27**,** 1451-1461.

PENMAN, H. L. (1940) Gas and vapour movements in the soil I. The diffusion of

vapours through porous solids. *Journal of Agricultural Science,* 30**,** 437-462.

PERRINS, W. T., MCKENZIE, D. R. & MCPHEDRAN, R. C. (1979) TRANSPORT-PROPERTIES OF REGULAR ARRAYS OF CYLINDERS. *Proceedings of the Royal Society of London Series a-Mathematical Physical and Engineering Sciences,* 369**,** 207-225.

PHATTARANAWIK, J., JIRARATANANON, R. & FANE, A. G. (2003) Effect of pore size distribution and air flux on mass transport in direct contact membrane distillation. *Journal of Membrane Science,* 215**,** 75-85.

PHELAN, F. R. & WISE, G. (1996) Analysis of transverse flow in aligned fibrous porous media. *Composites Part a-Applied Science and Manufacturing,* 27**,** 25-34.

RAHLI, O., TADRIST, L., MISCEVIC, M. & SANTINI, R. (1997) Fluid flow through randomly packed monodisperse fibers: The Kozeny-Carman parameter analysis. *Journal of Fluids Engineering-Transactions of the Asme,* 119**,** 188-192.

RANGANATHAN, S., PHELAN, F. R. & ADVANI, S. G. (1996) A generalized model for the transverse fluid permeability in unidirectional fibrous media. *Polymer Composites,* 17**,** 222-230.

RANTANEN, J., ALFTHAN, N., IMPIO, J., KARINSALO, T., MALMIVAARA, M., MATALA, R., MAKINEN, M., REHO, A., TALVENMAA, P. & TASANEN, M. (2000) Smart clothing for the arctic environment. IEEE *4th International Symposium on Wearable Computers*.

RENEKER, D. H., YARIN, A. L., FONG, H. & KOOMBHONGSE, S. (2000) Bending instability of electrically charged liquid jets of polymer solutions in electrospinning. *Journal of Applied Physics,* 87**,** 4531-4547.

SADIQ, T. A. K., ADVANI, S. G. & PARNAS, R. S. (1995) EXPERIMENTAL INVESTIGATION OF TRANSVERSE FLOW-THROUGH ALIGNED

CYLINDERS. *International Journal of Multiphase Flow,* 21**,** 755-774.

SAFFMAN, P. G. (1971) BOUNDARY CONDITION AT SURFACE OF A POROUS MEDIUM. *Studies in Applied Mathematics,* 50**,** 93-101.

SAMPSON, W. W. (2003) A multiplanar model for the pore radius distribution in isotropic near-planar stochastic fibre networks. *Journal of Materials Science,* 38**,** 1617-1622.

SANGANI, A. S. & ACRIVOS, A. (1982) SLOW FLOW PAST PERIODIC ARRAYS OF CYLINDERS WITH APPLICATION TO HEAT-TRANSFER. *International Journal of Multiphase Flow,* 8**,** 193-206.

SANGANI, A. S. & YAO, C. (1988) TRANSPORT PROCESSES IN RANDOM ARRAYS OF CYLINDERS .2. VISCOUS-FLOW. *Physics of Fluids,* 31**,** 2435-2444.

SHARMA, S. & SIGINER, D. A. (2010) Permeability Measurement Methods in Porous Media of Fiber Reinforced Composites. *Applied Mechanics Reviews,* 63**,** 020802.

SHEN, C. & SPRINGER, G. (1981) *Environmental Effect on Composite Materials,* Springer.

SHI, Y., XIAO, J., PAN, M. & YUAN, R. (2006) A fractal permeability model for the gas diffusion layer of PEM fuel cells. *Journal of Power Sources,* 160**,** 277-283.

SHIH, F. S. (1967) LAMINAR FLOW IN AXISYMMETRIC CONDUITS BY A RATIONAL APPROACH. *Canadian Journal of Chemical Engineering,* 45**,** 285-294.

SKARTSIS, L., KHOMAMI, B. & KARDOS, J. L. (1992) RESIN FLOW THROUGH FIBER BEDS DURING COMPOSITE MANUFACTURING PROCESSES .2. NUMERICAL AND EXPERIMENTAL STUDIES OF NEWTONIAN FLOW THROUGH IDEAL AND ACTUAL FIBER BEDS.

Polymer Engineering and Science, 32**,** 231-239.

SMITH, W. F. (2004) *Foundations of Materials Science and Engineering,* McGraw-Hill.

SMITH, W. F. & HASHEMI, J. (2006) *Foundations of materials science and engineering,* McGraw-Hill Higher Education.

SOBERA, M. P. & KLEIJN, C. R. (2006) Hydraulic permeability of ordered and disordered single-layer arrays of cylinders. *Physical Review E,* 74**,** 036301.

SONG, Y. S., CHUNG, K., KANG, T. J. & YOUN, J. R. (2004) Prediction of permeability tensor for three dimensional circular braided preform by applying a finite volume method to a unit cell. *Composites Science and Technology,* 64**,** 1629-1636.

SONG, Y. S., HEIDER, D. & YOUN, J. R. (2009) Statistical Characteristics of Out-of-Plane Permeability for Plain-Woven Structure. *Polymer Composites,* 30**,** 1465-1472.

SPAID, M. A. A. & PHELAN, F. R. (1997) Lattice Boltzmann methods for modeling microscale flow in fibrous porous media. *Physics of Fluids,* 9**,** 2468-2474.

STYLIANOPOULOS, T., YECKEL, A., DERBY, J. J., LUO, X. J., SHEPHARD, M. S., SANDER, E. A. & BAROCAS, V. H. (2008) Permeability calculations in three-dimensional isotropic and oriented fiber networks. *Physics of Fluids,* 20**,** 123601.

SUBBIAH, T., BHAT, G. S., TOCK, R. W., PARARNESWARAN, S. & RAMKUMAR, S. S. (2005) Electrospinning of nanofibers. *Journal of Applied Polymer Science,* 96**,** 557-569.

SULLIVAN, R. R. (1942) Specific Surface Measurements on Compact Bundles of Parallel Fibers *Journal of Applied Physics,* 13**,** 725-730.

TAHIR, M. A. & TAFRESHI, H. V. (2009) Influence of fiber orientation on the

transverse permeability of fibrous media. *Physics of Fluids,* 21**,** 083604.

TAMAYOL, A. & BAHRAMI, M. (2009) Analytical determination of viscous permeability of fibrous porous media. *International Journal of Heat and Mass Transfer,* 52**,** 2407-2414.

TAMAYOL, A. & BAHRAMI, M. (2010a) Parallel Flow Through Ordered Fibers: An Analytical Approach. *Journal of Fluids Engineering-Transactions of the Asme,* 132**,** 114502.

TAMAYOL, A. & BAHRAMI, M. (2010b) Transverse Permeability of Fibrous Porous Media. *Proceedings of the 3rd International Conference on Porous Media and its Applications in Science and Engineering.* Montecatini, Italy.

TAMAYOL, A. & BAHRAMI, M. (2011) Transverse permeability of fibrous porous media. *Physical Review E,* 83**,** 046314.

TAMAYOL, A., BAHRAMI, M. & ASME (2009) PARALLEL FLOW IN ORDERED FIBROUS STRUCTURES: AN ANALYTICAL APPROACH. 5th Symposium on Fundamental Issues and Perspectives in Fluid Mechanics FEDSM2009-78166, 1311-1321

TAO, Y. X., BESANT, R. W. & REZKALLAH, K. S. (1991) UNSTEADY HEAT AND MASS-TRANSFER WITH PHASE-CHANGES IN AN INSULATION SLAB - FROSTING EFFECTS. International Journal of Heat and Mass Transfer, 34, 1593-1603.

TOMADAKIS, M. M. & ROBERTSON, T. J. (2005) Viscous permeability of random fiber structures: Comparison of electrical and diffusional estimates with experimental and analytical results. *Journal of Composite Materials,* 39**,** 163-188.

TOMADAKIS, M. M. & SOTIRCHOS, S. V. (1991) KNUDSEN DIFFUSIVITIES AND PROPERTIES OF STRUCTURES OF UNIDIRECTIONAL FIBERS. *Aiche journal,* 37**,** 1175-1186.

TOMADAKIS, M. M. & SOTIRCHOS, S. V. (1993a) EFFECTIVE DIFFUSIVITIES AND CONDUCTIVITIES OF RANDOM DISPERSIONS OF NONOVERLAPPING AND PARTIALLY OVERLAPPING UNIDIRECTIONAL FIBERS. *Journal of Chemical Physics,* 99**,** 9820-9827.

TOMADAKIS, M. M. & SOTIRCHOS, S. V. (1993b) ORDINARY AND TRANSITION REGIME DIFFUSION IN RANDOM FIBER STRUCTURES. *Aiche Journal,* 39**,** 397-412.

TUNG, K. L., SHIAU, J. S., CHUANG, C. J., LI, Y. L. & LU, W. M. (2002) CFD analysis on fluid flow through multifilament woven filter cloths. *Separation Science and Technology,* 37**,** 799-821.

WANG, C. Y. (2000) On the diffusion past a staggered array of rectangular fibers. *Chemical Engineering Science,* 55**,** 6079-6084.

WANG, M. R., HE, J. H., YU, J. Y. & PAN, N. (2007a) Lattice Boltzmann modeling of the effective thermal conductivity for fibrous materials. *International Journal of Thermal Sciences,* 46**,** 848-855.

WANG, Q., MAZE, B., TAFRESHI, H. V. & POURDEYHIMI, B. (2006) A note on permeability simulation of multifilament woven fabrics. *Chemical Engineering Science,* 61**,** 8085-8088.

WANG, Q., MAZE, B., TAFRESHI, H. V. & POURDEYHIMI, B. (2007b) On the pressure drop modeling of monofilament-woven fabrics. *Chemical Engineering Science,* 62**,** 4817-4821.

WANG, Y., CHO, S., THIEDMANN, R., SCHMIDT, V., LEHNERT, W. & FENG, X. (2010) Stochastic modeling and direct simulation of the diffusion media for polymer electrolyte fuel cells. *International Journal of Heat and Mass Transfer,* 53**,** 1128-1138.

WEE, J. H. (2007) Applications of proton exchange membrane fuel cell systems. *Renewable and Sustainable Energy Reviews,* 11**,** 1720-1738.

WHEAT, J. A. (1963) The Air Flow Resistance of Glass Fiber Filter Paper. *The Canadian Journal of Chemical Engineering,* 41**,** 67-72.

WIGGINS, E. J., CAMPBELL, W. B. & MAASS, O. (1939) Determination of the specific surface of fibrous materials. *Canadian Journal of Research,* 17**,** 318-324.

WIKI (2012). http://en.wikipedia.org/wiki/Nanofiber.

WU, X. Q., LI, J. L. & SHENOI, R. A. (2007) A new method to determine fiber transverse permeability. *Journal of Composite Materials,* 41**,** 747-756.

XU, G. & WANG, F. (2005) Prediction of the permeability of woven fabrics. *Journal of industrial textiles,* 34**,** 243-254.

YAZDCHI, K., SRIVASTAVA, S. & LUDING, S. (2011) Microstructural effects on the permeability of periodic fibrous porous media. *International Journal of Multiphase Flow,* 37**,** 956-966.

YU, B. (2008) Analysis of flow in fractal porous media. *Applied Mechanics Reviews,* 61**,** 050801.

YU, B. M. (2005) Fractal character for tortuous streamtubes in porous media. *Chinese Physics Letters,* 22**,** 158-160.

YU, B. M. & LEE, L. J. (2000) A simplified in-plane permeability model for textile fabrics. *Polymer Composites,* 21**,** 660-685.

YU, B. M. & LI, J. H. (2001) Some fractal characters of porous media. *Fractals-Complex Geometry Patterns and Scaling in Nature and Society,* 9**,** 365-372.

YU, B. M. & LIU, W. (2004) Fractal analysis of permeabilities for porous media. *Aiche journal,* 50**,** 46-57.

ZALC, J. M., REYES, S. C. & IGLESIA, E. (2004) The effects of diffusion mechanism and void structure on transport rates and tortuosity factors in complex porous structures. *Chemical Engineering Science,* 59**,** 2947-2960.

ZAMEL, N., LI, X. & SHEN, J. (2009) Correlation for the Effective Gas Diffusion Coefficient in Carbon Paper Diffusion Media. *Energy & Fuels,* 23**,** 6070-6078.

ZHANG, Q., LI, B. Y. & SUN, W. W. (2011) Heat and sweat transport through clothing assemblies with phase changes, condensation/evaporation and absorption. *Proceedings of the Royal Society a-Mathematical Physical and Engineering Sciences,* 467**,** 3469-3489.

ZHONG, W. H., CURRIE, I. G. & JAMES, D. F. (2006) Creeping flow through a model fibrous porous medium. *Experiments in Fluids,* 40**,** 119-126.

ZHOU, F., KUENTZER, N., SIMACEK, P., ADVANI, S. G. & WALSH, S. (2006) Analytic characterization of the permeability of dual-scale fibrous porous media. *Composites Science and Technology,* 66**,** 2795-2803.

ZHU, Q. Y., XIE, M. H., YANG, J. & LI, Y. (2010) Investigation of the 3D model of coupled heat and liquid moisture transfer in hygroscopic porous fibrous media. *International Journal of Heat and Mass Transfer,* 53**,** 3914-3927.